



Universiteit
Leiden
The Netherlands

Solitary Waves and Fluctuations in Fragile Matter

Upadhyaya, N.

Citation

Upadhyaya, N. (2013, November 5). *Solitary Waves and Fluctuations in Fragile Matter*. *Casimir PhD Series*. Retrieved from <https://hdl.handle.net/1887/22138>

Version: Not Applicable (or Unknown)

License: [Leiden University Non-exclusive license](#)

Downloaded from: <https://hdl.handle.net/1887/22138>

Note: To cite this publication please use the final published version (if applicable).

Cover Page



Universiteit Leiden



The handle <http://hdl.handle.net/1887/22138> holds various files of this Leiden University dissertation.

Author: Upadhyaya, Nitin

Title: Solitary waves and fluctuations in fragile matter

Issue Date: 2013-11-05

Cover Page



Universiteit Leiden



The handle <http://hdl.handle.net/1887/22138> holds various files of this Leiden University dissertation.

Author: Upadhyaya, Nitin

Title: Solitary waves and fluctuations in fragile matter

Issue Date: 2013-11-05

SOLITARY WAVES AND
FLUCTUATIONS IN FRAGILE MATTER

PROEFSCHRIFT

Ter verkrijging van de graad van Doctor aan de
Universiteit Leiden, op gezag van Rector Magnificus
Prof. Mr. C.J.J.M Stolker, volgens besluit van het
College voor Promoties te verdedigen op dinsdag 5
november 2013 klokke 13:45 uur
door

NITIN UPADHYAYA

GEBOREN TE HYDERABAD, INDIA IN 1981

PROMOTIECOMMISSIE

Promotor

Prof. dr. M.L. van Hecke

Co-Promotor

Dr. V. Vitelli

Overige leden

Prof. dr. E.R. Eliel

Prof. dr. H. Schiessel

Prof. dr. C.W.J. Beenakker

Dr. Y. Shokef (Tel Aviv University)

Dr. B. Tighe (Technische Universiteit Delft)

CASIMIR PHD SERIES, DELFT-LEIDEN, 2013-28
ISBN 978-90-8593-169-0

THIS WORK IS PART OF THE RESEARCH PROGRAMME
OF THE FOUNDATION FOR FUNDAMENTAL RESEARCH
ON MATTER (FOM), WHICH IS PART OF THE NETHER-
LANDS ORGANISATION FOR SCIENTIFIC RESEARCH
(NWO).

CONTENTS

1	INTRODUCTION	1
1.1	Strongly non-linear waves in fragile matter	2
1.1.1	Hertz interaction for elastic bodies	2
1.1.2	A prelude to non-linear waves	3
1.1.3	Examples of fragile matter in one dimension	5
1.1.4	Examples of fragile matter in two dimensions	6
1.2	Disorder as an effective viscosity ?	12
1.3	This Thesis	14
	GRANULAR INTERFACES	17
2	GRANULAR INTERFACES	19
2.1	Simulations	20
2.2	Quasi-particle model	20
2.3	Weak disorder	21
2.4	Strong disorder : $A \ll 1$	22
	DISORDERED PACKINGS	27
3	AMORPHOUS PACKINGS	29
3.1	Exponential attenuation : weak disorder	29
3.2	Strong disorder	32
3.3	Long wavelength waves	33
3.4	Similarity solution	35
	FLUCTUATIONS AND EMERGENT HYDRODYNAMICS	39
4	FLUCTUATIONS AND EMERGENT PROPERTIES	41
4.1	Virial relation	41
4.2	Hydrodynamical modes	44
	THERMAL FLUCTUATIONS	53
5	SOLITARY WAVE IN FLUCTUATING BACKGROUND	55
5.1	The anti-Soliton	58
5.2	Langevin Equation	58
5.3	Mean and variance	62
5.4	Simulations	63
5.4.1	Fluctuation induced rigidity	65
5.4.2	Comparison with analytics	66

	SHEAR FRONTS IN RANDOM SPRING NETWORKS.	69
6	SHEAR FRONTS IN RANDOM SPRING NETWORKS	71
6.1	Linear regime	72
6.1.1	Early time	72
6.1.2	Late Times	75
6.2	Non-linear regime	76
	SUPPLEMENTARY MATERIAL	83
A	NESTERENKO SOLITARY WAVE	85
A.1	Quasi-particle interpretation	87
B	SOLITARY WAVE SOLUTION	89
B.1	Rosenau approximation	89
B.2	Solitary wave solution	90
C	HYDRODYNAMICAL MODES AND POWER SPECTRUM	93
C.1	Hydrodynamic modes	93
c.1.1	Longitudinal Current Density	95
D	FLUCTUATION DISSIPATION THEOREM	97
E	LINEAR NON-QUASISTATIC REGIME	101
E.1	From oscillatory rheology	101
E.2	Fractional equation	104
E.3	Non-linearity from harmonic springs	105
F	IDEAS FOR FURTHER WORK ON THERMAL AND QUANTUM FLUCTUATIONS	107
F.1	Approximate method to simulate quantum zero point energy	108
F.1.1	Simple harmonic oscillator	109
F.2	Chain of harmonic oscillators	110
F.3	Random network of harmonic springs	110
F.3.1	Fluctuation induced rigidity	111
F.4	Simulation	114
F.4.1	Planck Spectrum	114
F.4.2	Limiting forms	116
	BIBLIOGRAPHY	119
	SUMMARY	125
	SAMENVATTING	129
	CURRICULUM VITAE	133
	PUBLICATIONS	135

INTRODUCTION

Materials are conventionally classified in one of three states of matter: solid, liquid or gas. However, many commonly available materials may be easily arranged to display novel properties, that defy their simple classification into any of the above states of matter. Consider for instance, a block of steel, see Fig . (1.1). It is clearly a solid – if we hammer one end gently, the material remains intact and we hear sound. Now, construct out of the block of steel many smaller steel balls and pack them together so that the balls just touch each other. What happens if we now hit one end of this packing ?

No matter how gently you touch the sample, super-sonic waves (waves that travel faster than the sound speed of the medium) , rather than ordinary sound, will propagate in the packing. This happens no matter how hard (or soft) the constituent balls are. Surprisingly then, this simple aggregate of steel balls already uncovers a unique state of matter, that we will call *fragile matter*.

What is the origin of such an extreme response ? The paradigm of solids is the long range ordering of identical constituents (such as atoms) that interact harmonically for small displacements from their equilibrium lattice spacing. Within such approximations, their response to any external mechanical perturbation is linear and is embodied in a finite elastic moduli that also endows the solid with a finite speed of sound. Higher order non-linear terms conventionally appear as small perturbations around a response that is predominantly linear.

By contrast, in the above example of a granular aggregate of steel balls just in contact with their nearest neighbours, both the linear elastic moduli and speed of sound drop to zero. This extreme *softness* stems directly from the local strongly *non-linear* interaction between macroscopic balls in contact since the inter-particle interaction now no longer has a harmonic part. Moreover, this behaviour is independent of the material the ball is made of which could be as hard as steel or as soft as bubbles - it is a result of continuum elasticity that dictates the nature of the interaction between macroscopic objects in contact [1]. This is just one example of how *fragility* originates. Note, the

In fragile matter near their critical point, energy propagates through strongly non-linear waves that travel faster than the speed of sound

notion of a granular aggregate of steel balls as constituting a state of matter, is now at one higher level of abstraction: we are considering the collective behaviour of an aggregate of macroscopically solid balls and studying its mechanical (collective) response.

Interestingly, fragility itself can also arise from a global criteria, for instance in a weakly connected network of cross-linked polymers that are often modelled as a random network of harmonic springs. Here, *softness* in linear response can arise irrespective of the strength of the local spring constant, provided that the number of mechanical constraints is too low to maintain rigidity. In these physical systems, the disordered arrangement of particles plays a pivotal role in shaping the mechanical response by causing the particle displacement field in response to strains applied at the boundaries, to be very heterogeneous (not mimic the direction of strains applied at the boundaries). Such displacements are called *non-affine* and by absorbing a substantial part of the energy supplied at the boundaries, these displacements allow new configurations to minimize the energy, causing a vanishingly small linear response[2, 3, 4].

In many materials (see Fig. (1.2)), it is often the interplay between the nature of the constituents (that dictates their interaction locally) and how they are arranged in the material (global criteria), that together determine the nature of the elastic response. Note here, the notions of *fragility* and *softness* are only to stress the unusual behaviour within the regime of linear response and does not necessarily imply a breaking apart of the material.

In the following sections, we now give some examples of the kinds of unusual behaviour that arise in simple (often idealized) model systems, that are used to study fragile states of matter.

1.1 STRONGLY NON-LINEAR WAVES IN FRAGILE MATTER

1.1.1 Hertz interaction for elastic bodies

As alluded to above, the strongly non-linear interaction potential between macroscopic bodies in contact is often a source of fragility. Here, we provide a simple intuitive explanation of the origins of a strongly non-linear elastic response. Detailed analytic derivation may be found in Lev Landau's book on the Theory of Elasticity [5].

Fragility can arise from local non-linear interactions and/or emerge as a collective phenomenon where disorder plays a pivotal role.

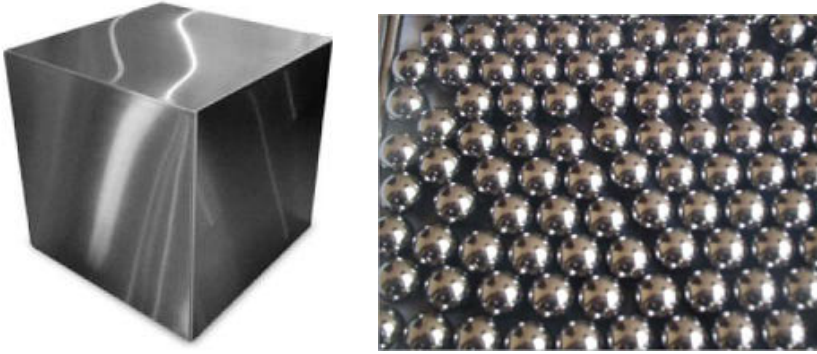


Figure 1.1: A block of steel (left) has a finite speed of sound (6000 m-sec). However, if we cut the block of steel into smaller steel balls and arrange the balls such that they are just touching each other, we uncover a new mechanical state where the sound speed is zero. Energy propagation therefore happens through strongly non-linear waves. This extreme response follows from the non-linear inter-particle interaction and motivates calling this new state as *fragile matter*. Source for figures: *google*.

When two macroscopic objects are brought into contact an elastic deformation δ is generated, as illustrated in Fig. 1.3 [1]. If a ball of radius R is squeezed against a flat wall, it is compressed in the longitudinal direction and expands in the transverse direction. Simple geometric considerations reveal that the radius of the area of contact is approximately $(R\delta)^{\frac{1}{2}}$ (see Fig. 1.3). Therefore in the contact area, the deformation (or strain) γ can be estimated by dividing the longitudinal deformation δ by this radius: $\gamma = \frac{\delta}{(R\delta)^{\frac{1}{2}}} \sim \delta^{\frac{1}{2}}$. According to linear elasticity, for small strains, the stress σ is proportional to the strain γ so that $\sigma \sim \delta^{\frac{1}{2}}$. The corresponding force f is obtained by multiplying the stress by the area of contact, which is proportional to $R\delta$, see the dashed circle in the Figure. The Hertzian law of interaction then follows: $f \sim \delta^{\frac{3}{2}}$, where only the dependence on δ has been kept explicitly. Note that, despite the linear stress-strain relation for the balls material, their interaction force is non-linear.

1.1.2 A prelude to non-linear waves

Consider now a general oscillator of the form described above with a return force given by $f \sim \delta^{\alpha-1}$, where δ is the displace-



Figure 1.2: Real examples of fragile matter: (left) a polymer like network of biological muscle fibres , (center) an amorphous packing of tennis balls and (right) bubbles. Source for figures : *google*.

ment from the equilibrium position and $\alpha \geq 2$. In the absence of any dissipation, the total mechanical energy is conserved and is the sum of kinetic and potential energies:

$$E = \frac{1}{2} \left(\frac{d\delta}{dt} \right)^2 + \delta^\alpha. \quad (1.1)$$

Since E is a constant, we obtain a differential equation for the variable δ ,

$$\left(\frac{d\delta}{dt} \right) = \sqrt{2(E - \delta^\alpha)}, \quad (1.2)$$

solving which, we obtain the time period of oscillation

$$T = \sqrt{2} \int_{-A}^A \frac{d\delta}{A^\alpha - \delta^\alpha}, \quad (1.3)$$

where, we have defined the amplitude of oscillation $A = E^{\frac{1}{\alpha}}$. Defining a new variable $t = \left(\frac{\delta}{A}\right)^\alpha$, the integral can be simplified and expressed in the form a Beta integral

$$T = \frac{2\sqrt{2}}{A^{\frac{\alpha-2}{2}}} \int_0^1 dt t^{\frac{1}{\alpha}-1} (1-t)^{-\frac{1}{2}} \quad (1.4)$$

with the solution

$$T = \frac{2\sqrt{2}}{A^{\frac{\alpha-2}{2}}} \frac{\Gamma\left(\frac{1}{2}\right) \Gamma\left(\frac{1}{\alpha}\right)}{\Gamma\left(\frac{1}{2} + \frac{1}{\alpha}\right)}. \quad (1.5)$$

Notice now, the time period or equivalently, the frequency of oscillation depends upon the amplitude as $\omega \sim A^{\frac{\alpha-2}{2}}$ for $\alpha > 2$ (non-linear oscillator) but is independent of the amplitude for $\alpha = 2$ (harmonic oscillator).

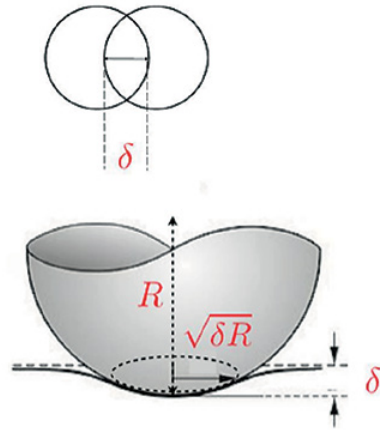


Figure 1.3: Schematic illustration of the origin of non-linear Hertz law of interaction between macroscopically large bodies interacting elastically. The top inset shows two spheres with an overlap δ . In the bottom figure, a sphere is pressing against a flat surface that causes both compression by an amount δ and lateral deformation proportional to $\delta^{1/2}$. source : *Shocks in fragile matter* [1]

This dependence of the frequency of oscillation upon the initial condition or the amplitude of excursion is the crucial difference between a harmonic oscillator with a linear restoring force (simply called a linear oscillator, such as the simple pendulum) and a non-linear oscillator and already alludes to the notion of non-linear waves. Recall, a linear non-dispersive wave typically assumes the form $\psi(x, t) = A G(x - ct)$, where A is the amplitude, $c = \omega/k$ is the constant speed of sound that only depends on the material properties of the medium, k is the wave-number and ψ, G are some general functions. Roughly then, since for a non-linear wave the frequency of oscillation is a function of the amplitude $\omega \equiv \omega(A)$, therefore the speed of propagation also depends upon the amplitude of the wave $c(A)$. In subsequent sections, we will explore specific examples where the dependence of the speed of propagation of the wave on its amplitude will signal the onset of a non-linear regime.

1.1.3 Examples of fragile matter in one dimension

One of the simplest example of fragile matter is a one dimensional chain of spherical macroscopic beads that are just in contact with their two nearest neighbours. Since this is a perfectly

ordered arrangement, we could try to define an effective spring constant from the second derivative of the interaction potential. Consider an interaction potential of the generalized Hertz form, i.e., $V(\delta) \sim \delta^\alpha$, where $\alpha > 2$ is the non-linear exponent. The case $\alpha = \frac{5}{2}$ corresponds to the Hertz law of interaction for linear macroscopic objects as described in section 1.1.1.

Using the second derivative of the potential to define an effective spring constant, we find, $K_{\text{eff}} \sim \delta^{\alpha-2}$. For a vanishingly small initial overlap, $\delta \equiv \delta_0 \rightarrow 0$, and we see that for $\alpha > 2$, $K_{\text{eff}} \rightarrow 0$, while for $\alpha = 2$, it is a finite constant. Since the speed of sound is related to the effective spring constant as $c \sim \sqrt{K_{\text{eff}}}$, we find that in a system that is initially un-stressed $\delta_0 \rightarrow 0$ (and has an interaction potential that has no harmonic part), the speed of sound in the medium is zero. Such a unique mechanical state, characterized by the absence of any sound, is referred to as *sonic vacuum*[6].

Sonic vacuum is the unique mechanical state characterized by the absence of linear sound.

Consequently, mechanical strains that arise for instance, in response to an impulse given to one of the beads, evolve into strongly non-linear waves that propagate as spatially compact excitations known as solitary waves. Note, in this example we have considered a chain of macroscopic beads (or balls) arranged in a line. In principle, this allows the possibility for the beads to break contact with each other. However, the state of sonic vacuum defined above simply stems from the non-linear power law interaction potential and exists even if we replace the beads with point nodes that interact with a non-linear spring, where both spring stretching and compression are accommodated. In subsequent sections, we will explore these examples in more detail.

1.1.4 Examples of fragile matter in two dimensions

As a minimal two dimensional model for fragile matter with disorder, we consider an amorphous packing of frictionless spheres (or disks) that interact repulsively upon overlap (including the possibility of no overlap as in hard disks). The unique control parameter specifying such a system is the packing fraction, ϕ defined as the ratio of the volume occupied by the spheres to the total volume of the sample. Extensive simulations have revealed the existence of a critical packing fraction ϕ_c , at which the packing undergoes a jamming (or rigidity) transition - below ϕ_c , the particles do not overlap and the energy, pressure and number of contacts between particles is zero. Above, ϕ_c

the energy, pressure, number of contacts, shear and bulk moduli are non-zero and scale with the distance from the critical point; $\delta\phi = \phi - \phi_c$.

If the interaction potential between particles that overlap by an amount δ is $V(\delta) \sim \delta^\alpha$, then for $\alpha = 2$ (harmonic interaction), the bulk modulus at the critical point is finite, but it is found that the shear modulus still vanishes. This is an example where fragility arises macroscopically and here, the amorphous arrangement of the spheres plays a crucial role. For $\alpha > 2$ (strongly non-linear interaction), the local spring constant defined as the second derivative of the interaction potential (as in the one dimensional example) vanishes in the limit $\delta_0 \rightarrow 0$. Consequently, at the critical point both the bulk and shear modulus are zero.

Another extensively studied model for fragile systems is a random network of harmonic springs that may be derived from the amorphous packing of spheres by replacing their centres with nodes and by modelling the interaction between neighbouring overlapping spheres with springs that can both, stretch and compress (two sided interaction). Such a random network of springs is often also used as a starting point to model polymer networks and glasses. Here, the control parameter is the average number of nodes each node is connected to, i.e., z . If we start with a loose arrangement of spheres, then at the rigidity transition, ϕ_c , the average connectivity z also jumps discontinuously from zero to a critical value $z_c = 2d$ (also called the isostatic value z_{iso}), that according to Maxwell's criteria marks the onset of mechanical rigidity for a loose particulate system in d dimensions. The mechanical properties above the critical value, are seen to scale with the distance from the critical value as $\delta z = z - z_c$.¹

In these examples, the vanishing of one or both the elastic moduli near the critical point leads to *fragility* that dictates their mechanical properties well beyond the critical point itself. We next explore as a consequence, some of the non-linear excitations that result when we strain at a uniform rate, one of the boundaries of the above model systems.

¹ Once a random network is used as a model under study though, there is no constraint in making $z < z_{\text{iso}}$ (due to springs that connect neighbouring nodes, it is no longer a loose arrangement of particles) and the mechanical properties below the isostatic value constitutes an active area of research.

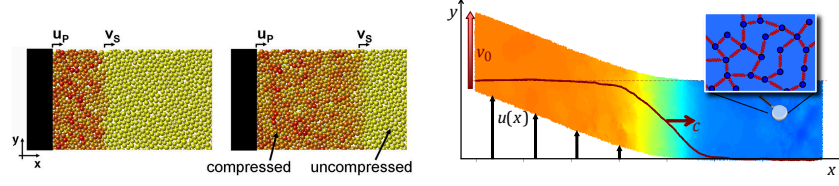


Figure 1.4: Schematic illustration of *left*: compressing an amorphous packing of soft frictionless disks close to the critical packing fraction ϕ_c with a piston moving at a uniform speed u_p . This results in a velocity field (illustrated in red) that corresponds to a uni-axial shock front that propagates along the direction of compression (x -direction) at a speed $v_s \sim u_p^{\frac{\alpha-2}{\alpha}}$. *right*: shearing a random network of harmonic springs close to the isostatic value z_c results in a shear front that propagates transverse to the direction of shearing. The velocity field is defined by averaging the longitudinal speeds of nodes. For high strain rates, the speed of propagation of non-linear shear fronts depends upon the applied strain rate as $v_f \sim \gamma^{1/2}$.

1.1.4.1 Compression shocks in amorphous packings:

Consider first the two dimensional packing of soft frictionless disks close to the critical point ϕ_c (see Fig. (1.4) left panel), where overlapping nearest neighbours interact with a purely non-linear potential of the form $V(\delta) \sim \delta^\alpha$, $\alpha > 2$. As shown in Fig. (1.4) left panel, compressing one end of the packing at a uniform rate u_p results in a compressive shock front (red field) that propagates along the direction of compression at a speed $v_s \sim u_p^{\frac{\alpha-2}{\alpha}}$ (see Fig. (1.5)). Since on either side of the shock front the number of disks is conserved, the relation between the driving speed u_p and the front speed v_s may be obtained from the conservation of number density.

In a frame of reference moving at the front speed v_s , the flux q to the left of the front equals the flux to its right- $q_l = \rho_l(u_p - v_s) = \rho_r(0 - v_s) = q_r$. This is known as the Rankine-Hugoniot condition for the shock speed:

$$v_s = u_p \frac{\rho_l}{\rho_l - \rho_r}. \quad (1.6)$$

Assuming now, that the average overlap between disks in the un-compressed region (right of the front) is δ_0 and in the compressed region (left of the front) is δ_s , the respective number densities in the two regions are $\rho_l = \frac{1}{2R-\delta_s}$ and $\rho_r = \frac{1}{2R-\delta_0}$,

where R is the average radii of the disks. Substituting in Eq. (1.6), we arrive at $v_s = u_p \frac{2R - \delta_0}{\delta_s - \delta_0}$ which for strongly non-linear fronts $\delta_s \gg \delta_0$, yields $v_s \sim \frac{u_p}{\delta_s}$.

Next, we make the working assumption that the particles enveloped within the region of the shock (see Fig. (1.4) red region) satisfy a Virial-like relation, i.e., in steady state, there exists a balance between the disk kinetic energies and the induced potential energy $u_p^2 \sim \delta_s^\alpha$. Then, the average compression induced by the propagating front is $\delta_s \sim u_p^{\frac{2}{\alpha}}$. This non-trivial scaling relation is a consequence of the non-linear local interactions and is verified numerically[26]. Thus, for strongly non-linear shocks, the shock speed is related to the driving rate via

$$v_s \sim \frac{u_p}{\delta_s} = u_p^{\frac{\alpha-2}{\alpha}}. \quad (1.7)$$

As alluded to earlier, this is a defining feature of non-linear waves: the speed of propagation depends upon the amplitude of the wave, unlike for linear sound waves, where the speed of propagation is independent of the amplitude (for instance, if $\alpha = 2$, v_s becomes independent of u_p). As shown in Fig. (1.5) left panel, this scaling relation is in very good agreement with numerical findings (shown for $\alpha = \frac{5}{2}$) and is also confirmed in recent experiments [7].

1.1.4.2 *Densification fronts in hard sphere gas below the critical point:*

In a recent experimental study, it is shown that uni-axially compressing a two dimensional loose assembly of hard binary disks below the jamming critical density ϕ_j , leads to a densification front that travels along the direction of compression, leaving the region enveloped by the front jammed at ϕ_j [8]. This is analogous to the red region shown in Fig. (1.4) left panel, except that for hard disks, the maximum packing fraction saturates at $\phi_j < \phi_c$. Since the number of disks behind and ahead of the front is conserved, the Rankine-Hugoniot condition Eq. (1.6) still holds. However, for hard disks, the region to the left of the front can be compressed to its maximum density ϕ_j and thus the front speed is simply related linearly to the driving speed $v_s = u_p \frac{\phi_j}{\phi_j - \phi_0}$, where $\phi_0 < \phi_j$ is the initial packing fraction. Notice, this relation is also obtained by taking the hard sphere limit of Eq. (1.7) : $v_s \sim \lim_{\alpha \rightarrow \infty} u_p^{\frac{\alpha-2}{\alpha}} = u_p$.

1.1.4.3 Shear fronts in random spring networks:

Next, we consider a random network of nodes connected by harmonic springs in the vicinity of the critical point, with an average connectivity $z > z_c$. Here, fragility manifests in the vanishingly small shear modulus that scales linearly with the distance from the critical point $G \sim \Delta z$. Consequently, as we approach the critical point from above, the transverse speed of sound $c \sim \sqrt{G}$ also drops to zero.

This limited window of linear response near the critical point, manifests in a non-linear constitutive stress-strain relation (in the frequency independent regime) for the shear stress as a function of shear strain applied at the boundary: [2]-

$$\sigma = G\gamma + \kappa\gamma|\gamma|. \quad (1.8)$$

Here, $\sigma \equiv \sigma_{xy}$ is the coarse grained shear stress, γ is the shear strain and κ is the coefficient of the first non-linear term (independent of Δz). Upon comparing the two terms on the right hand side, we find the critical strain $\gamma_c = \frac{G}{\kappa}$, beyond which the elastic response is predominantly non-linear. Note that, as we approach the critical point, $\Delta z \rightarrow 0$, the critical strain $\gamma_c \rightarrow 0$ and thus, an infinitesimally small strain elicits a strongly non-linear response. Since the constitutive random spring network is composed of purely harmonic springs, the strongly non-linear response near the critical point, highlights the macroscopic fragility of these networks, although the origins of non-linearity remain local (see Supplementary Information E).

The dynamics of energy propagation can now be explored by conducting numerical experiments analogous to the ones considered previously for an amorphous packings of frictionless spheres, but now in the transverse direction. Here, it is found that by shearing one edge of the sample at a uniform rate below the critical strain rate γ_c (in dimensionless units, the strain and strain rates coincide), initially gives rise to a transient super-diffusive spreading of the transverse velocity field away from the shearing zone, see Fig. (1.4) right panel. At later times however, this crosses over into a well defined shear front that propagates with the transverse speed of sound $c \propto \sqrt{G}$. Interestingly though, the linear shear fronts are not in a steady state, i.e., their widths continue to increase with time. We understand this behaviour as arising from the increasingly heterogeneous elastic displacement field near the critical point, that makes the random spring networks an over-damped system, despite no microscopic mechanism for dissipation being present. This unique

feature is a direct evidence of how the underlying network disorder manifests in the properties of the shear front, causing their widths to spread diffusively with time [9].

For strain rates $\gamma > \gamma_c$, the constitutive stress-strain relation described by Eq. (1.8) is non-linear and results in supersonic shear fronts. From Eq. (1.8), we identify a *non-linear modulus* $G_{nl} = G + \kappa\gamma$, and consequently a characteristic non-linear speed of propagation that is a function of the applied strain rate:

$$v_f = \sqrt{\frac{G_{nl}}{\rho}} = \sqrt{c^2 + \frac{\kappa\gamma}{\rho}}. \quad (1.9)$$

Notice, for $\gamma \ll \gamma_c$, the front speed approaches the transverse speed of sound c and is independent of the strain rate (driving amplitude). On the other hand, for $\gamma \gg \gamma_c$, the front speed becomes independent of c (and hence Δz), and depends only upon the applied strain as $v_f \propto \gamma^{\frac{1}{2}}$, this we classify as the strongly non-linear regime.

In Fig. (1.5), right panel, we see the analytically predicted speed of propagation Eq. (1.9) (solid lines) compared against numerical findings (symbols) for a range of Δz . For $\gamma < \gamma_c$, the speed of propagation is independent of the applied strain rate and agrees very well with the numerically determined transverse speed of sound. For $\gamma > \gamma_c$, we observe non-linear fronts that propagate at speeds that depends on the applied strain rate and the numerical findings are in very good agreement with the analytical estimate in Eq. (1.9). For $\gamma \gg \gamma_c$, we enter a strongly non-linear regime where the front speed depends quadratically upon the applied strain rate as $v_f \propto \gamma^{\frac{1}{2}}$ while becoming independent of Δz .

The behaviour of shear fronts in the strongly non-linear regime is analogous to the strongly non-linear compressional fronts observed in amorphous packings of soft frictionless disks where for sufficiently large driving speeds, $v_s \sim u_p^{\frac{1}{5}}$ (for $\alpha = \frac{5}{2}$ independent of the packing fraction). Thus, we find that despite the disparate sources of fragility (local versus global), the physics of energy propagation in the form of strongly non-linear waves is one of the defining features of fragile matter near their critical point. Note also, despite the differing exponents that capture the front speed as a function of driving rate, in both cases, the front speeds in the strongly non-linear regime is independent of the underlying microstructure, not being dependent on the distance from the critical point ($\delta\phi$ or δz).

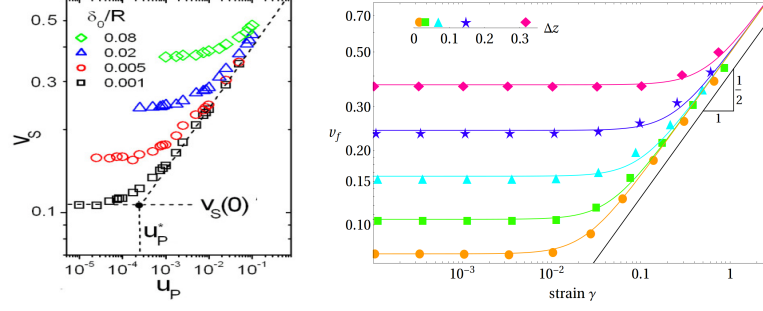


Figure 1.5: The front speed as a function of applied strain rate for *left*: compressional shocks in a jammed amorphous packing of soft frictionless disks for $\alpha = \frac{5}{2}$ in agreement with the relation $v_s \sim u_p^{1/5}$ (dashed line) for high strain rates. The symbols correspond to numerical data of the front speed, obtained for a range of initial packing fractions δ_0 . *right*: shear fronts in random network of harmonic springs shown for a range of coordination numbers Δz . The solid lines correspond to the analytical prediction Eq. (1.9) while symbols correspond to numerical data for the front speed.

1.2 DISORDER AS AN EFFECTIVE VISCOSITY ?

Understanding the nature of disorder in amorphous materials is still an arduous task. In particular, for fragile matter near the critical point, the breakdown of linear elasticity and the resulting non-linear response makes a quantitative analysis difficult. Notwithstanding, disorder has some clear signatures in the dynamical response of these systems, that we could try to explore.

At a simpler, qualitative level, the process of defining uniaxially propagating fronts involves an averaging over the degrees of motion transverse to the direction of propagation. See for instance Fig. (1.4), where for compressional fronts propagating along the horizontal x - direction, an averaging of the particle speeds over the transverse y - direction is necessary. Similarly for the shear fronts, an averaging along the horizontal direction is implied. For amorphous packings, this process thus necessarily involves ignoring a part of the energy that is being supplied at the boundaries. The net result is that this loss of energy effectively acts as a source of dissipation, that we refer to as an effective viscosity. The way this effective viscosity manifests in the properties of the propagating fronts however, differs in details.

The steadily propagating compressional shocks in amorphous packings are a consequence of the interplay between locally non-linear inter-particle interaction potential and the granular nature of the medium, that acts as a source of dispersion. The shock widths are thus a few grain diameters and happen to be, independent of the shock amplitude. As a result, the leakage of energy (or the effective viscosity) into degrees of motion transverse to the direction of propagation of the front, do not effect the shock width but act as a small perturbation that smooths out the shape of the shock profiles, in contrast to the oscillatory profiles observed in more ordered packings [26].²

By contrast, both the linear and non-linear shear fronts observed in random spring networks are a macroscopic phenomenon. The increasingly heterogeneous (non-affine) elastic displacement field close to the isostatic value, spills a large part of the energy into degrees of motion transverse to the ones being excited at the boundaries. For shear fronts, this amounts to a loss of energy into longitudinal excitations and several numerical studies have indicated that this loss diverges with the distance from the critical point $l^* \sim \Delta z^{-1/2}$. Consequently, both in the linear and non-linear regimes, random spring networks are found to be over-damped and the propagating fronts never achieve a steady state. Instead, their widths continue to grow with time. For instance, upon rescaling the temporal diffusive spreading of the linear shear fronts for strain rates $\gamma < \gamma_c$, the front widths are observed to be dictated by the diverging length l^* . Since this effect mimics the effect of viscosity (in setting the width of the shock transition region), disorder emerges as an effective viscosity that diverges as the critical point [9].

The densification fronts observed below the hard disk jamming density ϕ_j are found to be in a steady state and satisfy a Burgers-like non-linear diffusion equation. Like the shear fronts in random spring networks, a diverging length scale $l_j \sim (\phi_j - \phi_0)^{-0.65}$ sets the widths of the propagating fronts that now scales as $\eta = u_p l_j$, where u_p is the driving speed [8]. Physically, the length scale l_j here is found to be the characteristic length scale associated with longitudinal velocity-velocity correlation function.

² It is not the intention to convey here that these observations are obvious. We are only drawing some of these conclusions after having done the numerical experiments.

1.3 THIS THESIS

As part of this thesis, we will try to understand the interplay between the strongly non-linear waves and the underlying disorder, in models of fragile matter that are in the vicinity of the critical point. For instance, to better understand the role of disorder in jammed amorphous packings close to their critical packing fraction, we will study what happens to an impulse that is imparted at one of the edges of such a packing. This is in contrast to the compression experiments discussed previously, where an amorphous packing of soft frictionless disks is compressed at a uniform rate resulting in steadily propagating shock fronts. Rather, the study of impulse propagation will somewhat simplify the analysis and bring to the fore, the role played by disorder as a mechanism that continually takes energy away from the propagating excitation.

As our first step towards this, we will consider a two dimensional hexagonal packing of soft frictionless disks that are just in contact with their nearest neighbours and thereby, constitute a state of sonic vacuum (upon overlap the disks interact with the nonlinear Hertz potential). As the simplest form of disorder, we will consider an isolated impurity that we model as an interface that separates two hexagonal packings composed of disks with different masses so that on one side of the interface all the disks (particles) have a mass m_1 and on the other side all the disks have a mass m_2 . The elastic isotropy of the hexagonal lattice will essentially reduce the study of impulse propagation to a one dimensional problem, whose analytic solitary wave solutions are by now well established. Consequently, by mapping the resulting solitary wave excitation to a quasi-particle with an effective mass, we will be able to (approximately) understand the interaction of the solitary wave with the interface for different choices of mass ratios $A = m_2/m_1$.

Our understanding of the solitary wave behaviour across the interface will equip us with some approximate analytical tools to then study the problem of solitary wave propagation in a hexagonal lattice with particle masses distributed randomly. Subsequently, we will find a good estimate of how increasing the disorder (variance in mass distribution), increases the damping rate of the propagating solitary wave.

For a larger variance in the mass distribution, we will find a new regime of wave propagation and an associated decay rate. We will see that it is no longer possible to identify a propagat-

ing solitary wave except at the very early stages of the evolution of the impulse. Instead, we will find that the initial impulse soon transitions into a triangular shock like propagating front whose amplitude decays as it traverses the medium. This extreme limit of high disorder in particle masses then provides us with a link to the physics of impulse attenuation in amorphous packings where again an initial impulse transitions into a triangular shock front whose amplitude decays with the same power law exponent as in the hexagonal packing.

The attenuation of the impulse then leads to some interesting consequences. As noted, disorder will cause the energy initially localized in an impulse to be distributed throughout the amorphous packing (of finite size). Consequently, in a system with no intrinsic mechanism to dissipate energy, the particles will continue to fluctuate forever. This we imagine as a granular analogue of temperature where the passage of the impulse effectively fluidizes the amorphous packing and where the energy of the impulse plays a role that is analogous to temperature (but not really in thermal equilibrium). As a consequence, the emergent mechanical state will have a finite bulk modulus and a viscosity that we will see is consistent with the description of a one dimensional fluid in equilibrium (recall, we started with an amorphous packing at the critical point where it has vanishingly small bulk and shear modulus).

The emergence of a granular analogue of temperature and a fluctuation induced rigidity then motivates us to study an example of fragile matter that is explicitly coupled to a source of thermal fluctuation. The coupling to the heat bath forces the system to be truly in a state of thermal equilibrium. As the simplest toy model, we will adopt a one dimensional chain of strongly non-linear Hertz springs coupled to a heat bath. We will then study the propagation of an impulse along this chain and find that for small thermal fluctuations, the impulse again evolves into the same solitary wave solution that are the characteristic excitations in a granular chain of beads. By mapping the solitary wave to a quasi-particle, we will find that its dynamics can be described in analogy with that of a Brownian particle.

In the last chapter, we will shift our attention to another model of fragile matter: a two dimensional disordered network of linear springs, where the loss of rigidity (vanishing shear modulus) is a collective phenomenon. By shearing one edge of the sample at a uniform rate we will study the resulting dynamics, finding both a linear and non-linear regime for the propa-

gation of the shear front. In addition, within the linear regime, we will find that at early times, there is no front propagation but only a super-diffusive spreading of the energy away from the shearing edge.

GRANULAR INTERFACES

In order to build up the tools to study the propagation of strongly non-linear solitary waves in a two dimensional amorphous material, we begin here by looking at the interaction of the solitary wave with an isolated impurity modelled as a granular interface formed between two hexagonal lattices comprising particles with different masses. By treating the solitary wave as a quasi-particle with an effective mass, we construct an intuitive (energy and linear momentum conserving) discrete model to predict the amplitudes of the transmitted and reflected solitary waves generated when an incident solitary wave, parallel to the interface, moves from a lighter/-denser to a denser/lighter granular hexagonal lattice ‡.

‡ This chapter builds on the work done in the master's thesis by A. Tichler (2012) . Further research ideas evolved out of discussions with V. F. Nesterenko ,V. Vitelli and L.R. Gomez and are presented in reference [39]. Thanks to L.R. Gomez for simulations and accompanying figures.

GRANULAR INTERFACES

In this chapter, we start with the two dimensional problem of determining the reflection and transmission of a strongly non-linear solitary wave-front incident upon an interface between two hexagonal lattices both in a sonic vacuum (zero sound speed), but with different particle masses specified by the ratio $A = m_2/m_1$. We treat the solitary wave as a quasi-particle with an effective mass and model the interaction with a two-dimensional granular interface, as an elastic collision process conserving energy and linear momentum that is validated by simulations. Here, two distinct scenarios emerge valid approximately for - (a) $A \sim 1$ and (b) $A \ll 1$.

In the case $A \sim 1$, the incident solitary waves evolves into two new solitary waves, a leading one that is transmitted into the lighter medium and a smaller one, that is either reflected or transmitted depending upon the mass ratio being greater or less than 1. This is simply modelled as an elastic disintegration of a solitary wave. In the $A \ll 1$ case, the solitary waves moves from a much denser medium to a lighter medium and it is seen that the last row of "heavy" beads at the interface, absorbs on a "fast" time scale the main part of the energy and linear momentum of the incident solitary wave-front (assumed parallel to the interface) and detaches from the heavy medium while repeatedly colliding with the the lighter medium, see Fig. (2.1) (c). Through this process, the last row decelerates on a "slower" time scale, and generates a train of asymptotically well separated solitary waves in the "lighter" sonic vacuum. Crucial to understanding this phenomenon is the role of contact breaking at the interface and the resulting break-down of the continuum approximation that we model using an elastic collision process between the heavy beads and the solitary wave quasi-particle.

We then apply our understanding from the study of parallel interfaces, to study how a solitary wave that is incident at an angle to the interface, moves from one medium to another. Here, we find that the angles of refraction and reflection of the the leading solitary waves that are generated as a result of the elastic disintegration, are surprisingly well captured by a granular

analogue of Snell's law that holds irrespective of the solitary wave-front amplitude, for small angles of incidence.

2.1 SIMULATIONS

In order to investigate the solitary wave scattering at a two dimensional granular interface, we perform molecular dynamics simulations for a hexagonal packing of 10^4 frictionless spherical grains, using periodic boundary conditions. As shown in Fig. (2.1), an interface is introduced by assigning a mass m_1 to the rows of grains on its left (shown in red) and a mass m_2 to rows on its right (shown in yellow). Both portions of the hexagonal lattice are comprised of grains with zero initial overlap and equal diameters. Two grains of radius R and masses $\{m_i, m_j\}$ at positions $\{\vec{x}_i, \vec{x}_j\}$ interact via a one-sided non-linear repulsive potential following Hertz law [5]

$$V_{ij} = \frac{K_{ij}}{\alpha} \delta_{ij}^{\frac{5}{2}} \quad (2.1)$$

only for positive compressional strains $\delta_{ij} \equiv 2R - |\vec{x}_i - \vec{x}_j| > 0$, otherwise $V_{ij} = 0$, when $\delta_{ij} \leq 0$. Here, the interaction parameter $K_{ij} = \frac{2}{3}RE_{ij}^*$ is expressed in terms of the effective Young's modulus of the two particles, E_{ij}^* , see Ref. [20] for more details. Consequently, due to the non-linear interaction potential and absence of any initial overlap between grains, both the hexagonal lattices are in a state of sonic vacuum. At $t = 0$, we impart to the left-most row a speed u_p and subsequently integrate Newton's equations of motion numerically subject to periodic boundary conditions perpendicularly to the direction of propagation. As seen in Fig. (2.1) (a), we see a well defined solitary wave that propagates along the direction of impact.

2.2 QUASI-PARTICLE MODEL

We take advantage of the isotropic elasticity of the hexagonal lattice to assume that the dynamics of a solitary wave-front parallel to the interface, as in Fig. (2.1), is effectively one dimensional and governed, in the continuum limit, by the non-linear wave equation Eq. (A.10):

$$\xi_{tt} = c^2 \left[\xi^{\frac{3}{2}} + \frac{2R^2}{5} \xi^{\frac{1}{4}} (\xi^{\frac{5}{4}})_{xx} \right]_{xx}, \quad (2.2)$$

where c is a material constant and $\xi(x, t)$ is the strain field $\xi(x, t) = -\partial_x u(x, t)$ expressed in terms of the particle displace-

ment field, $u(x, t)$, along the x direction. The left-hand side of Eq. (2.2) is the standard inertia term, the second term on the right-hand side captures non-linear dispersive effects, while the first arises from the restoring force as in the wave-equation, if one considers that the force is not linear, but it depends on $\xi^{3/2}$ according to Hertz law.

As discussed in the previous chapter, a strongly nonlinear solitary wave solution of Eq. (2.2) can be derived analytically [6] and it has been validated by extensive simulations and experiments mostly on granular chains [15, 6, 23, 24, 17, 33, 26, 27]. Crucially, the total energy $E = \frac{P^2}{2m_{\text{eff}}}$ carried by the solitary wave depends quadratically on its total momentum P , which allows the interpretation of the solitary wave as a quasi-particle with an effective mass $m_{\text{eff}} \approx 1.4m$. We next use this quasi-particle interpretation of the solitary wave to study its interaction with a two dimensional granular interface.

2.3 WEAK DISORDER

If the ratio of bead masses on either side of the interface $A = \frac{m_2}{m_1}$ is nearly equal to 1, an initial solitary wave excitation is seen to split at the interface into two new solitary waves: a leading solitary wave that crosses the interface into the new medium and a smaller solitary wave, that is either reflected back or transmitted depending on the mass ratio being greater or less than one. The quasi-particle notion of the solitary wave provides a simplified model to study the interaction of the solitary wave with the granular interface as an elastic collision process (conserving momentum and energy) resulting in the disintegration of the initial solitary wave into two new solitary waves [17, 39]

$$P_0 = P_1 + P_2, \quad (2.3)$$

$$\frac{P_0^2}{2m_{1,\text{eff}}} = \frac{P_1^2}{2m_{1,\text{eff}}} + \frac{P_2^2}{2m_{2,\text{eff}}} \quad (2.4)$$

where, P_0 is the momentum of the incident solitary wave, P_1 is the momentum of the smaller reflected or transmitted solitary wave and P_2 is the momentum of the leading transmitted solitary wave. Solving, we obtain

$$P_1 = \frac{P_0 (1 - A)}{(1 + A)}, \quad (2.5)$$

where $A \equiv \frac{m_{2,\text{eff}}}{m_{1,\text{eff}}}$ and

$$P_2 = \frac{2P_0}{1+A}. \quad (2.6)$$

The predicted momentum P_1, P_2 are found to be in good agreement with numerical data in both one and two dimensional granular interfaces for $A \sim 1$ [17, 39]. Since this case is well studied and we will make further use of it in a later chapter where the validity of this result will be explicitly used (Chapter 3), we now turn to discussing the more novel observations when the mass ratio $A \ll 1$.

2.4 STRONG DISORDER : $A \ll 1$

As shown in Fig. (2.1)(a), the initial impulse imparted to the left most beads, leads to the generation of a non-linear wave front parallel to the interface that travels towards the right with a speed $V_s \sim u_p^{1/5}$ analogously to solitary waves in granular chains [6]. At t_0 , all the energy and linear momentum P_0 of the incident solitary wave is concentrated in the "heavy" (red) chain of beads and we have an undisturbed chain of "light" (yellow) beads. At later times, shown in Fig. (2.1)(b), when the solitary wave has interacted with the interface, we see a ruptured interface with one of the inter-facial rows of heavy (red) beads "dancing" in contact with the lattice of lighter (yellow) beads, throttling the generation of an oscillatory wave profile in the lighter lattice close to the interface. This oscillatory wave is subsequently disintegrated into a sequence of separate solitary waves, as shown in Fig. (2.1)(c). The separate solitary waves propagate with different speeds (dependent on their amplitude), while a second collision of the "dancing" interfacial row of particles, shown in Fig. (2.1)(d), generates a second delayed solitary-wave train with smaller amplitudes.

The notion of the solitary wave as a quasi-particle again allows us to construct a simple quasi one-dimensional model for the generation of the solitary wave train, illustrated schematically in Fig. (2.2). At t_0 , we assume that a chain of *light* yellow beads is uncompressed and all the energy and linear momentum P_0 , carried by the incident solitary wave, is concentrated in the *heavy* red interfacial particle. At a subsequent time t_1 a single solitary wave is generated in the *light* chain by reducing the energy and linear momentum of the interfacial heavy particle. We apply conservation of energy and linear momen-

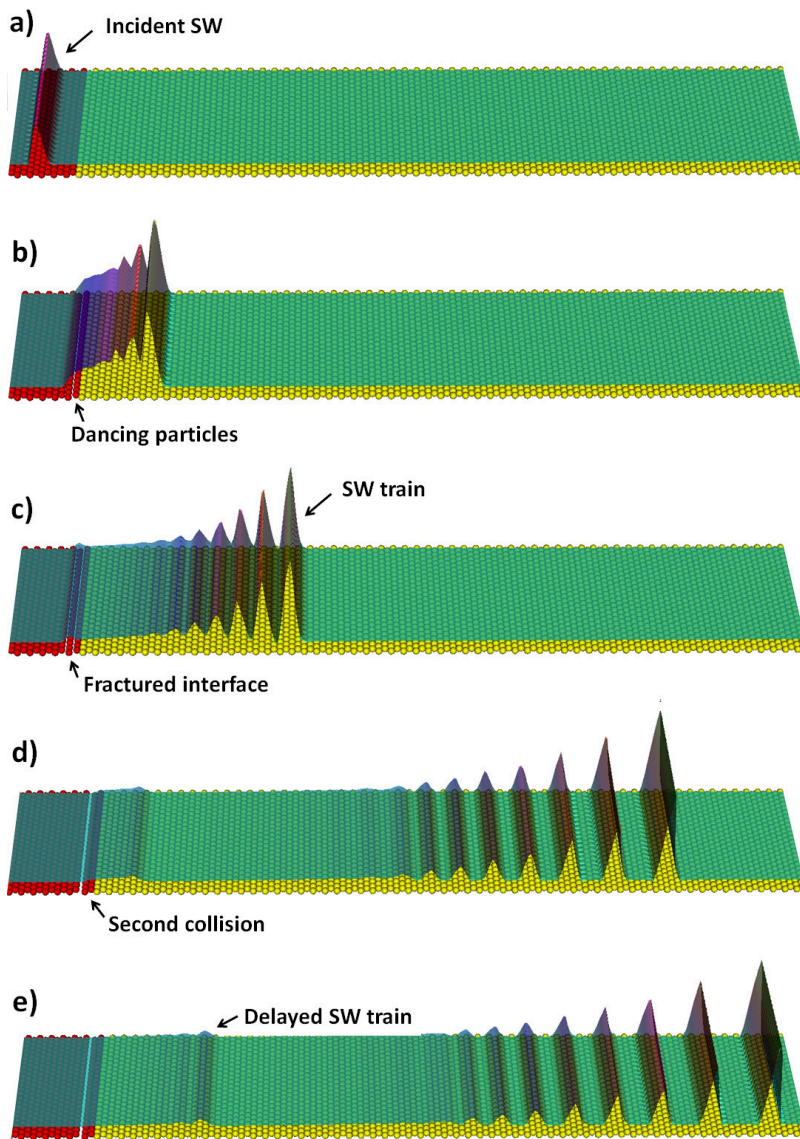


Figure 2.1: Time sequence leading to the generation of a solitary wave train in simulations. The (red) beads on the left of the interface constitute the heavier medium with mass m_1 and the (yellow) beads on the right of the interface constitute the lighter medium with mass m_2 . The mass ratio $\Lambda \equiv \frac{m_2}{m_1} = 0.125$. The velocity field overlayed in green, denotes the instantaneous speeds of the beads.

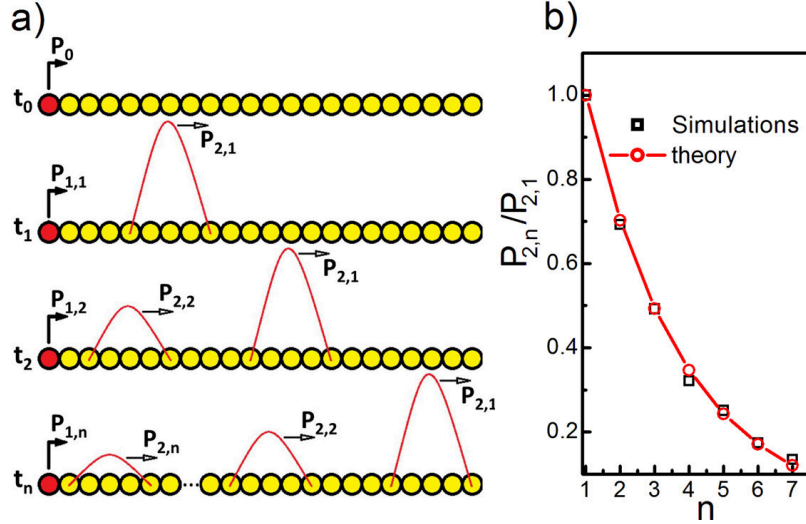


Figure 2.2: (a) Schematic illustration of our model for the formation of a solitary-wave train, side-view. (b) Momentum ratios $\frac{P_{2,n}}{P_{2,1}}$ between the n -th solitary wave and the leading one in the train for $A = \frac{m_2}{m_1} = 0.125$. Red circles are the theoretical predictions while the black squares are the numerical values from the simulations of Fig. (2.1).

tum to the collision process between the “dancing” bead with mass m_1 and the solitary wave, treated as a quasiparticle with mass $m_{2,\text{eff}}$. Note, it is here that the effective mass of the solitary wave becomes crucial to our understanding of the process, unlike the case for $A \sim 1$, where the collision is between two solitary waves with effective masses that are rescaled by the same constant value (≈ 1.4) and thus cancel out. We calculate the momentum of the “dancing” interfacial particle $P_{1,1}$ after the first collision as

$$P_{1,1} = \frac{P_0 (B - 1)}{(B + 1)}, \quad (2.7)$$

where $B \equiv \frac{m_1}{m_{2,\text{eff}}}$. The momentum $P_{2,1}$ carried by the first leading solitary wave at $t = t_1$ is

$$P_{2,1} = \frac{2P_0}{B + 1}. \quad (2.8)$$

At time t_2 another independent single solitary wave is generated in the “light” chain, further reducing the energy and linear momentum of the “dancing” interfacial particle. Upon applying conservation of energy and linear momentum, as before, and assuming that the first solitary wave does not participate

in this process, we find the momentum of the “dancing” particle at $t = t_2$, $P_{1,2}$, and of the second solitary wave, $P_{2,2}$, as

$$P_{1,2} = \frac{P_0 (B - 1)^2}{(B + 1)^2}, P_{2,2} = \frac{2P_0 (B - 1)}{(B + 1)^2}. \quad (2.9)$$

Upon iterating this process n times (assuming that the generation of each solitary wave occurs independently and does not interfere with the previous or subsequent solitary wave), we find that the “heavy” interfacial bead at $t = t_n$ is left with a linear momentum $P_{1,n}$ while the n -th solitary wave carries momentum $P_{2,n}$ given by

$$P_{1,n} = \frac{P_0 (B - 1)^n}{(B + 1)^n}, P_{2,n} = \frac{2P_0 (B - 1)^{n-1}}{(B + 1)^n}. \quad (2.10)$$

Fig. (2.2)(b) illustrates the favorable comparison of $\frac{P_{2,n}}{P_{2,1}} = \left(\frac{B-1}{B+1}\right)^{n-1}$ against numerical data (red circles) for $A = 0.125$. The amplitudes of the delayed secondary sequence of solitary waves generated is neglected in our approximate model.

DISORDERED PACKINGS

In the previous chapter we found that approximating the solitary wave as quasi-particle, provides us with a simple model to study its interaction with an isolated granular interface characterized by mass mismatch. Upon crossing the interface, the solitary wave was seen to disintegrate into approximately two solitary waves when the mass ratio is small. This suggests that if we keep track of the leading transmitted solitary wave as it propagates through a series of well separated interfaces as a model for a medium with mass disorder, we will find the solitary wave amplitude to decrease with distance.

In this chapter, we study numerically and analytically the decay of the solitary wave excitations in such a two dimensional mass disordered and amorphous packings of grains that are just in contact with their nearest neighbours. We find that there is a regime of weak mass disorder, where the solitary wave excitation generated in response to an impulse decays exponentially at early times, with a rate that depends upon the amount of disorder. In the long time limit, the initially well defined solitary wave soon transitions into a triangular shock like profile, whose amplitude decays as a power law with an exponent that is consistent with $\frac{1}{2}$ and independent of the amount of disorder. Additionally, there is a regime of strong disorder where the quasi-particle model is not adequate to model the interaction of the solitary waves with the material inhomogeneities. Rather in this regime, the power law decay is the dominant mechanism of attenuation and we observe this in hexagonal lattices with strong mass disorder (large variance in masses) as well as in jammed amorphous packings close to their critical packing fraction*.

* The research ideas presented in this chapter evolved out of discussions with L. R. Gomez and V. Vitelli and are part of Reference[45]. Thanks to L.R. Gomez for the 2D simulations and accompanying figure 3.3.

AMORPHOUS PACKINGS

We now consider, simple models of a disordered two dimensional packing. As a first step, we begin with a hexagonal lattice of particles that are just in contact with their nearest neighbours, but with particle masses distributed as a normal random variable. We again excite the packing with an impulse imparted to one end of the sample and follow the evolution of the excitation. Here, we find two distinct regimes of attenuation of the initial impulse excitation.

3.1 EXPONENTIAL ATTENUATION : WEAK DISORDER

For weak mass disorder (or a small variance in masses), a well defined solitary like wave is formed in response to an impulse. As the initial solitary wave propagates through the packing, it begins to attenuate and we find the initial stages of this attenuation to be well approximated as an exponential decay (see Fig. (3.3), left panel top inset).

In the last chapter, we used the quasi-particle approximation of the solitary wave to study the disintegration of a solitary wave across a mass interface [17, 39]. Consider again, an interface between two regions of sonic vacuum with grain masses m_1, m_2 respectively. For mass ratios $A = \frac{m_2}{m_1}$ close to 1, a solitary wave initially moving with amplitude P_0 is seen to split into two new solitary waves, with momentum P_1, P_2 that may be obtained using an elastic collision model that conserves the quasi-particle energy and momentum -

$$\begin{aligned} P_0 &= P_1 + P_2, \\ \frac{P_0^2}{m_{1,\text{eff}}} &= \frac{P_1^2}{m_{1,\text{eff}}} + \frac{P_2^2}{m_{2,\text{eff}}} \end{aligned} \quad (3.1a)$$

from where, we obtain

$$P_1 = \left(\frac{1-A}{1+A} \right) P_0, \quad (3.2a)$$

$$P_2 = \left(\frac{2A}{1+A} \right) P_0. \quad (3.2b)$$

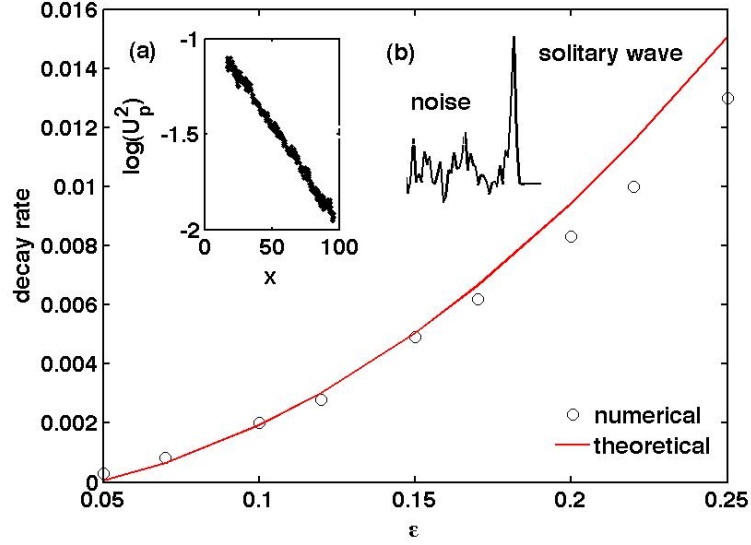


Figure 3.1: (a) The exponential decay of the solitary wave energy U_p^2 as a function of distance x along a one dimensional chain of granular particles with mass disorder modelled as a normal random variable with mean 1 and variance ϵ^2 . (b) The noisy state comprising of a non-linear superposition of several smaller solitary waves left behind by the leading solitary wave as it interacts with the disorder. The main panel compares the exponent in Eq. (3.6) (solid red line) against numerical data (black circles).

Thus, the ratio of transmitted to incident energy is

$$\frac{m_{1,\text{eff}} P_2^2}{m_{2,\text{eff}} P_0^2} \equiv \frac{T_E}{T_0} = \frac{4A}{(1+A)^2}. \quad (3.3)$$

In order to study the propagation of the solitary wave in a medium with weak mass inhomogeneity, consider a chain of beads with the mass ratio of neighbouring beads i, j related via $m_i = A_{i,j} m_j$, where $A_{i,j} = 1 + N_{i,j}(0, \epsilon^2)$. The normal random variable $N_{i,j}(0, \epsilon^2)$ has mean 0 and variance ϵ^2 . Upon appealing to the localized nature of the solitary wave (its width being around 5 bead diameters and also independent of the amplitude of the solitary wave), we treat each bead as an interface and invoke the quasi-particle elastic collision model.

Thus, the energy of the leading solitary wave after the first collision is

$$\begin{aligned} T_1 &= \frac{1 + \epsilon N_1(0, 1)}{(1 + \frac{\epsilon}{2} N_1(0, 1))^2} T_0 \\ &\approx \left[(1 + \epsilon N_1(0, 1)) \left(1 - \epsilon N_1(0, 1) + \frac{3}{4} \epsilon^2 N_1^2(0, 1) \right) \right] T_0 \\ &\approx \left[1 - \frac{1}{4} \epsilon^2 N_1^2(0, 1) \right] T_0, \end{aligned}$$

where, we have retained terms up to order ϵ^2 . Iterating this process n - times, we find that the solitary wave energy after it has propagated n beads diameters is approximately

$$T_n \approx \left[1 - \frac{1}{4} \epsilon^2 N_n^2(0, 1) \right] \cdot \left[1 - \frac{1}{4} \epsilon^2 N_1^2(0, 1) \right] T_0. \quad (3.4)$$

Retaining terms only to order ϵ^2 , we find

$$\begin{aligned} \frac{T_n}{T_0} &\approx 1 - \frac{1}{4} \epsilon^2 \sum_{k=1}^n N_k^2(0, 1), \\ &\approx 1 - \frac{1}{4} \epsilon^2 \chi^2(n), \end{aligned} \quad (3.5)$$

where, $\chi^2(n)$ is the chi function with an expectation value n . Taking the mean, we obtain that the average solitary wave energy after propagating n beads diameters reads

$$\frac{\langle T_n \rangle}{T_0} \approx 1 - \frac{1}{4} n \epsilon^2 \approx e^{-\frac{n}{4} \epsilon^2}. \quad (3.6)$$

As shown in the inset to Fig. (3.3) top inset, this estimate is in very good agreement with numerical observations on an hexagonal packing and for the solitary wave attenuation in weakly-disordered granular chains [34]. Note, as the solitary wave propagates through a disordered lattice, at each subsequent collision with the material inhomogeneity, a smaller excitation in addition to a leading solitary wave is generated. This is the simplest example of how disorder effectively acts as a source of dissipation for the solitary wave, despite no source of microscopic dissipation being present in the lattice. We refer to this regime of attenuation, where the initial stages of exponential decay can be well captured, as the weakly disordered regime. Note, the reason we do not obtain an exact quantitative match in two dimensional packings is because in constructing

our quasi-one dimensional model, we are inevitably ignoring transverse degrees of motion that are necessarily excited. However, the exponential decay is in very good agreement with numerical studies on one dimensional lattices, including the pre-factor $\frac{1}{4}$ for small ϵ , see Fig. (3.1) [34].

3.2 STRONG DISORDER

Our study in the previous chapter on the formation of a solitary wave train across an interface for mass ratios $A \ll 1$, provides an important prelude to the propagation of a solitary wave in a strongly disordered lattice. Consider for instance, a hexagonal lattice with masses distributed normally but with a large variance in the grain masses. Here, numerical observations reveal that an initial solitary wave (still modelled approximately by the Nesterenko solitary wave) soon transitions into a triangular shock like propagating front whose amplitude decays as a power law, while the regime of exponential decay is barely identifiable, see Fig. (3.3) middle inset.

What is the manifestation of multiple scattering by strong heterogeneity around the mechanical state of sonic vacuum ?

As may be anticipated by the formation of the solitary wave train during a collision with a strong heterogeneity, if multiple such closely located regions of strong disorder are present, multiple overlapping solitary waves will be formed. In turn, the solitary wave train will not have the occasion to separate into isolated solitary waves, since that requires a homogeneous region for them to separate asymptotically. As a result, we are only able to follow the evolution of an envelope of many such solitary waves and the spatial extent of the envelope continues to grow as more and more wave trains are generated. Eventually we find that such an envelope spans several hundred grain diameters and acquires a nearly triangular shock like profile.

The power law decay in this regime, reveals a striking similarity for the long time decay in a hexagonal packing with weak mass disorder, the dominant regime of decay in a hexagonal packing with strong mass disorder (large ϵ) as well as the dominant mechanism of decay in amorphous jammed packings, see Fig. (3.3). In all these cases, a triangular shock like profile emerges, whose leading edge decays as a power law x^{-r} with an exponent approximately $r \approx 0.5$ (solid red line). This exponent seems to be independent of the amount of disorder.

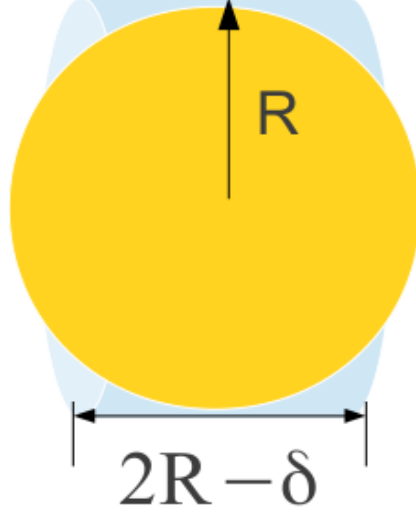


Figure 3.2: The cylindrical box around a sphere for an effective medium description. Here, R is the radius of the sphere and cylinder, while δ is the average compression.

In a recent study, the existence of very long wavelength triangular shock like fronts in a one dimensional chain of granular particles is established [43]. Here, we find that due to material inhomogeneities, an initial excitation in two dimensional disordered packings, naturally evolve into long wavelength shock solutions and their power law decay may be captured approximately (ignoring transverse excitations) from the conservation of energy [31, 43]. Below, we review the derivation of the long wavelength waves and then provide an intuitive argument for its power law decay in a disordered packing.

3.3 LONG WAVELENGTH WAVES

Here, we review the long wavelength waves that are derived for a coarse grained variable representing an averaged compressional field [43]. We first define a mass density averaged over a cylindrical segment containing a single sphere (see Fig. (3.2)):

$$\rho = \frac{m}{\pi R^2 (2R - \delta)} \quad (3.7)$$

$$\approx \frac{m}{2\pi R^3} \left(1 + \frac{\delta}{2R}\right), \quad (3.8)$$

or $\rho = \rho_0 + \rho'$, where $\rho_0 = \frac{m}{2\pi R^3}$ and $\rho' = \rho_0 \frac{\delta}{2R}$. Here, δ is the average or coarse grained compression. Defining a coarse

grained pressure p as the contact force between spheres divided by the cross-sectional area πR^2 (see Fig. (3.2)) of the chain, we find

$$p = \frac{\sqrt{2}}{3} \frac{E}{1-\nu^2} \frac{R^{1/2}}{\pi R^2} \delta^{3/2} \approx A \rho'^{3/2}, \quad (3.9)$$

where $A = \frac{4E}{3\pi\rho_0^2}(1-\nu^2)$, see Eq. (A.1) for the prefactors. If we define v as the velocity field, the equations for mass and momentum continuity (Euler equations) are

$$\rho'_t = -(\rho v)_x, \quad (3.10)$$

$$(\rho v)_t = -(\rho v^2)_x - p_x. \quad (3.11)$$

Differentiating Eq. (3.10) once with respect to time (t), we obtain

$$\rho'_{tt} = -[(\rho v)_x]_t = -[(\rho v)_t]_x, \quad (3.12)$$

and substituting Eq. (3.11) for the last expression in the square brackets above, we find

$$\rho'_{tt} = (p + \rho v^2)_{xx} \approx A (\rho'^{3/2})_{xx} + O(\rho'^{5/2}). \quad (3.13)$$

where, the $O(\rho'^{5/2})$ corresponds to the leading term from $\rho v^2 = \rho_0 v^2$. Recall the discussion from the introductory chapter, where for compressional shocks, the particle speeds and average compression follow a Virial like relation $v^2 \sim \delta^{5/2}$ (see discussion following Eq. (1.6)). Consequently, if we assume the validity of this relation, then the particle speed scales as $v^2 \sim \rho'^{5/2}$ and is thus a higher order correction, that we ignore in Eq. (3.13). Shortly we will see that this relation is consistent with the form of the solution we obtain.

A subset of solution for Eq. (3.13) moving along the positive x - direction is (as can be verified by substituting into Eq. (3.13))

$$\rho'_t = \frac{4}{5} \sqrt{\frac{3A}{2}} (\rho'^{5/4})_x = -(\rho v)_x. \quad (3.14)$$

Now, if we compare the two terms on the right (to leading order), we find $\rho'^{5/4} \sim \rho_0 v$ and therefore, $v \sim \frac{\rho'^{5/4}}{\rho_0}$, consistent with our assumption in ignoring the term ρv^2 in Eq. (3.13).

Casting in terms of the compressional field, δ this reads

$$\delta_t = -\frac{4}{5} \sqrt{6KR^2} (\delta^{5/4})_x. \quad (3.15)$$

This equation represents a coarse grained compressional field propagating along the positive x direction. Note here, the similarity with the better know inviscid Burger's equation, where the non-linear exponent is 2 instead of $\frac{5}{4}$.

3.4 SIMILARITY SOLUTION

As discussed previously in our studies, the triangular shock like fronts evolve from an initial impulse excitation irrespective of the amount of disorder. However, since our medium is in a state of sonic vacuum (no sound waves) where the only known excitations are the Nesterenko solitary waves, any other initial excitation is likely to eventually decay into a train of (possibly overlapping) solitary waves. Indeed, the long wavelength solutions first studied for one dimensional granular lattices evolve from an initially Gaussian profile.

Consequently, our investigations suggest that any initial excitation will in the long time limit evolve into a triangular shock front. This is especially true for two dimensional disordered and amorphous packings, where the disorder will ensure the attenuation of any initial solitary like wave, irrespective of the amount of disorder.

Moreover, since the dynamical response we are trying to describe is still far from any equilibrium condition, we try to look for similarity solutions to Eq. (3.15), that are often characteristic of travelling wave solutions in the regime of *intermediate asymptotics* (independent of initial condition and still far from equilibrium).

The propagating solutions we have considered elsewhere in the thesis, for instance, the steadily propagating solitary wave solutions, are also a form of similarity solution, except that they are simple translations of each other (here, the name similarity draws from similar figures in geometry that are proportional to each other but not necessarily exactly equal). Like the propagating solutions, these help reduce a partial differential equation into an ordinary differential equation. Here, the basic idea is to look for solutions of the form $f(x, t) = t^m f(\eta)$ where $\eta = x t^n$ and m, n are chosen to reduce the partial differential equation into an ordinary differential equation (in our example, x, t are taken to be space and time variables respectively, but this is not necessary).

To motivate this idea, we first start with the better known heat equation $u_t = u_{xx}$ and look for its similarity solutions by substituting $u = t^m f(\eta)$. This results in

$$m t^{m-1} f + n t^{m+n-1} x f' = t^{m+2n} f'', \quad (3.16)$$

where, primes denote derivative with respect to $\eta = xt^n$. A choice of $m = 0, n = -\frac{1}{2}$ leads to $\eta = \frac{x}{t^2}$ and reduces the heat equation to

$$-\frac{1}{2}\eta f' = f'', \quad (3.17)$$

which is an ordinary differential equation with a solution $f \sim \exp(-\eta^2) = \exp(-\frac{x^2}{t})$. Thus, we obtain the characteristic Gaussian heat kernel.

We now apply this to the non-linear equation $\delta_t + \delta^{\frac{1}{4}}\delta_x = 0$ (omitting the constant in Eq. (3.15)). Substituting $\delta = t^m f(\eta)$ leads to

$$mt^{m-1}f + nt^{m+n-1}\eta f' + t^{\frac{m}{4}+m+n}f'f^{\frac{1}{4}} = 0. \quad (3.18)$$

Now, a choice $m = 0, n = -1$ reduces this to an ordinary differential equation

$$-\eta f' + f^{\frac{1}{4}}f' = 0, \quad (3.19)$$

with solutions are $f = \text{constant}$ or $f \sim \eta^4 \sim (\frac{x}{t})^4$. This is the similarity solution describing the long wavelength shock like compressional field.

In order to connect this solution to the velocity field that we probe during simulations, we next re-cast this solution in the form of a propagating velocity field. Upon integrating once with respect to x (to obtain the displacement field from the compressional strain) and differentiating once with respect to t , we obtain the corresponding solution for the particle velocity field $\phi(x, t) \sim (\frac{x}{t})^5$.

If we ignore the energy that goes into exciting the transverse degrees of motion (as discussed for compression shocks in Chapter 1, this is a reasonable working approximation for non-linear waves arising from strongly non-linear local interactions), the energy of the beads enclosed within the shock envelope is approximately conserved (in the longitudinal direction). Therefore,

$$E \sim \int_0^{x_f} dx \phi^2(x, t) \sim \frac{x_f^{11}}{t_f^{10}} = \text{constant}, \quad (3.20)$$

where x_f is the position of the shock front at a time t_f , see Fig. (3.3). Consequently, $t_f \sim x_f^{\frac{11}{10}}$. Thus, at the location of the shock front, the jump in the velocity field should scale as

$$\phi(x_f, t_f) \sim \frac{x_f^5}{x_f^{\frac{11}{2}}} \sim x_f^{-\frac{1}{2}}, \quad (3.21)$$

which indicates that the amplitude of front will decay as a power law with an exponent of $\frac{1}{2}$. As shown in Fig. (3.3), solid red lines, we do find this estimate to be in good agreement with the numerically determined exponent $r \approx 0.5$ for the decay of the shock front.

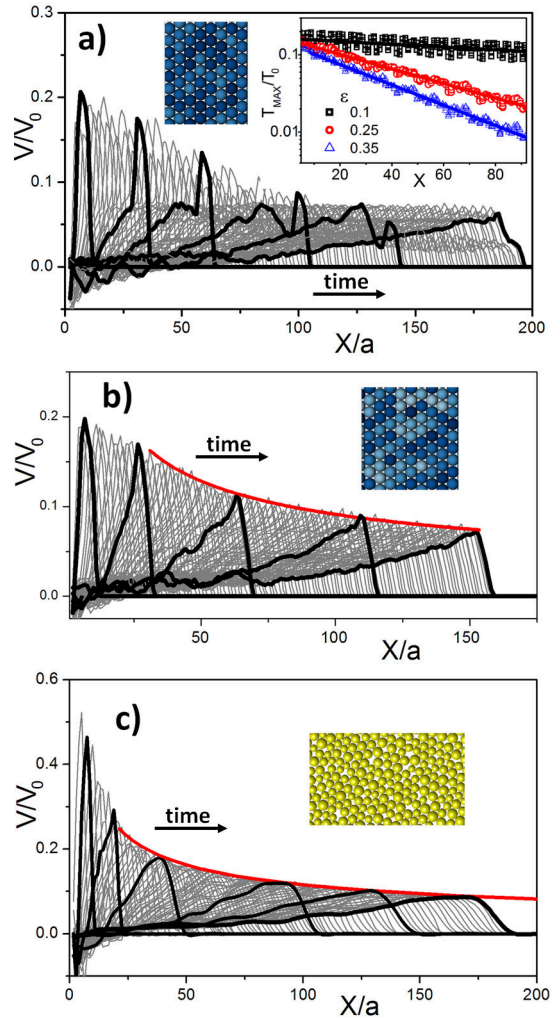


Figure 3.3: (a): The time evolution in response to an impulse in a hexagonal packing with weak mass disorder ϵ . An impulse response generates a solitary wave excitation that decays exponentially at early times. In the long time limit, a shock like triangular profile emerges whose leading edge decays as a power law with an exponent $\chi^{-0.5}$. (b) The time evolution in response to an impulse in a hexagonal packing with strong mass disorder ϵ . An impulse response generates a solitary wave excitation but the regime of exponential attenuation is barely identifiable. Instead, a shock like triangular profile soon emerges whose leading edge again decays as a power law with an exponent $\chi^{-0.5}$ (solid red line). (c) The time evolution in response to an impulse in a jammed amorphous packing prepared at a pressure of $P \sim 10^{-6}$ and an average overlap between grains $\delta_0 \sim 10^{-4}$. An impulse response still generates a solitary wave excitation but like (b), a shock like triangular profile soon emerges whose leading edge decays as a power law with an exponent $\chi^{-0.5}$ (solid red line).

FLUCTUATIONS AND EMERGENT HYDRODYNAMICS

Up till now, we have seen that for amorphous packings of soft frictionless disks close to their critical packing fraction, an initial impulse excitation evolves into a solitary like wave, that is progressively attenuated by disorder. For a finite size packing, what happens to the energy that was initially localized in the form of the solitary wave at very long times?

In this chapter, we demonstrate that the particle fluctuations generated by the solitary-wave decay, can be viewed as a granular analogue of temperature, that fundamentally alters the state of the packing. The presence of fluctuations leads to two emergent macroscopic properties absent in the unperturbed granular packing: a finite pressure that scales with the injected energy (akin to a granular temperature) and a wavenumber dependent viscosity that is consistent with the observations in one dimensional fluids*.

* The research ideas presented in this chapter evolved out of discussions with V. Vitelli and L. R. Gomez and are part of Reference [45]. Thanks to L.R. Gomez for Fig 4.1.

FLUCTUATIONS AND EMERGENT PROPERTIES

The simple model that we have used to understand the regime of exponential decay of the solitary wave amplitude (for weak disorder) suggests that at each subsequent collision with an inhomogeneity, the solitary wave splits approximately into two solitary waves- a leading pulse (the main degree of freedom that is damped exponentially as a result) and a smaller solitary wave, that is either reflected or transmitted depending upon the mass ratio *. Therefore, once we allow sufficient time for the leading solitary wave to disintegrate completely such that a leading pulse is no longer distinguishable from the background, we expect to reach a state comprised of several smaller solitary waves with different energies, see Fig. (4.1)(bottom). The solitary waves in turn interact with each other in-elastically, (as a consequence of the Nesterenko equation of motion being non-integrable [6]) and thus their interaction may be thought of as inherently dissipative. However, in addition to these processes that seek to distribute the energy initially concentrated in a single solitary wave excitation into multiple smaller solitary waves, the structural disorder in two dimensional amorphous packings also spills a part of the energy into transverse degrees of motion. Through a series of such intrinsic dissipative mechanisms, we eventually reach a fluctuating equilibrium-like state that spans the entire finite-sized packings under-investigation.

4.1 VIRIAL RELATION

As a check to demonstrate the emergence of an equilibrium like state, we compute the distribution of energies between the kinetic and potential degrees of freedom - the Virial relation. We first recall the Virial relation for a general (non) linear oscillator.

Consider a one dimensional oscillator whose Hamiltonian is

$$H = \frac{p^2}{(2m)} + q^\alpha, \quad (4.1)$$

* Here, we are sidestepping the question pertaining to the identity of the transmitted solitary wave, i.e., whether it is a new solitary wave with a smaller amplitude or the old one that has been attenuated

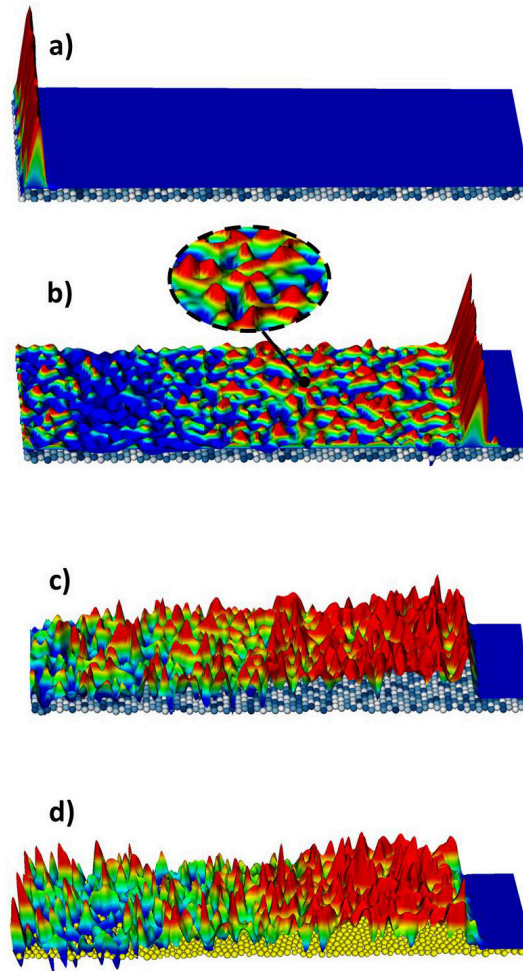


Figure 4.1: (a) A schematic illustration of how a hexagonal packing at zero pressure (with vanishing longitudinal and transverse sound speeds) and weak mass disorder, responds to an impact at one of its ends, by generating a solitary wave excitation. (b) As the solitary wave propagates and interacts with the weak mass inhomogeneity, its amplitude decays. The decay at early times is nearly exponential and the process of energy loss is such, that it excites several smaller solitary waves. Over the long run, a noisy state (velocity fluctuations) spanning the size of the packing emerges (zoomed region). (c) The initial solitary wave is now no longer identifiable in a hexagonal packing with strong mass disorder. Instead we observe a triangular shock like profile that is defined as an envelope over the smaller excitations. In this regime, the decay of the leading edge follows a power law. Eventually, no leading propagating edge is visible. (d) Similar to the strongly disordered hexagonal packing, no initial solitary wave is seen in a jammed amorphous packing. Instead, an impulse excitation soon evolves into the universal triangular shock-like profile. These plots, show the particle velocity field where the front amplitudes and positions have been rescaled for better illustration.

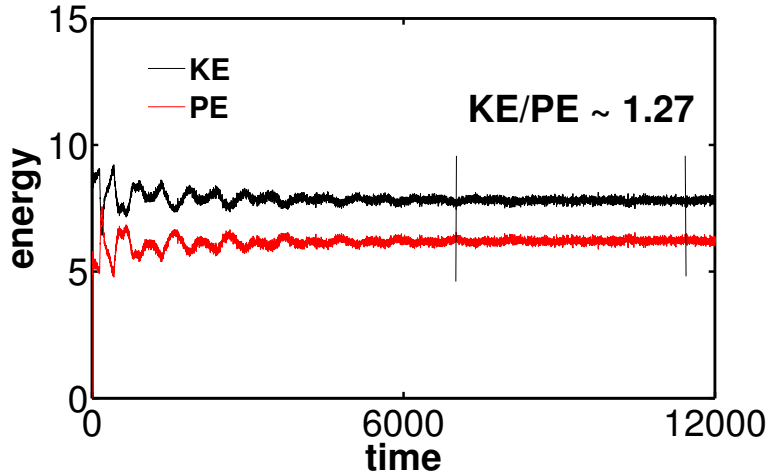


Figure 4.2: The virial relation in the quasi-equilibrium state showing the ratio between kinetic energy (KE) and potential energy (PE) to be approximately $KE/PE \approx 1.27$.

where, p, q are the generalized momentum and position coordinates. The equipartition theorem states that under suitable assumptions of thermal equilibrium, the following is satisfied:

$$\left\langle x_n \frac{\partial H}{\partial x_n} \right\rangle = k_B T \quad (4.2)$$

where $x_n = p, q$ is a generalized coordinate. Thus, $\frac{p^2}{m} = k_B T$ and $\alpha q^\alpha = k_B T$. Therefore, the kinetic energy is $KE = \frac{p^2}{(2m)} = \frac{k_B T}{2}$ and the potential energy is $PE = q^\alpha = \frac{k_B T}{\alpha}$ with their ratio being $KE/PE = \frac{\alpha}{2}$.

For the harmonic oscillator, $\alpha = 2$ and thus, we recover the usual equipartition of energy between quadratic degrees of freedom. However, for a non-linear oscillator, say of the Hertz form considered previously, the corresponding ratio is $\frac{5}{4}$. In other words, on an average the kinetic energy is greater than the potential energy for $\alpha > 2$. Intuitively, for $\alpha > 2$ and small displacements from equilibrium, the non-linear return force is weaker (or the potential is said to be softer) than for the corresponding harmonic oscillator. Thus, such a particle is “free” more of the time, and consequently, has a higher kinetic energy.

In Fig. (4.2), we verify this relation in the asymptotic state that an amorphous packing reaches, once we allow sufficient time for the initial impulse excitation to no longer be identifiable. We find that in this state, the ratio of kinetic and potential energies, does indeed approach the Virial limit. Recall, all model

systems we have considered so far, represent macroscopic objects in contact and a-priori, temperature is not a relevant variable. However, the agitations induced by the decaying solitary wave cause the packing of frictionless disks to acquire a state, that mimics an equilibrium like state, where the initial solitary wave energy plays the role of temperature (although not truly in thermal equilibrium).

4.2 HYDRODYNAMICAL MODES

In order to rationalize the physics behind this fluctuating state that at first appears to be just noise (see Fig. (4.1), bottom panels), we assume the existence of small wave-number k and small frequency ω , longitudinal (l) and transverse (t) hydrodynamical modes and obtain their power spectral densities, as follows.

In order to obtain hydrodynamical modes from the velocity field of fluctuating particles, we use the statistical mechanical definition of particle current density, defined as

$$\mathbf{j}(\mathbf{r}, t) = \frac{1}{\sqrt{N}} \sum_{i=1}^N \mathbf{v}_i(t) \delta(\mathbf{r} - \mathbf{r}_i(t)), \quad (4.3)$$

where, N is the number of particles and bold-face variables correspond to two dimensional Cartesian coordinates. The Fourier transform of the Cartesian component α , is given by

$$j_\alpha(\mathbf{k}, t) = \frac{1}{\sqrt{N}} \sum_{i=1}^N v_{i\alpha}(t) e^{i\mathbf{k} \cdot \mathbf{r}_i(t)}. \quad (4.4)$$

Assuming now, that the hydrodynamical collective modes propagate along the x -direction (assumed isotropy of the amorphous packing), i.e., $\mathbf{k} = (k, 0)$, we let $\alpha = x$ or y , which allows us to define the corresponding longitudinal or transverse current density auto-correlation functions as

$$C_{l,t}(k, t) = \langle j_{l,t}^*(\mathbf{k}, 0) j_{l,t}(\mathbf{k}, t) \rangle, \quad (4.5)$$

where the angular brackets denote ensemble averaging over the initial time. The longitudinal/transverse spectral densities are then obtained as the Fourier transform of the respective current density auto-correlation functions as,

$$P_{l,t}(k, \omega) = \int_{-\infty}^{\infty} dt e^{i\omega t} C_{l,t}(k, t). \quad (4.6)$$

The Fourier transforms defined in Eq. (4.6) are evaluated using Fast Fourier transform from simulation data.

Within the linearized hydrodynamical description, the longitudinal power spectral density is of the form (see Supplementary Information C for a detailed derivation)

$$P_l \propto \frac{\omega^2 \eta k^2}{[\omega^2 - \omega_0^2]^2 + (\omega \eta k^2)^2}, \quad (4.7)$$

while the transverse power spectral density is of the form

$$P_t \propto \frac{\eta k^2}{\omega^2 + (\eta k^2)^2}. \quad (4.8)$$

Here, η is the coefficient of viscosity in the Navier-Stokes equation and $\omega_0 = ck$ is the linear longitudinal dispersion curve, where c is the speed of sound. Thus, the longitudinal modes (or current fluctuations) propagate at the speed of sound (obtained from the linear dispersion relation) and are damped by viscous effects, manifest in the half-width at half-maximum of the power spectral density that scales as h.w. $\sim \eta k^2$. On the other hand, the transverse modes are non-propagating, but instead, are damped exponentially in time, at a rate equal to ηk^2 , which is also its half-width at half-maximum. This coincides with our intuitive understanding, that fluids have a finite bulk modulus (longitudinal sound speed), but no shear modulus.

Shown in Fig. (4.3), right panel (b), are the longitudinal (red squares) and transverse (red circles) dispersion curves that are obtained numerically by projecting the respective power spectral densities (Fig. (4.3) right panel (a)) into the $k - \omega$ plane. For comparison are shown, the corresponding longitudinal (black squares) and transverse (black circles) dispersion curves for a highly compressed jammed packing far from the critical density, prepared at a pressure of $P \sim 10^{-1}$. Since the total potential energy of a jammed packing is related to its pressure via $E \sim P^{5/3}$, the numerical data shown for the emergent state, corresponds to an impact speed $U_p \approx 2.0$ in order to generate a solitary wave in the weakly compressed packings ($P \sim 10^{-6}$) with an energy E_{SW} that is comparable to the energy of the highly compressed packing E_{PC} to facilitate a more meaningful comparison between the two states.

As seen in Fig. (4.3) right panel (b), highly compressed jammed packings behave as ordinary solids with a finite bulk and shear modulus and this translates into a finite sound speed manifest in the linear regime of the longitudinal (black squares)

and shear (black circles) dispersion curves. In contrast, exciting a jammed packing prepared at a vanishingly small pressures (that a-priori has nearly zero longitudinal and shear sound speeds), leads to a linear dispersion regime for the longitudinal modes, but no such regime is obtained for the transverse modes. The slope of the linear regime in the longitudinal dispersion curves, corresponds to the speed of long wavelength hydrodynamical sound modes. Defining the sound speed c as the second derivative of the induced potential energy; E_{SW} ; leads to the relation, $c \sim E_{SW}^{\frac{1}{2}}$ [38], closely matching the numerical data in Inset to Fig. (4.3) right panel (b), red squares. Thus, the speed of the long wavelength hydrodynamical sound modes scales with the energy of the initial solitary wave E_{SW} injected into the system [45].

This is analogous to the scaling relation for pre-compressed jammed packings at a finite packing fraction δ_0 , where the sound speed is found to scale as $c \sim E_{PC}^{\frac{1}{2}}$, with E_{PC} being the potential energy due to the finite pre-compression δ_0 . Thus, in so far as longitudinal sound modes are concerned, a rigidity induced by statically compressing a marginally compressed packing is analogous to the rigidity induced by exciting a marginally compressed packing with a finite energy wave. Note therefore, one can easily replace the source of energy by a heat bath and thereby obtain a thermally induced rigidity upon making the substitution $E \rightarrow k_B T$. However, unlike a state that is truly in thermal equilibrium, an external perturbation over the fluctuating state created by the disintegration of a solitary wave, will further raise its energy due to the absence of a fluctuation-dissipation mechanism. The emergent state is thus at best described as a quasi-equilibrium state.

In contrast to the longitudinal modes, the transverse modes obtained by energizing a marginally compressed packing do not show a well defined linear regime, see Fig. (4.3) right panel (b), red circles. This is in stark contrast from a statically compressed jammed packing where a linear transverse dispersion regime (owing to the finite shear modulus) with a slope that scales with the amount of pre-compression (and does not depend upon the solitary wave energy injected) as $c \sim E_{PC}^{\frac{1}{2}}$ is expected (Fig. (4.3) right panel (b), black circles). Thus, the shear modes excited by injecting energy into a packing near its critical point are purely diffusive and the medium does not develop a finite shear modulus. There is therefore a profound dif-

Fluidization of the jammed packing endows it with a finite bulk modulus.

ference between the resultant states obtained by (a) statically compressing a granular packing near its critical point versus (b) injecting energy either in the form of an excitation or thermally. In the former case, one obtains a solid-like medium with finite bulk and shear moduli, while in the latter, we fluidize the medium. This means that, even after the non-linear wave excitations (characteristic of the jamming point) are strongly attenuated, one cannot describe the system purely in terms of the normal modes of a (linear elastic) solid because the system has *de facto* become a fluid. This is one of the key conclusions of this work and it heralds the signature property of packings at the jamming threshold: they are fragile. See also Chapter 6, where we find that the initial response (below a length scale) of a fragile network of harmonic springs is independent of the details of the network connectivity and does not contain any propagating modes.

In Fig. (4.3) right panel (c), we show how the half width (inverse lifetime τ) of the longitudinal hydrodynamical modes depends anomalously upon the wavenumber as $\tau^{-1} \sim k^{1.6}$. For purely hydrodynamical modes obeying the Navier-Stokes equation, the half width scales with the wave number as $hw \sim \eta k^2$, where η is the shear viscosity, see Eq. (4.7). However, extensive numerical and analytical studies have shown that in one dimension the time correlation functions (whose long time integrals by definition correspond to macroscopic transport properties such as diffusivity and shear viscosity) do not decay exponentially but display long time tails, decaying as power laws instead [40, 41, 42].

This phenomenon indicates the breakdown in low dimensions of the standard mean field approximation embedded in the Navier-Stokes equation – the strength of fluctuations is too strong for simple coarse-grained theories to hold. Note, the Navier-Stokes equation is conventionally expressed without any fluctuating noise term. For three and two dimensional equilibrium fluids, noise produces a small correction to the dynamics of large scale and long time time properties ($k \rightarrow 0, \omega \rightarrow 0$), the same is not true in one dimension [46, 47]. In addition, as we review below, the non-linear term that we dropped while linearizing the equations of motion (see Supplementary Information C) is no longer justified for the description of an equilibrium fluid in one dimension. (Although the packings are two-dimensional, their emergent hydrodynamic description is effectively one-dimensional because of the longitudinal binning

inherent in our description of the packing. This for instance ignores the effect of particles diffusing in the transverse directions.)

For simplicity, we consider the one dimensional Burger's equation stirred with a random force as a model for a one dimensional fluid-

$$\frac{\partial v}{\partial t} + v \frac{\partial v}{\partial x} = \nu \frac{\partial^2 v}{\partial x^2} - \lambda \frac{\partial \eta}{\partial x}, \quad (4.9)$$

where ν is the fluid viscosity, ν is the kinematic viscosity and $\lambda \frac{\partial \eta}{\partial x}$ is the random stirring force such that in d -dimension ($d=1$ here):

$$\langle \eta(x, t) \rangle = 0 \quad (4.10)$$

$$\langle \eta(x, t) \eta(x', t') \rangle = 2D \delta^d(x - x') \delta(t - t'). \quad (4.11)$$

The Burger's equation (without random stirring) is obtained from the Navier-Stokes equation by ignoring the compressibility (pressure gradient term). As discussed earlier, the finite compressibility leads to propagating modes in the dispersion relation and the width of the power spectral density is measured in a frame that is moving at the speed of sound. Thus, the propagating modes only shifts the peak and do not effect the scaling properties of the width [47]. (Note, the Navier-Stokes equation is obtained from Newtons equations of motion written for a fluid particle. We can consider the Navier-Stokes with a noise term as the equivalent of a Langevin equation phenomenologically written for a fluid particle that is perturbed by thermal fluctuations.)

We can re-write this equation in terms of the potential function $v = -\lambda \frac{\partial \phi}{\partial x}$ to arrive at the Kardar-Parisi-Zhang (kpz) equation [48]:

$$\frac{\partial \phi}{\partial t} = \nu \frac{\partial^2 \phi}{\partial x^2} + \frac{\lambda}{2} \left(\frac{\partial \phi}{\partial x} \right)^2 + \eta. \quad (4.12)$$

Now consider rescaling the variables: $x \rightarrow bx'$, $t \rightarrow b^z t'$ and $\phi \rightarrow b^\xi \phi'$. In terms of the primed variables, Eq. (4.12) becomes [48]

$$\frac{\partial \phi}{\partial t} = b^{z-2} \nu \frac{\partial^2 \phi}{\partial x^2} + b^{\xi+z-2} \frac{\lambda}{2} \left(\frac{\partial \phi}{\partial x} \right)^2 + \eta', \quad (4.13)$$

where, $\eta' = b^{z-\xi} \eta(bx', b^z t')$ and therefore

$$\langle \eta'(x, t) \eta'(x', t') \rangle = 2D b^{z-d-2\xi} \delta^d(x - x') \delta(t - t'). \quad (4.14)$$

Therefore, the transport coefficients in the primed coordinates are $\nu' \rightarrow b^{z-2}\nu, \lambda' \rightarrow b^{\xi+z-2}\lambda$ and $D' \rightarrow b^{z-2\xi-d}D$.

Suppose, we now ignore the non-linear coefficient, that is $\lambda = 0$. Then, the transport coefficients are scale invariant for $z = 2$ and $\xi = \frac{(2-d)}{2}$. For this choice of exponents, we find the combination $\frac{x}{t^{\frac{1}{2}}}$ is invariant, as expected for ordinary diffusion.

However, around this point, λ scales as $b^{\frac{2-d}{2}}$. For $d < 2$, this is a relevant parameter and it is no longer possible to ignore the non-linear term. Thus, it is necessary for us to include both a fluctuating term and the non-linear term while describing equilibrium properties of a one dimensional fluid ($d=2$ is the critical dimension for fluids). By carrying out this analysis with the non-linear term and enforcing the invariance of λ under scale transformations (due to Galilean invariance of the Navier-Stokes equation) and of $D/\nu \sim k_B T$ (that scales as the equilibrium temperature of the fluid), we find the relevant exponents are $z = \frac{3}{2}, \xi = \frac{1}{2}$ [48, 47]. (Note, in this description the fluid itself is assumed not to be near a phase transition.)

With $z = \frac{3}{2}$, we therefore find the invariant combination to be $\frac{x}{t^{\frac{2}{3}}}$. The behaviour thus corresponds to a super-diffusive spreading of information, i.e.,

$$x^2 \sim t^{\frac{4}{3}}. \quad (4.15)$$

In order to see how super-diffusion effects the scaling of half-width with wave-number, we first define a time dependent diffusivity, i.e.,

$$x^2 \sim t^{\frac{4}{3}} = D(t)t \quad (4.16)$$

,where $D(t) \sim t^{\frac{1}{3}}$. The time correlation function associated with this diffusivity then scales as

$$C(t) \sim t^{\frac{1}{3}-1} = t^{-\frac{2}{3}} \quad (4.17)$$

since, $D \sim \int C(t)dt$. The Fourier transform of the time correlation function therefore scales as

$$C(\omega) \sim \omega^{-\frac{1}{3}} \quad (4.18)$$

For small wavenumbers near the linear regime of the dispersion curves $\omega \sim k$ and therefore, $C(k) \sim k^{-\frac{1}{3}}$. Since a transport

coefficient is associated with the low frequency limit of the correlation function in frequency space, i.e.,

$$D \sim \lim_{k \rightarrow 0} \int C(t) e^{-ikt} dt \quad (4.19)$$

$$\sim \lim_{k \rightarrow 0} C(k), \quad (4.20)$$

we find that the wave-number dependent diffusivity should scale as $D(k) \sim k^{-\frac{1}{3}}$. Consequently for small wave-numbers, the half-width scales as $hw \sim D(k)k^2 = k^{-\frac{1}{3}}k^2 = k^{\frac{5}{3}}$. This is close to the value we observe in simulations.

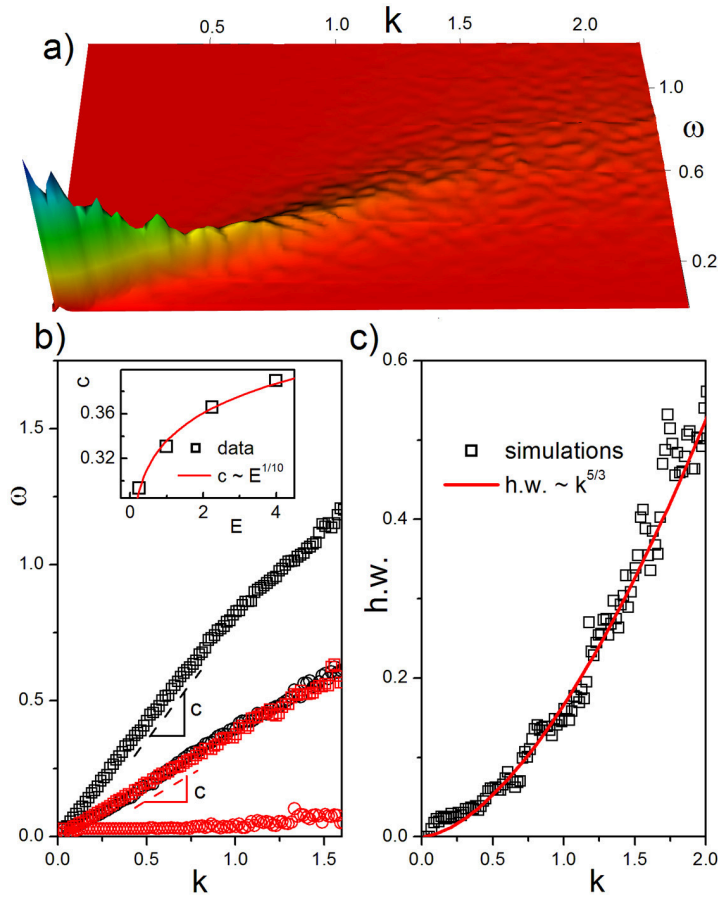


Figure 4.3: (a) The power spectral density for longitudinal modes that emerge in marginally compressed amorphous packings ($P \sim 10^{-6}$) by the complete disintegration of an initial solitary wave excitation. (b) The red squares shows the numerical data for the longitudinal dispersion curves. The slope of the linear regime scales with the energy of the solitary wave as $c \sim E^{1/10}$ for Hertzian interaction, that we identify with long wavelength longitudinal hydrodynamical modes. In contrast, the red circles shows the numerically obtained data for the transverse dispersion curve where no linear regime is seen. The shear mode is therefore non-propagating. For comparison, shown are linear dispersion curves for longitudinal (black squares) and transverse (black circles) obtained for highly compressed jammed packings, prepared at a pressure $P \sim 10^{-1}$. (c) The half-width obtained numerically from the longitudinal modes as a function of wavenumber on a linear scale and compared against the analytical estimates $h.w. \sim k^{5/3}$ (solid red line).

THERMAL FLUCTUATIONS

We found in the last chapter, that the attenuation of a solitary wave eventually leads to the emergence of an equilibrium like state, where particle fluctuations mimic thermal fluctuations. However, the system is not truly in a state of equilibrium, since there is no mechanism (such as an explicit coupling to a heat bath), to dampen external perturbations.

In this chapter, we therefore take a slight departure from our theme on the study of solitary wave propagation in disordered two dimensional packings and turn to the study of a strongly non-linear one dimensional chain of oscillators that is initially in the state of sonic vacuum, that we then couple to a heat bath. Like the granular analogue of temperature, thermal fluctuations induce an entropic rigidity. We then explore the propagation of a strongly non-linear solitary wave in this background of thermal fluctuations and environmental drag, and find an effective Langevin equation to describe the propagation of the solitary wave quasi-particle. This gives us the mean damping rate and thermal diffusion of the solitary wave quasi-particle that we compare against numerical results from a Langevin dynamic simulation. In addition, we find that a one dimensional chain composed of two sided non-linear springs, also supports an expansion solitary wave, as companion to the compressive solitary waves observed for macroscopic particles [†].

[†] The research ideas presented in this chapter evolved out of discussions with A.M. Turner and V. Vitelli and are part of Reference [62].

SOLITARY WAVE IN FLUCTUATING BACKGROUND

In linear elastic solids, phonons are the basic mechanical excitations responsible for energy propagation. By contrast, as discussed in the previous chapters, an aggregate of macroscopic grains just in contact with their nearest neighbours constitute a novel elastic material where solitary waves or shocks replace phonons as the basic excitations [32, 49, 26]. The origin of these strongly non-linear waves can be traced to the fact that, unlike the case of harmonic springs, the repulsive force between two grains in contact does not depend linearly on the relative compression. So far, little effort has been directed to determine the fate of these strongly non-linear excitations in a background of thermal fluctuations because temperature is clearly not a parameter relevant to the elastic response of macroscopic grains.

However, as we saw in chapter 4, an impulse excitation attenuates as it propagates through a two dimensional amorphous packing and interacts with the inhomogeneities. In turn, the aggregate of grains get effectively thermalized by the energy that leaks away from the solitary wave and the final state of the packing changes to a fluid-like state, suggesting the notion of a granular analogue of temperature. Unlike a system truly in thermal equilibrium, this new state is at best categorized as a quasi-equilibrium state since an analogous fluctuation-dissipation mechanism to maintain the state of equilibrium is so far not known to exist.

Notwithstanding, granular aggregates at zero pressure are just one example of a broader class of materials that can be prepared in a unique mechanical state called *sonic vacuum* [32]. Grafted colloidal particles [50] and ultra-cold atoms in optical lattices [51] are microscopic systems that allow for tunable non-linear interactions, while being naturally coupled to a source of fluctuation (thermal or quantum). Much like the granular analogue of temperature, these fluctuations restore rigidity and generate long wavelength phonon modes [52, 38]. However, the physics of very high amplitude strain propagation is still predominantly non-linear and resembles the state of sonic vacuum perturbed by background fluctuations. This extreme regime is

particularly relevant for energy transport in some biological systems, where transport occurs through localized non-linear excitations with energy significantly higher than the thermal energy [55, 56].

Moreover, systems such as polymer networks and colloidal glasses undergoing an unjamming transition are also characterized by vanishing elastic moduli as the coordination number or packing fraction are lowered towards the critical point [57]. The effect of thermal fluctuations on the *non-linear* response of materials undergoing an unjamming transition is relatively unexplored, despite they are obvious examples of a sonic vacuum state at zero temperature [53, 58, 59]. Note, that in the case of jamming the linear elastic moduli can be lowered towards zero even if the microscopic interactions are harmonic, simply because there are not enough forces to prevent floppy motions.

In this chapter, we now focus on strongly non-linear mechanical waves propagating in a background of small thermal fluctuations, a non-equilibrium problem that lies outside the realm of perturbation theory. The starting point of conventional perturbation methods is a linear elastic solid, possibly at finite temperature, perturbed by small anharmonic terms. By contrast, we adopt as a starting point the fully non-linear state of sonic vacuum whose elementary excitations are long-lived solitary waves [60]. Subsequently we *switch on* temperature as a small perturbation that creates a background of thermal fluctuations.

As a minimal model that is analytically tractable, we study impulse propagation in a one dimensional lattice of non-linear springs with a tune-able power law interaction. In addition to the compressive solitary waves seen in a lattice of macroscopic grains with one-sided repulsive interaction, we find an accompanying anti-solitary wave solution for the lattice of non-linear springs with two sided interactions. By coupling the lattice to a heat bath, we then study the effects of the thermal fluctuations on the leading solitary wave generated in response to an impulse of energy much higher than the background thermal energy. Our approach in a nutshell is to treat the solitary wave as a quasi-particle and derive an effective Langevin equation that describes its stochastic dynamics. We corroborate our analytical predictions for the damping rate and thermal diffusion of the solitary waves with Langevin dynamic simulations.

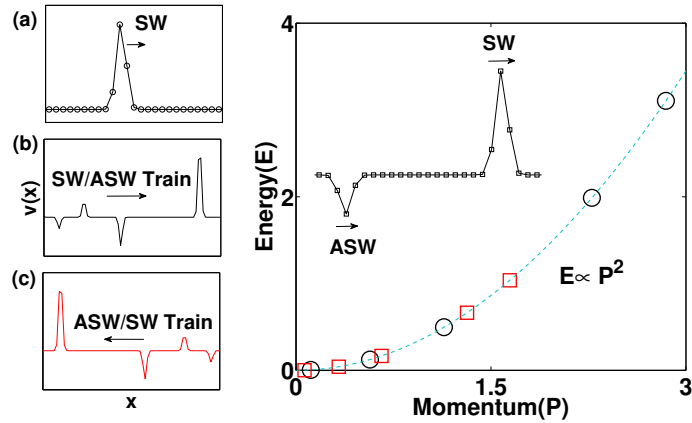


Figure 5.1: *left:*(a) Velocity profile of the compressive solitary wave (SW) generated in an athermal chain of beads with one sided interaction. (b-c) Velocity profiles showing the formation of a train of SW-ASW pair for two-sided non-linear springs. A single particle is initially given an impulse to the right, generating a train led by a SW moving in the direction of the impulse (b), while simultaneously generating a symmetric train led by an ASW moving in the opposite direction. *right:* The energy momentum relation for the leading SW/ASW in the three cases shown in the left panel following the energy (E) momentum (P) relation $E = \frac{P^2}{2m_{\text{eff}}}$. *inset:* Zoom in of the leading SW-ASW pair from left panel (b).

5.1 THE ANTI-SOLITON

In Fig. (5.1), we demonstrate that the compressional solitary wave (SW) excitation discovered by Nesterenko in a chain of non-cohesive beads is also seen in a lattice of springs with two sided interactions. However, unlike the case of a one sided potential, each compressive SW generated in response to an impulse is accompanied by a corresponding expansion solitary wave (formed by local stretching of springs) of the same magnitude but moving in the opposite direction. This anti solitary wave (ASW) is not sustained by beads interacting with purely repulsive potentials – the beads would merely loose contact.

The anti-soliton is not sustained by beads interacting with purely repulsive potentials.

In Fig. (5.1) left panel, we show the SW/ASW excitations for (a)beads , (b-c) particles connected by springs. In Fig. (5.1), right panel, we plot the energy-momentum relation for the leading SW/ASW demonstrating that SW excitations in a lattice of repulsive beads have the same effective mass m_{eff} (as defined in Eq. (A.17)) as a SW and ASW in two-sided springs. As shown in Fig. (5.1) left panel (b-c), the leading SW-ASW generated in response to an impulse imparted to one of the particles towards the right (direction of arrow) is followed by a train of alternating SW-ASW's excitations, of progressively smaller magnitudes. The smaller SW/ASW's are generated as the particle initially imparted the impulse, recoils with its left-over energy. This process is repeated several times, leading to the generation of the train of smaller excitations. Since the speed of propagation depends upon the amplitude, the SW and ASW that start propagating together initially (appearing bounded), eventually separate and become clearly distinguishable.

5.2 LANGEVIN EQUATION

The classical energy-momentum relation (see Fig. (5.1) right panel) satisfied by the SW motivates the interpretation of the solitary wave as a quasi-particle [32, 17]. For small perturbations, the SW can still be treated as a quasi-particle provided the effects of the perturbations accrue gradually such that the SW retains its functional form. We now apply this adiabatic approximation to derive an effective Langevin equation for the SW quasi-particle when the lattice of springs is coupled to a

heat bath. Recall first, the Langevin equation for a particle of mass m undergoing Brownian motion in one dimension is

$$\begin{aligned}\frac{dx}{dt} &= v, \\ \frac{dE}{dt} &= -2\frac{\zeta}{m}K + \sqrt{\frac{2\beta^2K}{dt}}N(0,1).\end{aligned}\quad (5.1)$$

Here, E, K are the total and kinetic energies respectively, ζ, β are the dissipation and diffusion coefficients related via the fluctuation dissipation theorem $\beta^2 = 2\zeta k_B T/m^2$, where k_B is the Boltzmann constant. $N(0, 1)$ is a normal random variable with mean 0 and variance 1, and encapsulates the effects of random fluctuations during the time interval $t, t + dt$. For a free particle of unit mass moving with speed v , $E = K = \frac{1}{2}v^2$ and upon substituting in Eq. (5.1), we recover the Langevin's equation conventionally expressed as the rate of change of momentum of the particle [63].

We now derive an equation analogous to Eq. (5.1) for the compressive solitary wave quasi-particle. Identifying the lattice spacing a as a characteristic length scale and $\omega = \sqrt{\frac{k}{m}}a^{\alpha-2}$ as an inverse time scale, the equation of motion for the compressive displacement field $\phi(x, t)$ in dimensionless units reads-

$$\phi_{tt} - \frac{1}{12}\phi_{xxtt} + [(-\phi_x)^{\alpha-1}]_x = 0 \quad (5.2)$$

where subscripts denote partial derivatives with respect to space x and time t . Eq. (5.2) is a simplified form of the Nesterenko equation [32, 49], see Supplementary Information I for details. The first two terms express the rate of change of momentum while the third term represents the force. Although the solitary wave solution to Eq. (5.2) is not exact (lacking compact support), Eq. (5.2) provides a good approximation while being analytically more tractable especially since we are interested in keeping the non-linear exponent α general [49, 26]. Note that the equation for the ASW (stretching) is obtained by modifying the third term $+ [(-\phi_x)^{\alpha-1}]_x \rightarrow -[(\phi_x)^{\alpha-1}]_x$ in Eq. (5.2). Upon substituting $\delta = -\phi_x$ for the compressive SW or $\delta = \phi_x$ for the expansive ASW, we find the same functional forms for the solitary wave solutions in both cases.

In analogy with the Langevin equation for a particle, we model the coupling to a heat bath as the sum of two contributions-

an external drag and a random fluctuating force, phenomenologically introduced into the equation of motion as :

$$\phi_{tt} - \frac{1}{12}\phi_{xxtt} + [(-\phi_x)^{\alpha-1}]_x = -\gamma \left(\phi_t - \frac{1}{12}\phi_{txx} \right) + \sqrt{\frac{2\gamma}{\alpha\Gamma dt}} \left(\eta(x, t; t + dt) - \frac{1}{\sqrt{12}}\eta_x(x, t; t + dt) \right) \quad (5.3)$$

where $\gamma = \frac{\zeta}{m\omega}$ is the dimensionless drag coefficient that couples to the momentum $\Pi = \left(\phi_t - \frac{1}{12}\phi_{txx} \right)$. It is useful to define a coupling constant $\Gamma = \frac{k\alpha^\alpha}{\alpha k_B T}$ as the ratio of potential to thermal energy in terms of which, the dimensionless diffusion coefficient is $D = \frac{2\gamma}{\alpha\Gamma}$. The last (noise) term on the right of Eq. (5.3) in conjunction with Π , satisfies the fluctuation dissipation theorem [64] (see Supplementary Information 3 for details). Here, $\eta(x, t; t + dt)$ is a Gaussian random noise during the time interval $t, t + dt$ with the moments $\langle \eta(x, t; t + dt) \rangle = 0$ and $\langle \eta(x, t; t + dt)\eta(x', t'; t' + dt') \rangle = \delta(x - x')\delta(t - t')$ respectively, where angular brackets denotes ensemble averaging.

To study the propagation of the SW in a background of thermal fluctuations, we now make a working assumption based on the quasi-particle approximation to the SW: whenever the energy of the SW, $E \equiv E_{SW} \gg k_B T$, the SW functional form is unaltered and only its amplitude $A(t)$ becomes time-dependent. The amplitude $A(t)$ is the collective variable for the SW quasi-particle and other properties of the solitary wave, such as its energy and momentum may be determined from it. Note, the width of the SW is independent of its amplitude and therefore we do not consider its time dependence [64].

From Eq. (5.2), the conserved energy is

$$E = \int dx \left(\frac{1}{2}\phi_t^2 + \frac{1}{24}\phi_{tx}^2 + \frac{1}{\alpha}(-\phi_x)^\alpha \right), \quad (5.4)$$

and the energy of the SW may be obtained by integrating Eq. (B.27) over the width of the SW of order W . (This avoids including the energy of small SW that separate from the main wave). Using Eq. (5.2), the rate of change of energy is,

$$\frac{dE}{dt} = \sqrt{\frac{D}{dt}} \int dx \eta(x, t; t + dt) \left(\phi_t + \frac{1}{\sqrt{12}}\phi_{tx} \right) - 2\gamma K \quad (5.5)$$

where, K is the kinetic part of the energy,

$$K = \int dx \left(\frac{1}{2}\phi_t^2 + \frac{1}{24}\phi_{tx}^2 \right). \quad (5.6)$$

The last term on the right of Eq. (5.5) describes the possible mechanisms of decay of the SW by “friction” from the heat bath (γ). The first term is the fluctuating part of the energy. In the following, we make the assumption (verified numerically) that the coupling to the heat bath is more important and therefore, any drag induced by background phonons is negligible.

Solving for the SW solution from Eq. (5.2), we find $\phi_t = A\psi$, where

$$\psi(x, t) = \text{sech}^{\frac{2}{\alpha-2}} \left(\frac{x - V_s t}{W} \right) \quad (5.7)$$

is the functional form of the SW with amplitude A , speed $V_s = A^{\frac{\alpha-2}{\alpha}}$ and width $W = \frac{1}{\sqrt{3(\alpha-2)}}$ in units of the lattice spacing, see Supplementary Information I for details. The SW energy, kinetic energy, and momentum may now be expressed in terms of the collective variable A :

$$E = A^2 \int dx \psi^2(x, t) = A^2 I_E \quad (5.8)$$

and from the the virial theorem,

$$K = \frac{\alpha}{\alpha+2} E = \frac{\alpha}{\alpha+2} I_E A^2 \quad (5.9)$$

Additionally, the solitary wave momentum is

$$P = A \int dx \psi(x, t) = A I_P. \quad (5.10)$$

Here,

$$I_E = \int dx \text{sech}^{\frac{4}{\alpha-2}} \left(\frac{x}{W} \right) \quad (5.11)$$

$$I_P = \int dx \text{sech}^{\frac{2}{\alpha-2}} \left(\frac{x}{W} \right), \quad (5.12)$$

are constants obtained by integrating over all space [49].

Substituting for E and K in terms of A , we cast Eq. (5.5) into the form of an ordinary Langevin equation (with additive noise) for the collective variable $A(t)$,

$$\frac{dA}{dt} = \sqrt{\frac{2\gamma}{\alpha \Gamma I_E^2 A(t)^2 dt}} \int dx \eta(x, t; t + dt) \left(\phi_t + \frac{1}{\sqrt{12}} \phi_{tx} \right) - \frac{\alpha\gamma}{\alpha+2} A \quad (5.13)$$

where, $\phi \equiv \phi(x, t)$. Eq. (5.13) is the central result of our work whose analytical predictions we derive and test numerically in

the next sections. The first term can be written as $\frac{1}{\sqrt{dt}}\eta_A(t, t + dt)$, where η_A is a white noise signal; that is, its correlations are given by $\langle \eta_A(t)\eta_A(t') \rangle = \frac{2\gamma}{(\alpha+2)I_E\Gamma}\delta(t-t')$. Using the fact that the correlations of $\eta(x, t)$ are described by delta-functions, the correlations of $\eta_A(t)$ can be related to the kinetic energy Eq. (5.6), which can be replaced by $\frac{\alpha}{\alpha+2}I_E A(t)^2$.

5.3 MEAN AND VARIANCE

Taking the expectation value (ensemble average) of Eq. (5.13), we find

$$\frac{d\langle A \rangle}{dt} = -\frac{\alpha\gamma}{\alpha+2}\langle A \rangle, \quad (5.14)$$

where, owing to the noise term $\eta(x, t; t + dt)$ (which acts between times $t; t + dt$) and $\phi_t(x, t)$ (which is a solution at time t) being statistically independent, the expectation value $\langle \eta(x, t; t + dt)\phi_t(x, t) \rangle = 0$. Consequently, the solitary wave amplitude decays as

$$\langle A \rangle = A_0 e^{-\frac{\alpha\gamma}{\alpha+2}t} \quad (5.15)$$

where, A_0 is the initial solitary wave amplitude. Note, the effective damping rate $\gamma' = -\frac{\alpha\gamma}{\alpha+2}$ is independent of inverse temperature Γ but rescales with the exponent of the non-linear potential α .

Similarly, we solve for the variance of the solitary wave amplitude or equivalently, the variance in the square root of energy. Re-defining, $D = \frac{\gamma}{2\alpha\Gamma I_E^2}$, we solve for the variance in the solitary wave amplitude by first evaluating the differential $d[A^2] = A^2(t + dt) - A^2(t)$, by substituting $A(t + dt) = A(1 - \frac{\alpha\gamma}{\alpha+2}dt) + \sqrt{Ddt} \int dx \eta(x, t; t + dt) \left(\psi + \frac{1}{\sqrt{12}}\psi_x \right)$ from Eq. 5.14 and retaining terms to order $0(\sqrt{dt})$ [65, 66],

$$\begin{aligned} d[A^2] &= -\frac{2\alpha\gamma}{\alpha+2}A^2dt + 2A\sqrt{Ddt} \int dx \eta(x, t; t + dt)\xi(x, t) + \\ &\quad + Ddt \iint dx dx' \eta(x, t; t + dt)\eta(x', t; t + dt)\xi(x, t)\xi(x', t) \end{aligned} \quad (5.16)$$

where for brevity, we have defined $\xi(x, t) = \left(\psi(x, t) + \frac{1}{\sqrt{12}}\psi_x(x, t) \right)$. Taking the expectation value, the second term on the right van-

ishes (as discussed for the mean) and using the property that the noise term is delta-correlated in space, we obtain

$$\frac{d[\langle A^2 \rangle]}{dt} = -\frac{2\alpha\gamma}{\alpha+2}\langle A^2 \rangle + D \int dx \left(\psi + \frac{1}{\sqrt{12}}\psi_x \right)^2.$$

The last term when expanded gives twice the solitary wave kinetic energy $2K$, see Eq. (5.6), plus an integral $\frac{2}{\sqrt{12}} \int dx \psi \psi_x$, that vanishes by symmetry for the SW solution. Moreover, the SW kinetic energy is related to its total energy via the virial relation $K = \frac{\alpha}{\alpha+2}E$. Hence, we obtain the ordinary differential equation correct to order dt -

$$\frac{d\langle A^2 \rangle}{dt} = -\frac{2\alpha\gamma}{\alpha+2}\langle A^2 \rangle + 2DI_E \frac{\alpha}{\alpha+2}. \quad (5.17)$$

Solving, the differential equation subject to the initial condition $\langle A^2 \rangle_{t=0} = A_0^2$ and substituting for D , we obtain,

$$\langle A^2 \rangle = A_0^2 e^{-\frac{2\alpha\gamma}{\alpha+2}t} + \frac{1}{2I_E \alpha \Gamma} \left(1 - e^{-\frac{2\alpha\gamma}{\alpha+2}t} \right). \quad (5.18)$$

Using Eq. (5.15), this may be expressed as

$$\text{var}(A) = \langle A^2 \rangle - \langle A \rangle^2 = \frac{1}{2I_E \alpha \Gamma} \left(1 - e^{-\frac{2\alpha\gamma}{\alpha+2}t} \right). \quad (5.19)$$

Using the relation in Eq. (5.8), we rewrite the above equation as

$$\text{var}(\sqrt{E}) = \frac{1}{2\alpha\Gamma} \left(1 - e^{-\frac{2\alpha\gamma}{\alpha+2}t} \right). \quad (5.20)$$

The coefficient $\frac{1}{2\alpha\Gamma}$ reduces to $\frac{k_B T}{2}$ when the energy is not measured in units of ka^α , so this expression is analogous to the velocity variance of a Brownian particle. Note, for large α , the SW is effectively one particle wide and thus Eq. (5.20) captures the correct thermal equilibration of the particle energy with the heat bath. However, for the dynamics of the SW, Eq. (5.20) is only useful as long as the SW is identifiable against the background thermal energy, that is $E_{SW} \gg \Gamma^{-1}$.

The SW quasi-particle in a background of thermal fluctuations behaves as Brownian particle.

5.4 SIMULATIONS

We consider a one dimensional chain consisting of $N = 1024$ particles each having a mass m placed regularly on a lattice with spacing a (spring rest length) interacting pair-wise with a

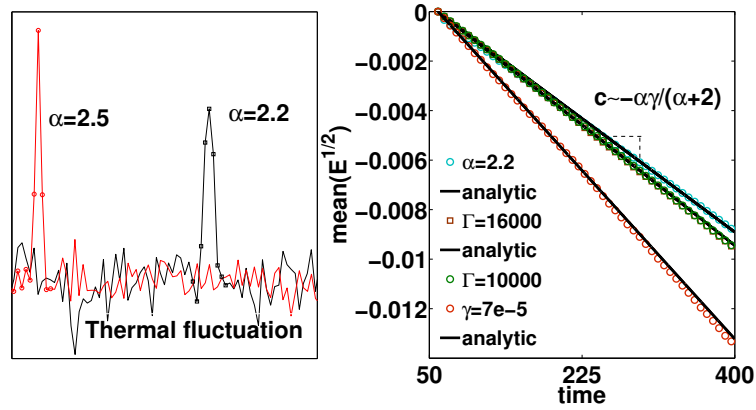


Figure 5.2: *left*: Snapshot of two solitary waves in a background of thermal fluctuations for $\alpha = 2.5$ (red) and $\alpha = 2.2$ (black). *right*: the attenuation of the solitary wave as a function of time for various values of γ, Γ , and α . When not indicated, $\alpha = 2.5, \Gamma = 10^4$ and $\gamma = 5 \times 10^{-5}$. The data for these values is shown with green circles; the other data corresponds to changing one parameter, $\alpha = 2.2$ (black circles), $\Gamma = 1.6 \times 10^4$, (brown squares) and $\gamma = 7 \times 10^{-5}$ (red circles) compared with the analytic expression in Eq. (5.15) represented by solid lines. The initial $E_{SW} = 0.5$.

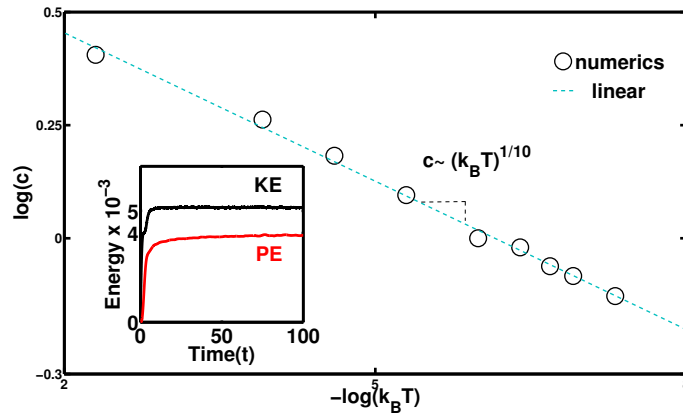


Figure 5.3: The sound speed computed from the dispersion curves for a range of Γ (inverse temperature) for $\alpha = \frac{5}{2}$. The circles are from numerical simulation while the dashed blue line is a linear fit, giving a slope of 0.11 for $\alpha = \frac{5}{2}$, close to the expected value $\frac{\alpha-2}{2\alpha}$. The inset shows the kinetic and potential energy approaching thermal equilibrium, where their ratio satisfies the virial relation $KE/PE = \alpha/2$.

nearest neighbour interaction $V(\delta) = \frac{\kappa}{\alpha} (\delta)^\alpha$, where δ is the compression/stretching induced during the dynamics. We model the coupling to the heat bath by numerically integrating Eq. (5.1) for each particle using the predictor-corrector algorithm [71]. In thermal equilibrium the mean kinetic energy is $\text{KE} \sim \frac{k_B T}{2}$ and potential energy is $\text{PE} \sim \frac{k_B T}{\alpha}$, where their ratio satisfies the virial relation, see Fig. (5.3), inset for $\alpha = 5/2$. In the following, all numerical data is presented in dimensionless units, ensemble averaged over 1000 samples.

5.4.1 Fluctuation induced rigidity

To extract the equilibrium properties in the thermalized state, we define the longitudinal current density of particles as $j(x, t) = \frac{1}{\sqrt{N}} \sum_{i=1}^N v_i(t) \delta(x - x_i(t))$, and its Fourier transform $j(k, t) = \frac{1}{\sqrt{N}} \sum_{i=1}^N v_i(t) e^{ikx}$, where k is the longitudinal collective mode along the x -direction. Thus, the corresponding longitudinal current density auto-correlation functions is $C(k, t) = \langle j^*(k, 0) j(k, t) \rangle$, where the angular brackets denote ensemble averaging over the initial time. The longitudinal power spectral density is then obtained as the Fourier transform of the respective current density auto-correlation functions as, $P(k, \omega) = \int_{-\infty}^{\infty} dt e^{i\omega t} C(k, t)$. The Fourier transforms defined above are evaluated using fast Fourier transform from simulation data. The sound speeds in Fig. (5.3) correspond to the linear part of the dispersion curves, obtained by projecting the power spectral densities on the frequency (ω)- wavenumber (k) plane. See Supplementary Information C for details.

In Fig. (5.3), we plot the sound speed from the slope of the dispersion curves for $\alpha = 5/2$ for a range of Γ . At thermal equilibrium, the mean kinetic energy and hence the temperature T satisfy the virial relation $T \sim \delta_T^\alpha$, where δ_T is the average displacement of the particles induced by thermal fluctuations. Defining the sound speed c as the second derivative of the induced potential energy leads to the relation, $c^2 \sim T^{\frac{\alpha-2}{\alpha}}$ [38]. For $\alpha = \frac{5}{2}$, we find $c \sim \Gamma^{-\frac{1}{10}} \sim (k_B T)^{\frac{1}{10}}$, closely matching the linear fit in Fig. 5.3. Thus, coupling the lattice of non-linear springs that is initially in its state of sonic vacuum (implying the absence of linear sound) to a heat bath, leads to hydrodynamical sound modes with a linear sound speed that scales with the temperature of the heat bath [38]. Note, setting $\alpha = 2$ (harmonic springs) yields a sound speed that is independent

By coupling a lattice of non-linear springs to a thermal bath, we see the emergence of entropic elasticity.

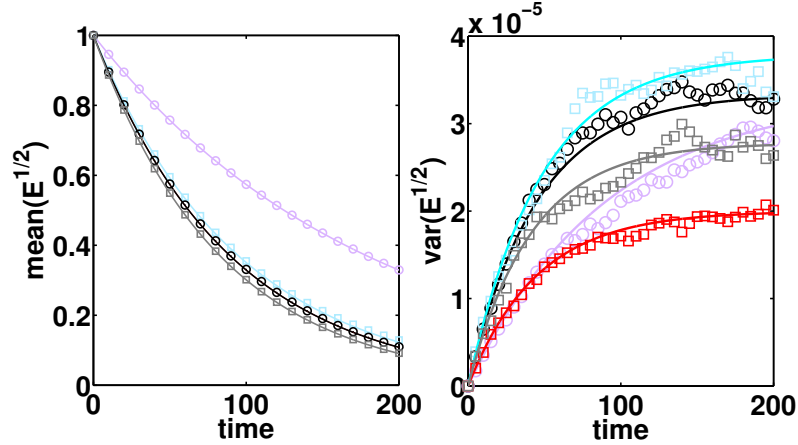


Figure 5.4: *left*: the numerically obtained mean solitary wave energy for $\alpha = 2.5, \gamma = 0.01$ (purple circles), $\alpha = 2.2, \gamma = 0.02$ (blue squares), $\alpha = 2.5, \gamma = 0.02$ (black circles), $\alpha = 3.0, \gamma = 0.02$ (gray squares) decaying exponentially compared against the analytical expression (solid curves). The mean decay rate is independent of the temperature Γ^{-1} . *right*: the numerically obtained variance of the solitary wave energy for $\alpha = 2.2, \gamma = 0.02, \Gamma = 6000$ (blue squares), $\alpha = 2.5, \gamma = 0.02, \Gamma = 6000$ (black circles), $\alpha = 3.0, \gamma = 0.02, \Gamma = 6000$ (grey squares), $\alpha = 2.5, \gamma = 0.01, \Gamma = 6000$ (purple circles) and $\alpha = 2.5, \gamma = 0.02, \Gamma = 10000$ (red squares) compared against the analytical expression Eq. (5.20) (solid curves).

of temperature while the limit $\alpha \rightarrow \infty$ yields $c \sim (k_B T)^{\frac{1}{2}}$, a result in agreement with the entropic elasticity for hard sphere colloidal crystals [52].

5.4.2 Comparison with analytics

Once the lattice reaches thermal equilibrium, we excite a solitary wave (SW) by imparting one of the particles an initial energy of order $E_{SW} = 0.5$ in dimensionless units. In Fig. (5.2) left panel, we show a snapshot of two SWs at the same time, propagating in a background of thermal fluctuations for $\alpha = 2.5$ (red) and $\alpha = 2.2$ (black). We see that the SW with lower α is wider and moves faster for the given amplitude, in qualitative agreement with the analytic widths $W \sim \frac{1}{\sqrt{3(\alpha-2)}}$ and speeds $V_s \sim A \frac{\alpha-2}{\alpha}$.

In Fig. (5.4) left panel, we plot the numerical data (symbols) for the attenuation of the SW amplitude as a function of time for various values of γ and α and we find a very good match to the analytic expression in Eq. (5.15) (solid curves). For the range of Γ explored, we find the damping rate is independent of temperature (Γ) but depends on the environmental drag γ and α .

In Fig. (5.4) right panel, we show the increase in the variance of SW amplitude (or the square root of its energy) as a function of time for multiple values of α , γ and Γ obtained numerically (symbols) and compare them with the complete analytical solution Eq.(5.20) finding good agreement. Notice, the final value of the variance correctly approaches the thermal energy, as expected for a Brownian particle. However, since the solitary wave is a dynamical object that decays under the influence of the external drag, once the solitary wave energy becomes comparable to the background thermal energy, it is no longer meaningful to consider it as a Brownian particle.

SHEAR FRONTS IN RANDOM SPRING NETWORKS.

We now shift our attention to another model of fragile matter: a two dimensional disordered network of harmonic springs. At a critical value of its mean connectivity, such a network becomes fragile: it undergoes a rigidity transition signalled by a vanishing shear modulus and transverse sound speed. We then investigate analytically and numerically the linear and non-linear visco-elastic response of these networks by probing the dynamics that result from shearing one edge of the sample at a uniform rate. Similar to our previous studies, we will find that close to the rigidity transition, the regime of linear response becomes vanishingly small and the tiniest shear strains generates non-linear shear shock waves. Moreover, we find that the response of the networks at early times is reminiscent of the emergent fluid like state we saw in Chapter 4. In this case, the emergent viscosity directly manifests in the super-diffusively growing widths of the nonlinear shock front*.

* The research ideas presented in this chapter evolved out of interesting discussions with V. Vitelli and S. Ulrich and are part of Reference [9]. Thanks to S. Ulrich for the simulations and accompanying figures.

SHEAR FRONTS IN RANDOM SPRING NETWORKS

As discussed in the introduction, a disordered network of harmonic springs constitutes another interesting model for fragile matter, where the loss of rigidity is a collective phenomenon. In this chapter, we turn to the study of this model by subjecting a two dimensional random network of harmonic springs (not coupled to any other local source of fluctuations) to a constant influx of energy, by shearing one of its edges at a uniform rate. We will then study the response of the network by following the evolution and propagation of the resulting shear excitations.

We construct computer models of weakly connected two dimensional random viscoelastic networks from highly compressed jammed packings of frictionless poly-disperse disks. One first identifies the disk centers as point particles (network nodes) and then models the interactions between overlapping disks using two sided harmonic springs of varying rest length to eliminate any pre-stress existing in the original jammed packings. The result is a highly coordinated ($z \approx 6$) spring network that serves as the seed from which families of networks with a wide range of z are generated by removing springs. See, Fig. (6.1).

Once the networks are generated, we shear the left most edge at a constant speed v_0 , and follow the evolution of the resulting shear velocity profile by averaging out the longitudinal particle speeds over bins along the x direction effectively creating a one dimensional front profile propagating in the x direction. Note here, it is useful to express the rate of shearing in terms of dimensionless parameter, that we define as the strain $\gamma = \frac{v_0}{v_f}$, where v_f is the speed of propagation of the front. In the following discussions, we will find two distinct regimes of shear front propagation - a linear regime for $\gamma < \gamma_c$ and a non-linear regime for $\gamma > \gamma_c$, where γ_c is the critical strain, to be defined later.

The dynamics is obtained by numerically integrating Newton's equations of motion (using the velocity Verlet method) subject to Lees-Edwards boundary conditions in the y -direction

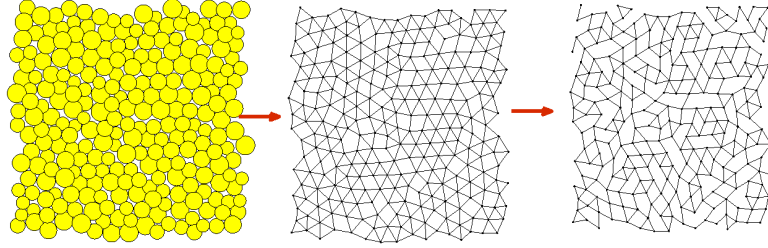


Figure 6.1: From a jammed packing of soft frictionless disks (left), we identify the disk centers with point nodes and model the interaction between overlapping disks as harmonic springs (middle). We then remove springs to obtain an ensemble of disordered spring networks with the desired coordination number (right).

and hard walls in the x -direction *. The samples are composed of up to $N = 10^5$ identical particles with mass m . In addition to the Hookean interaction (with a spring constant k) between connected particles, i, j , we include the effects of viscous dissipation: $\vec{f}_{\text{diss}}^{ij} = -b(\vec{v}^i - \vec{v}^j)$, where b is the microscopic damping constant, and $\vec{v}^{i,j}$ are the velocities of a pair of particles connected by a spring. Time is measured in units of $\sqrt{m/k}$ and the damping constant in units of \sqrt{km} , which is equivalent to setting $m = 1$ and $k = 1$. Lengths are measured in units of d the mean spring length at rest.

6.1 LINEAR REGIME

6.1.1 Early time

In the inset to Fig. (6.2), we plot the resulting velocity field (normalized by the shearing rate v_0) for times less than a critical transition time, i.e., $t < t_c$. Notice, the velocity field simply broadens away from the shearing edge that is located at $x=0$, while remaining centered there. Thus, in this regime, we do not observe any propagating shear fronts.

In the main panel of Fig. (6.2), we plot the width $w(t)$ of the velocity field as a function of time t . Expectedly, the width in-

* A hard wall can only move up and down as a whole, but no relative motion of the particles is allowed.

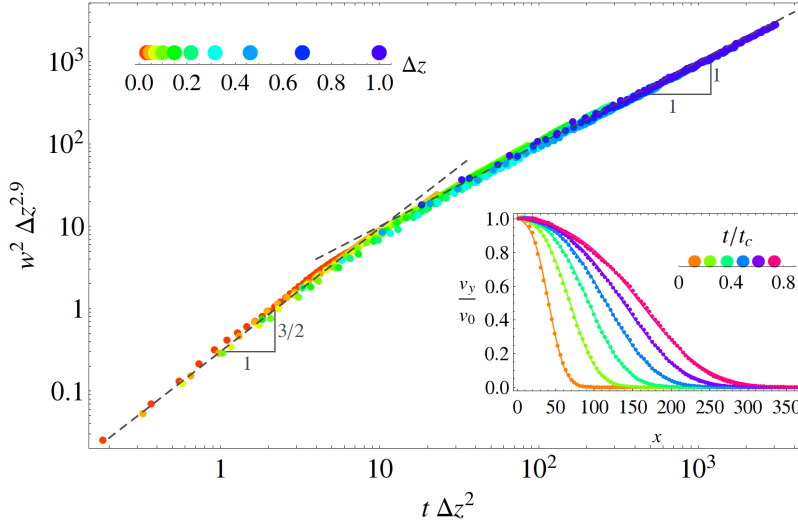


Figure 6.2: The main plot shows the time evolution of the squared front width, whereby the time axis has been normalized by $t_c \propto \Delta z^{-2}$ and the width axis by $\Delta z^{2.9}$. The inset shows the broadening at early times, $t < t_c$, of the velocity profiles, $v(x, t)$, in the \hat{y} direction, normalized by v_0 . Note the absence of front *propagation*, in contrast with the plot in the left inset of Fig. (6.3).

creases with time. At early times we find that $w^2 dz^3 \sim (tdz^2)^{\frac{3}{2}}$, implying, a super-diffusively increasing width:

$$w^2(t) \sim t^{\frac{3}{2}}. \quad (6.1)$$

However, at later times ($t > t_c$), there is a transition to a new regime where the width increases diffusively,

$$w^2(t) \sim \frac{t}{dz}. \quad (6.2)$$

Recall, particle diffusion in a medium can be characterized by a diffusion constant defined from the mean square displacement as:

$$\langle r^2(t) - r^2(0) \rangle = Dt^\xi, \quad (6.3)$$

where, $r(t)$ is the displacement, D is a characteristic diffusion constant and ξ is an exponent characterizing the nature of diffusion. If $\xi = 1$, we are in the regime of normal diffusion where the mean square displacement increases linearly with time and is consistent with the late time dynamics that we observe in Fig. (6.2) and Eq. (6.2). By contrast, a ξ different from 1 is considered

anomalous diffusion, with $\xi < 1$ being referred to as the sub-diffusive regime and $\xi > 1$ as the regime of super-diffusion. From Eq. (6.1), we find that a $\xi = \frac{3}{2}$ characterizes the broadening of the velocity field at early times.

In the super-diffusive regime, Eq. (6.3) can also be interpreted in the form

$$\langle r^2(t) - r^2(0) \rangle = D(t)t, \quad (6.4)$$

with a diffusivity that depends upon time ,i.e., $D(t) = Dt^{\xi-1}$ (see also Chapter 4). If $\xi > 1$, this implies that the diffusivity will continue to increase with time. However, we note from Fig. (6.2) that beyond a transition time t_c we enter the regime of normal diffusion that has a constant diffusivity. Thus, if we imagine that this transition process physically corresponds to a diffusivity that increases with time until it saturates to a constant value $\frac{1}{dz}$ (from Eq. (6.2)), we find the transition time,

$$Dt^{\xi-1} \sim \frac{1}{dz} \quad (6.5)$$

$$t \sim \left(\frac{1}{dz} \right)^{\frac{1}{\xi-1}}. \quad (6.6)$$

For $\xi = \frac{3}{2}$, the transition time is therefore

$$t_c \sim \frac{1}{dz^2}. \quad (6.7)$$

This explains the choice of normalization used in the axes of Fig. (6.2). Note, the critical transition time is exactly the critical time for transition from the so called non-quasistatic regime to the quasi-static regime, first studied for visco-elastic random spring networks using linear oscillatory rheology [4].

In the context of the transverse velocity field studied here, physically, the transition time represents the time required for the front width to increase to a large enough length scale so that wave numbers characterizing the front discontinuity only contains low frequency components and the network response can then be described by frequency independent elastic constants. The length scale up to which anomalous diffusion persists is then

$$l_c \sim t_c^{\frac{3}{4}} \sim \frac{1}{dz^{\frac{3}{2}}}. \quad (6.8)$$

This length scale can therefore be associated with the characteristic size of the network beyond which its response can be considered elastic, as we will see in the next section.

6.1.2 Late Times

At late times (for $t > t_c$), along with the transition to a regime where the width spreads diffusively, we also find the onset of front propagation, see inset to Fig. (6.3), with a speed that is characteristic of the network shear modulus. As discussed in the introductory chapter, for random spring networks near the rigidity transition critical point, the shear modulus scales linearly with the excess coordination number $G \sim dz$. In Fig. (6.4), we extract from the speed of front propagation, the corresponding shear modulus via the relation $c_s \sim \sqrt{G}$, and plot it as a function of dz , finding very good agreement with the expected scaling.

In addition, in Fig. (6.5), we extract the width of the propagating shear fronts as a function of dz (after normalizing out the diffusive spreading in time seen in Fig. (6.2)). As anticipated from the relation Eq. (6.2), we find a width that diverges with the excess coordination number $w^2 \sim \frac{1}{dz}$. Conversely, from the width of the propagating fronts we can define a transport coefficient, that we call the effective viscosity of the network $\eta_e \sim \frac{1}{dz}$. Phenomenologically, this amounts to a second order equation of motion for the transverse y - displacement field of the form

$$\rho \frac{\partial^2 y}{\partial t^2} = G \frac{\partial^2 y}{\partial x^2} + \eta_e \frac{\partial^3 y}{\partial x^2 \partial t}. \quad (6.9)$$

In turn, this equation can be derived from a visco-elastic stress-strain relation of the form:

$$\sigma = G\gamma + \eta_e \dot{\gamma}, \quad (6.10)$$

where $\gamma = \frac{\partial y}{\partial x}$. Thus, for $t > t_c$, the network response can be effectively described by time independent (or frequency independent) characteristic storage (G) and loss (η_e) moduli. As discussed in the introductory chapter, this is consistent with the recent studies that probe random visco-elastic spring networks by imposing a linear frequency dependent strain at the boundaries (oscillatory rheology), where the response of the networks in the quasi-static regime (for frequencies $\omega < \omega_c \sim dz^2$) is characterized by frequency independent storage modulus $G \sim dz$ and a frequency independent loss modulus $\eta \sim \frac{1}{dz}$. By contrast, for $\omega > \omega_c$, the complex moduli are frequency dependent. See Supplementary information F for more details, including a derivation of the velocity profiles in the frequency dependent regime.

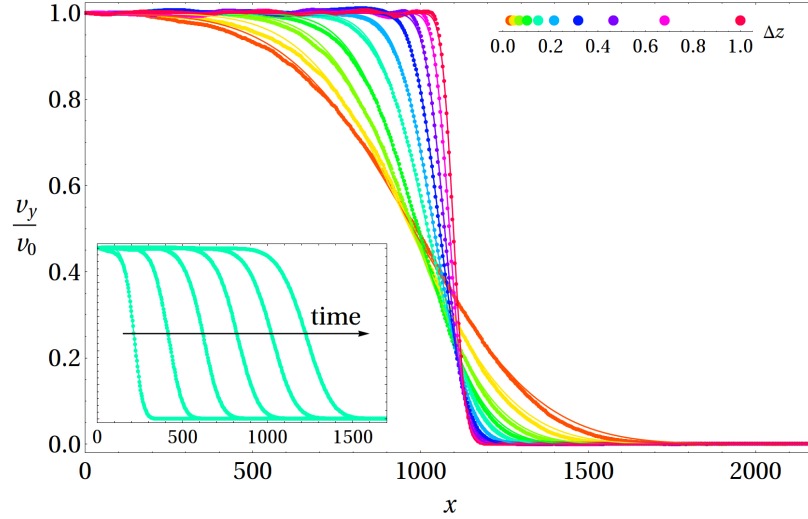


Figure 6.3: Shape of the linear wave profile. In the main plot, velocity profiles for different Δz are superimposed, with the smallest Δz corresponding to the widest profile. The damping coefficient is $b = 0.1$ and the time is chosen such that the wave has roughly reached the center of the sample. The left inset shows the wave front for $\Delta z = 0.15$ (same color as main plot) for different times. In all plots, data points are (averaged) profiles from the simulation and the solid lines are fits to analytical solution [9].

6.2 NON-LINEAR REGIME

For large strain rates i.e., $\gamma > \gamma_c$ the network response changes substantially, see Fig. (6.6). Compared to the inset in Fig. (6.2), we now find that even at early times, a well defined front propagates. At the same time, the front width continues to increase super diffusively with the same exponent $\xi = \frac{3}{2}$ as seen in the linear regime. However, unlike the case for $\gamma < \gamma_c$ where we found a cross-over to ordinary diffusion for times $t > t_c$, we no longer observe such a transition in the non-linear regime during the entire times probed in our simulations, see Fig. (6.7).

For a qualitative understanding of this network response for large strains, consider first, the one dimensional diffusion equation :

$$\frac{\partial u}{\partial t} = D \frac{\partial^2 u}{\partial x^2}. \quad (6.11)$$

Let us impose a field of the form $u = u_0 e^{i(kx - \omega t)}$. The solution is:

$$u = u_0 e^{\left(\frac{-t}{\tau_r}\right)} e^{ikx}, \quad (6.12)$$

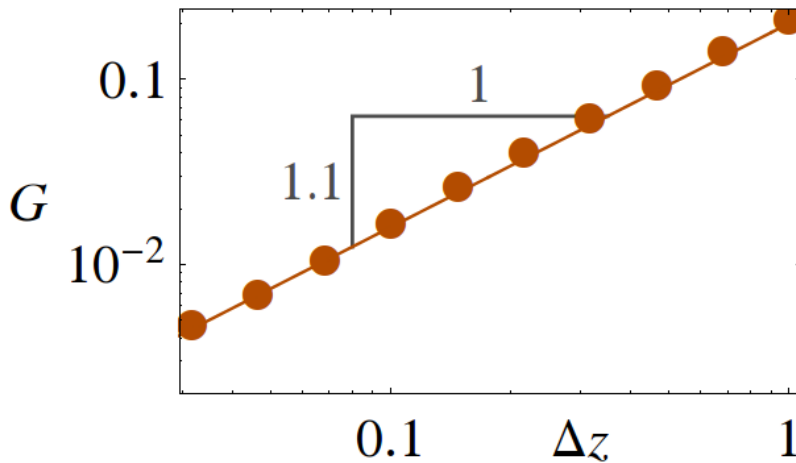


Figure 6.4: The shear modulus G versus Δz extracted from the speed of the linear front propagating in a homogeneously cut network.

where we have defined a response time t_r

$$t_r = \frac{1}{Dk^2}. \quad (6.13)$$

This implies that for large wave numbers (or small wavelength fluctuations), the response time for their decay is very small. However, at such short time scales, the continuum diffusion equation Eq. (6.11) should no longer be a good approximation to the physical processes since the diffusion equation is generally associated with the long wavelength and long time properties of the medium. In fluids for instance, one way to account for the short time response of the fluid is to introduce a diffusion kernel (memory function) [69]. Similarly, the anomalous wavenumber dependent viscosity that we observed in the quasi-equilibrium state of amorphous packings (see Chapter 4) is also related to the inability of fluids in low dimensions to respond instantaneously to fluctuations. Since the transport properties (such as diffusivity, viscosity, conductivity) are long time integrals of correlation functions, their time dependence typically correspond to correlation functions that do not decay exponentially but have a long time power law tail.

Similarly for the random spring networks, we find that their initial response in the linear regime is marked by a diffusivity that is time (frequency) dependent. Only when the diffusion causes the width to grow to large enough length scales of the order of l_c (small wave numbers), do we find a transition to a

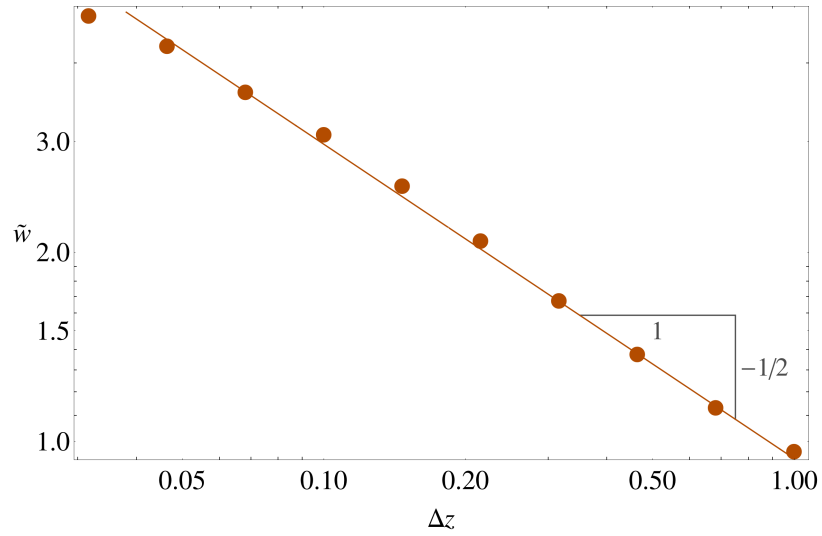


Figure 6.5: The main panel shows numerical data for the rescaled width $\tilde{w} \equiv \frac{w(t)}{\sqrt{t}}$ (or equivalently the effective viscosity η_e) versus Δz (dots) for homogeneously cut networks with $b = 0.1$. The solid line represents the scaling $\tilde{w} \propto \Delta z^{-1/2}$.

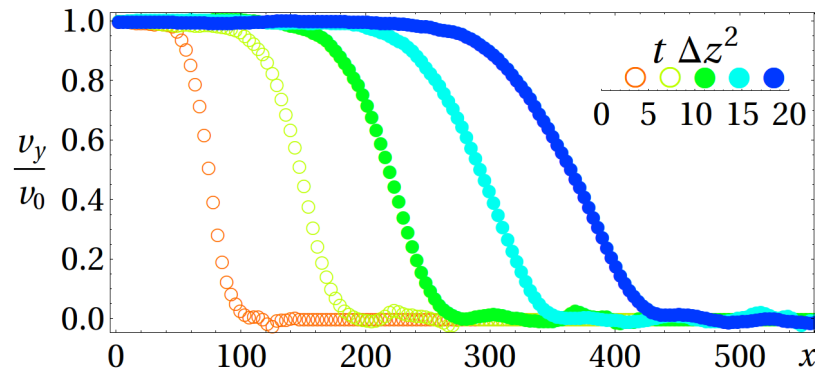


Figure 6.6: Evolution of a non-linear ($\frac{\gamma}{\gamma_c} = 6.8$) wave front for $\Delta z \approx 0.15$. Late times $t\Delta z^2 > 10$ are indicated by full circles.

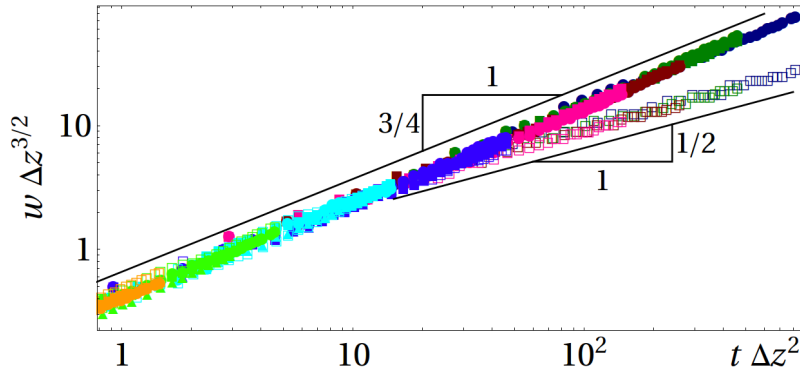


Figure 6.7: Time dependence of the widths in the non-linear regime. Different colors correspond to different Δz , as in the plot on the left. The full symbols correspond to the non-linear regime with $1.5 < \frac{\gamma}{\gamma_c} < 680$. The open symbols correspond to the linear regime ($\frac{\gamma}{\gamma_c} < 10^{-3}$).

regime where the transport process with a constant diffusivity may be defined. However, why is this regime not attained when the strain rates are large ?

Intuitively, for large strain rates, Eq. (6.11) is expected to be modified to include non-linear corrections of the form:

$$\frac{\partial u}{\partial t} + \kappa \frac{\partial u^n}{\partial x} = D \frac{\partial^2 u}{\partial x^2}, \quad (6.14)$$

where n is the index of non-linearity.

Consider the simplest non-linear term with $n = 2$ (such as in the Navier-Stokes equation without a pressure gradient term). How does this term respond to a perturbation of the form : $u = u_0 \cos(kx)$, that we considered previously. To leading order, we find $u^2 = u_0^2 \cos^2 kx$ and upon differentiating once with respect to the spatial variable x , we find a new term of the form $u_0^2 \sin(2kx)$ with a wavenumber $2k$. Once a perturbation with larger wavenumber is generated, the non-linear term responds again to this new perturbation, by generating another higher wavenumber, and this process thus keeps repeating, limited only by the largest wavenumber physically supported by the medium or by other dissipative processes. Thus, one effect of the non-linear term is that it acts as a source term that generates higher wavenumbers. This mechanism is similar to the generation of smaller and smaller eddies in the study of turbulence, where large wavenumbers represent the smaller eddies that are eventually dissipated by thermal processes, such as the one encapsulated in Eq. (6.13).

Thus, if the response of random spring networks at high strain rates is non-linear, then one effect of the non-linearity would be to act as a source for higher wave numbers. However, Eq. (6.13) also indicates that due to the generation of the higher wave numbers, the network will have to keep responding at short time scales to diffusive these fluctuations away. This, in a sense is the physical process modelled by Eq. (6.14). However, at short time scales, the response of random spring networks is no longer in the quasi-static regime with a constant diffusivity D and therefore, the non-linearity constantly forces the system to remain in the regime with a time dependent diffusivity. By contrast, in the linear regime, once the higher wave-numbers inevitably generated during the early phases of the network response (due to the sharper front discontinuities) have been dissipated away, the network gradually enters the regime of quasi-static visco-elastic response with constant material properties.

Is there a distinctive signature of the kind of non-linearity present in our system? As remarked in the introductory chapter, a non-linear response could lead to the generation of non-linear fronts, whose speeds depends upon the applied strain. In the main panel of Fig. (6.8), we plot the normalized front speed v_f/c versus the normalized strain rate, γ/γ_c for the random networks at various values of Δz . For $\gamma \gg \gamma_c$, we find $v_f \propto \gamma^{\frac{1}{2}}$. Thus, we find a non-linearity index $n = 2$. This index is consistent with the findings in reference [2], where close to the critical point, the stress response of random spring networks was seen to take the form

$$\sigma = G\gamma + \kappa\gamma|\gamma| \quad (6.15)$$

In the strongly non-linear regime, differentiating once with respect to spatial coordinate x (ignoring the term $G\gamma$), we can write the continuum equation of motion

$$\frac{\partial \sigma}{\partial x} = \rho \frac{\partial^2 y}{\partial t^2}, \quad (6.16)$$

where y is the shear displacement. Using Eq. (6.15), we obtain the non-linear equation

$$\frac{\partial^2 y}{\partial t^2} = \frac{\kappa}{\rho} \frac{\partial \gamma^2}{\partial x}. \quad (6.17)$$

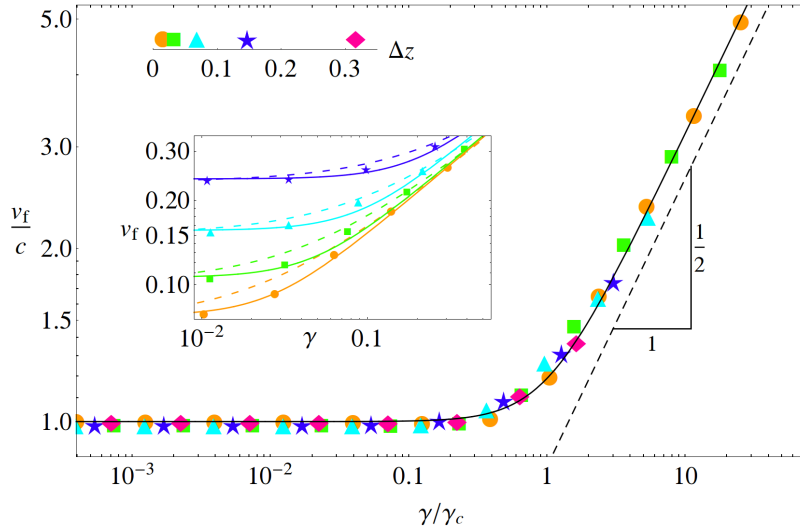


Figure 6.8: In the main panel, the normalized front velocity, v_f/c , is plotted as a function of the normalized strain γ/γ_c for a range of Δz . For $\gamma/\gamma_c \ll 1$, the front speed v_f is independent of the applied strain and corresponds to the linear speed of sound c . In the strongly non-linear regime $\gamma/\gamma_c \gg 1$, the front speed is independent of Δz and scales with the applied strain as $v_f \propto \gamma^{1/2}$ (straight black line). The solid curve is plotted using the relation $v_f = \frac{(G_0^2 + k_{nl}^2 \gamma^2)^{1/4}}{\sqrt{\rho}}$. The inset compares the solid curves from the main plot to the alternative relation $\tilde{v}_f = \sqrt{c^2 + \frac{k_{nl}\gamma}{\rho}}$ (dashed lines), clearly favouring v_f over \tilde{v}_f .

Differentiating once more with respect to x and noting that $\gamma = \frac{\partial y}{\partial x}$, we arrive at the second order non-linear wave equation:

$$\frac{\partial^2 \gamma}{\partial t^2} = \frac{\kappa}{\rho} \frac{\partial^2 \gamma^2}{\partial x^2}. \quad (6.18)$$

Comparing the two terms dimensionally, we can define a characteristic speed

$$v_f \sim \left(\frac{\kappa \gamma}{\rho} \right)^{\frac{1}{2}}. \quad (6.19)$$

In the strongly non-linear regime where the network response persists in the non-quasistatic regime with a front width that spreads super-diffusively, v_f is the only characteristic speed in the system. In essence, this is reminiscent of the effective sound speed we found in Chapter 4, where the effective sound speed depends upon the initial solitary wave energy as $c \sim E^{\frac{1}{10}}$. Since the solitary wave amplitude is related to the energy as $E \sim A^2$, the only characteristic speed in that medium was $c \sim A^{\frac{1}{5}}$. Consequently, one way to understand the response of the random spring network in the strongly non-linear regime is as a simple advection of the super-diffusive fronts with the characteristic speed v_f .

More-over, the critical strain for the transition from linear to non-linear regime can be obtained by comparing the two terms on the right of Eq. (6.15),

$$\gamma_c \sim dz. \quad (6.20)$$

In the main panel of Fig. (6.8), we do find a good collapse of the data, where strains have been normalized by the critical strain Eq. (6.20). Note also, for $\gamma < \gamma_c$ and at later times, the front speed is simply the speed of linear sound $c \sim \sqrt{G}$. Although the dynamics in the intermediate regime $\gamma \sim \gamma_c$ is complex, we do find well defined front propagation and indeed find a good collapse of the data for the front speed by the expression

$$v_f = \frac{(G^2 + \kappa^2 \gamma^2)^{\frac{1}{4}}}{\sqrt{\rho}} \quad (6.21)$$

that correctly captures the asymptotic front speeds.

SUPPLEMENTARY MATERIAL

NESTERENKO SOLITARY WAVE

In this supplementary chapter, we review the original derivation of the strongly non-linear Nesterenko wave equation and motivate, how its solitary wave solution may be interpreted as a quasi-particle with an effective mass [32].

Consider a one dimensional chain of identical spherical particles of radius R with an initial overlap δ_0 (see Fig. (A.1)), and interacting with a non-linear force of the Hertz form. If the displacement of particle i from its equilibrium position is u_i , then the equation of motion of the i -th particle is

$$\ddot{u}_i = A(\delta_0 - u_i + u_{i-1})^{\frac{3}{2}} - A(\delta_0 - u_{i+1} + u_i)^{\frac{3}{2}}, \quad (\text{A.1})$$

where $A = R^{\frac{1}{2}} 2^{-\frac{3}{2}} \Theta^{-1}$ and $\Theta = \frac{3(1-\nu^2)}{4E}$ is a material constant depending upon the Young's modulus E and Poisson's ratio ν . Here, double dots refer to two derivatives with respect to time t . If the displacement of the particles with respect to the initial pre-compression is small, i.e., $|u_{i-1} - u_i| \ll \delta_0$, the right hand side of Eq. (A.1) can be expressed as

$$\ddot{u}_i = A\delta_0^{\frac{3}{2}} \left[\left(1 + \frac{u_{i-1} - u_i}{\delta_0} \right)^{\frac{3}{2}} - \left(1 + \frac{u_i - u_{i+1}}{\delta_0} \right)^{\frac{3}{2}} \right]. \quad (\text{A.2})$$

Using the binomial expansion, i.e., $(1+x)^{\frac{3}{2}} \approx 1 + \frac{3}{2}x + \frac{3}{4}x^2 \dots$, the right hand side of Eq. (A.2) can be expressed as

$$\ddot{u}_i = c(u_{i+1} - 2u_i + u_{i-1}) + d(u_{i+1} - 2u_i + u_{i-1})(u_{i-1} - u_{i+1}) \quad (\text{A.3})$$

where, $c = \frac{3}{2}A\delta_0^{\frac{3}{2}}$, $d = \frac{3}{8}A\delta_0^{-\frac{1}{2}}$. For a long wavelength continuum approximation $L \gg a = 2R$, where a is the lattice spacing, we now make the simplification $u_i \rightarrow u(x) \equiv u$, where x is the continuum spatial variable. Thus, we obtain

$$u_{tt} = c(u(x+a) - 2u(x) + u(x-a)) + d(u(x+a) - 2u(x) + u(x-a))(u(x-a) - u(x+a)). \quad (\text{A.4})$$

Taylor expanding the right hand side and retaining terms to order a^4 , we obtain the weakly non-linear wave equation

$$u_{tt} = c_0^2 u_{xx} + 2c_0 \gamma u_{xxxx} - \epsilon u_x u_{xx}, \quad (\text{A.5})$$

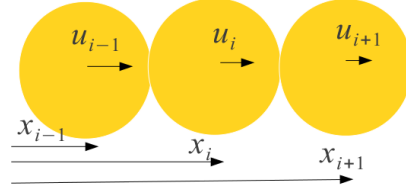


Figure A.1: Nearest neighbour particles in a one dimensional granular chain.

where, $c_0^2 = A\delta_0^{\frac{1}{2}}6R^2$, $\gamma = \frac{c_0}{6}R^2$, $\epsilon = c_0^2\frac{R}{\delta_0}$. Here, subscripts refer to partial derivatives with respect to space x and time t . This equation is known as the Boussinesq equation and under certain approximations, the solutions of this equation satisfy the better known Korteweg-De Vries (KdV) equation.

However, our main interest is in the other regime where $\delta_0 \rightarrow 0$ and thus the standard long wavelength approximation made above can no longer be used, since $|u_{i-1} - u_i| \gg \delta_0$. Consequently, we take the extreme limit and set $\delta_0 = 0$ (the spherical beads just touching other) in Eq. (A.1) and express it in the continuum space and time variables as

$$\ddot{u}_i = A \left[(u(x-a) - u(x))^{\frac{3}{2}} - (u(x) - u(x+a))^{\frac{3}{2}} \right], \quad (\text{A.6})$$

and Taylor expand as

$$\ddot{u}_i = A \left(u - au_x + \frac{a^2}{2}u_{xx} - \frac{a^3}{6}u_{xxx} + \frac{a^4}{24}u_{xxxx} - u \right)^{\frac{3}{2}} - (\text{A.7})$$

$$A \left(u - u - au_x - \frac{a^2}{2}u_{xx} - \frac{a^3}{6}u_{xxx} - \frac{a^4}{24}u_{xxxx} \right)^{\frac{3}{2}}. (\text{A.8})$$

Now performing a Binomial expansion around $(-u_x)$, we obtain the Nesterenko equation for strongly non-linear waves:

$$u_{tt} = c^2 \left[\frac{3}{2}(-u_x)^{\frac{1}{2}}u_{xx} + \frac{a^2}{8}(-u_x)^{\frac{1}{2}}u_{xxxx} - \frac{a^2u_{xx}u_{xxx}}{8(-u_x)^{\frac{1}{2}}} - \frac{a^2(u_x x)^3}{64(-u_x)^{\frac{1}{2}}} \right] \quad (\text{A.9})$$

where, $c^2 = (2R)^{\frac{5}{2}}\frac{A}{m}$ is just a rescaled material dependent parameter. Upon rewriting this equation in terms of the strain field $\xi = -u_x$, we obtain the equation in a more condensed form

$$\xi_{tt} = c^2 \left[\xi^{\frac{3}{2}} + \frac{2R^2}{5}\xi^{\frac{1}{4}}(\xi^{\frac{5}{4}})_{xx} \right]_{xx}. \quad (\text{A.10})$$

A travelling wave solution of Eq. (A.10) is obtained by looking for solutions of the form $\xi = \xi(x - v_s t)$, where v_s is the speed of propagation. Upon substituting in Eq. (A.10) and integrating twice [32], we obtain the solitary wave solution (see Supplementary Information B for a similar calculation in more detail)

$$\xi = \left(\frac{5 v_s^2}{4 c^2} \right)^2 \cos^4 \left(\frac{\sqrt{10}}{5a} (x - v_s t) \right). \quad (\text{A.11})$$

This represents a propagating strain field ξ . Often in simulations, it is easier to measure the velocity field $v(x, t) = u(x, t)_t = -v_s \xi(x, t)$. Thus, the solution in terms of the velocity field reads

$$v = \left(\frac{25 v_s^5}{16 c^4} \right) \cos^4 \left(\frac{\sqrt{10}}{5a} (x - v_s t) \right). \quad (\text{A.12})$$

where, we find that the amplitude of the wave depends upon the speed of propagation as $\xi_m \equiv u_p \sim v_s^5$. This is also the scaling relation we found for compressional shocks in amorphous packings in subsection 1.1.4.1. Notice, the width of the solitary wave is simple a few times the grain diameter a , $w = \frac{5a}{\sqrt{10}}$ and is independent of the speed of propagation v_s . This is unlike some well known weakly non-linear waves such the KdV equation, where the width also depends upon the speed of propagation.

A.1 QUASI-PARTICLE INTERPRETATION

The solitary wave kinetic energy K_{SW} , the potential energy U_{SW} , the total energy E_{SW} and momentum P_{SW} (i.e, sum of the respective kinetic, potential and total energies of the beads that are enveloped by the solitary wave) are-

$$K_{\text{SW}} = \frac{m v_s^2}{4R} \int dx \xi^2 = \left[\frac{(2R)^3 \xi_m^{\frac{5}{2}}}{\Theta \sqrt{10}} W_8 \right] \quad (\text{A.13})$$

$$U_{\text{SW}} = \frac{2A(2R)^{\frac{3}{2}}}{5} \int dx \xi^{\frac{5}{2}} = \left[\frac{(2R)^3 \xi_m^{\frac{5}{2}}}{\Theta \sqrt{10}} W_{10} \right] \quad (\text{A.14})$$

$$E_{\text{SW}} = \left[\frac{(2R)^3 \xi_m^{\frac{5}{2}}}{\Theta \sqrt{10}} (W_8 + W_{10}) \right] \quad (\text{A.15})$$

$$P_{\text{SW}} = \frac{m v_s}{2R} \int dx \xi = \left[\frac{(2R)^3 \xi_m^{\frac{5}{4}}}{\sqrt{\frac{3\Theta}{\pi\rho}}} W_4 \right]. \quad (\text{A.16})$$

where, $W_n = \int_0^{\pi/2} dx \cos^n x$ [17].

Now, the proportionality of the solitary wave kinetic energy K_{SW} and potential energy U_{SW} , gives the opportunity to describe its dynamics as a quasi-particle. Defining an equivalent particle of mass m_{SW} moving at a speed v_{SW} such that the solitary wave momentum and energy are $P_{SW} = m_{SW}V_{SW}$ and $E_{SW} = \frac{1}{2}m_{SW}V_{SW}^2$, one finds

$$m_{SW} = \frac{P_{SW}^2}{2E_{SW}} = \Omega m, \quad (\text{A.17})$$

where, $\Omega = \frac{W_4^2 \sqrt{10}}{W_8 + W_{10}} = 1.345$. Thus, the solitary wave is effectively like a particle with a rescaled mass $1.34m$, where m is the mass of the beads. Note, for many waves, differentiating E_{SW} with respect to P_{SW} gives the group velocity or the speed of propagation of the wave. However, here P_{SW} is not the canonical momentum and is physically related to the speed of the particles, not the wave.

An important relation to be used later, is between the solitary wave momentum P_{SW} , the mass of the beads m and the solitary wave speed of propagation v_s . Using $P_{SW} \equiv m \int dx \frac{du}{dt} \sim mv_s \int dx \xi$ and substituting the solitary wave solution for ξ , we find the relation

$$P_{SW} = mv_s \xi_m \int dx \cos^4 x, \quad (\text{A.18})$$

$$= mv_s^5 \left(\frac{5}{6} \pi \rho \Theta \right)^2 \int dx \cos^4 x, \quad (\text{A.19})$$

$$\sim m^3 v_s^5, \quad (\text{A.20})$$

where $\rho = \frac{m}{(4/3\pi R^3)}$. In Supplementary information B, we provide an alternative (albeit approximate) derivation of the strongly nonlinear Nesterenko wave equation that would allow us to express the solitary wave solution for any general nonlinear exponent $\alpha > 2$.

SOLITARY WAVE SOLUTION

In this supplementary chapter, we will derive the quasi-particle representation of the solitary wave using an approximation to the Nesterenko solitary wave equation, that is valid for a more general non-linear interaction potential with exponent $\alpha > 2$ [49].

B.1 ROSENAU APPROXIMATION

Here, we adopt as our starting point the Lagrangian for a one dimensional chain of identical spheres that are just touching each other, i.e., in the limit $\delta_0 \rightarrow 0$ (strongly nonlinear limit) -

$$L = \sum_n \frac{1}{2} m \dot{u}_n^2 - \frac{A}{\alpha} \left(\frac{u_n - u_{n+1}}{a} \right)^\alpha \quad (\text{B.1})$$

where, u_n is the displacement of the n -th sphere from its equilibrium position and $a = 2R$ is the lattice spacing. In order to avoid doing a Binomial expansion in powers of α , we will define the continuum field variable as

$$a\phi'(n + \frac{1}{2}) = u_{n+1} - u_n, \quad (\text{B.2})$$

where, primes denote derivative with respect to x . We now take the continuum limit, i.e., $u_n \rightarrow u(x) \equiv u$ and Taylor expand the right hand side about $x + \frac{a}{2}$:

$$a\phi'(x) \approx u + \frac{a}{2}u' + \frac{a^2}{8}u'' + \frac{a^3}{48}u''' - u + \frac{a}{2}u' - \frac{a^2}{8}u'' + \frac{a^3}{48}u'''. \quad (\text{B.3})$$

Integrating both sides once with respect to x , we obtain

$$\phi(x) = u + \frac{a^2}{24}u'', \quad (\text{B.4})$$

$$= \left(1 + \frac{a^2}{24} \frac{d^2}{dx^2} \right) u(x). \quad (\text{B.5})$$

Inverting the differential operator, we obtain

$$u(x) \approx \phi - \frac{a^2}{24}\phi''. \quad (\text{B.6})$$

Thus, in the continuum limit, the Lagrangian becomes

$$\frac{L}{m} = \int dx \frac{1}{2} \dot{u}^2(x) - \frac{A}{m\alpha} (\phi'(x))^\alpha \quad (\text{B.7})$$

$$= \int dx \frac{1}{2} \dot{\phi}^2 - \frac{a^2}{24} \dot{\phi} \phi'' - \frac{A}{m\alpha} (\phi')^\alpha. \quad (\text{B.8})$$

By using the Euler-Lagrange equation, we obtain the equation of motion as

$$\ddot{\phi} - \frac{a^2}{12} \dot{\phi}'' + \frac{A}{m} [(-\phi')^{\alpha-1}]' = 0. \quad (\text{B.9})$$

Note, ϕ here corresponds to the continuum displacement field. The corresponding equation in the strain field $\delta = -\phi'$ reads

$$\ddot{\delta} - \frac{a^2}{12} \dot{\delta}'' - \frac{A}{m} [\delta^{\alpha-1}]'' = 0. \quad (\text{B.10})$$

B.2 SOLITARY WAVE SOLUTION

The solitary wave solution of Eq. (B.10) can be obtained by looking for propagating solutions of the form $\delta(x, t) = \delta(x - v_s t)$:

$$\frac{v_s^2 a^2}{12} \delta'' - v_s^2 \delta + \frac{k}{m} \delta^{\alpha-1} = 0, \quad (\text{B.11})$$

which can be expressed in the form of Newton's-like equation

$$\delta'' = -\frac{12}{v_s^2 a^2} \left[-v_s^2 \delta + \frac{k}{m} \delta^{\alpha-1} \right] = -\frac{dW}{d\delta}. \quad (\text{B.12})$$

Multiplying both sides by δ' and integrating,

$$\int dx \delta' \delta'' = \int dx -\frac{dW}{d\delta} \delta', \quad (\text{B.13})$$

$$\int \frac{1}{2} d(\delta')^2 = \int -dW, \quad (\text{B.14})$$

$$\frac{1}{2} (\delta')^2 = -W(\delta). \quad (\text{B.15})$$

Integrating again, we find

$$\int \frac{d\delta}{\sqrt{-2W}} = \int dx. \quad (\text{B.16})$$

Substituting, $W(\delta) = \frac{12}{v_s^2 a^2} \left[\frac{k}{m\alpha} \delta^\alpha - \frac{v_s^2}{2} \delta^2 \right]$, and writing for brevity $A = \frac{12}{v_s^2 a^2} \frac{k}{m\alpha}$ and $B = \frac{6}{a^2}$, we need to integrate

$$\int \frac{d\delta}{\sqrt{2B\delta^2 - 2A\delta^\alpha}} = x, \quad (\text{B.17})$$

$$\int \frac{d\delta}{\sqrt{2\delta} \sqrt{B - A\delta^{\alpha-2}}} = x. \quad (\text{B.18})$$

Making the change of variables, $z^2 = B - A\delta^{\alpha-2}$, we find

$$\frac{-\sqrt{2}}{A(\alpha-2)} \int \frac{dz}{\delta^{\alpha-2}} = x, \quad (\text{B.19})$$

$$\frac{-\sqrt{2}}{(\alpha-2)} \int \frac{dz}{(\sqrt{B})^2 - z^2} = x. \quad (\text{B.20})$$

Therefore,

$$x = \frac{-1}{\sqrt{2B}(\alpha-2)} \left[\int \frac{dz}{\sqrt{B}-z} + \int \frac{dz}{\sqrt{B}+z} \right], \quad (\text{B.21})$$

yielding

$$s = -\sqrt{2B}(\alpha-2)x = \ln \frac{\sqrt{B}+z}{\sqrt{B}-z}, \quad (\text{B.22})$$

or

$$z = -\sqrt{B} \frac{1 - \exp -s}{1 + \exp -s}. \quad (\text{B.23})$$

Squaring and substituting $z^2 = B - A\delta^{\alpha-2}$,

$$B - A\delta^{\alpha-2} = B \frac{\exp s/2 - \exp -s/2}{\exp s/2 + \exp -s/2}, \quad (\text{B.24})$$

yielding,

$$\delta^{\alpha-2} = \frac{B}{A} \operatorname{sech}^2(s/2). \quad (\text{B.25})$$

Therefore, the solitary wave solution is

$$\delta = \left(\frac{m\alpha V_s^2}{2K} \right)^{\frac{1}{\alpha-2}} \operatorname{sech}^{\frac{2}{\alpha-2}} \left(\frac{\sqrt{3}}{2a} (x - V_s t) \right). \quad (\text{B.26})$$

We now note a few important properties of the solitary wave solution.

- The width of the solitary wave is approximately $w = \frac{2}{\sqrt{3}}$ times the lattice spacing $a = 2R$. Thus, unlike the Nesterenko solitary wave that is explicitly 5 particle diameters wide, the approximate width predicted by the solitary wave solution above is much less.
- However, due to the secant-hyperbolic function, Eq. (B.26) has an exponential tail. In principle this means, that unlike the Nesterenko solitary wave Eq. (A.12) that is zero outside 5 particle diameters (due to the zeros of cosine function), the above solution is never strictly zero. Thus, Eq. (B.26) is said to lack a compact support.

- The Hamiltonian and therefore the conserved energy corresponding to the Lagrangian Eq. (B.8) is

$$\frac{H}{m} = \int dx \frac{1}{2} \dot{\phi}^2 - \frac{\alpha^2}{24} \phi \dot{\phi}'' + \frac{\Lambda}{m\alpha} (\phi')^\alpha. \quad (\text{B.27})$$

Similarly, the momentum of the beads (not the canonical momentum) is simply,

$$\frac{P}{m} = \int dx \dot{\phi}. \quad (\text{B.28})$$

In conjunction, these two relations again allow us to interpret the solitary wave as a quasi-particle.

HYDRODYNAMICAL MODES AND POWER SPECTRUM

C.1 HYDRODYNAMIC MODES

In this supplementary section, we derive the longitudinal and transverse power spectral densities, that is used to obtain an understanding of the emergent state in Chapter 4 [72].

We begin with the fluid equations of continuity and the Navier-Stokes equation for the conservation of momentum [69] (ignoring any fluctuations in temperature of the system),

$$\frac{\partial}{\partial t} \tilde{\rho}(\mathbf{r}, t) + \nabla \cdot [\tilde{\rho}(\mathbf{r}, t) \tilde{\mathbf{v}}(\mathbf{r}, t)] = 0, \quad (\text{C.1})$$

where $\tilde{\rho}(\mathbf{r}, t) \equiv n_d(\mathbf{r}, t)$ is the particle number density per unit area and

$$m \frac{\partial}{\partial t} [\tilde{\rho}(\mathbf{r}, t) \tilde{\mathbf{v}}(\mathbf{r}, t)] + m \tilde{\rho}(\mathbf{r}, t) [\tilde{\mathbf{v}}(\mathbf{r}, t) \cdot \nabla] \tilde{\mathbf{v}}(\mathbf{r}, t) = -\nabla \tilde{p}(\mathbf{r}, t) + \eta_1 \{ \nabla^2 \tilde{\mathbf{v}}(\mathbf{r}, t) + \nabla [\nabla \cdot \tilde{\mathbf{v}}(\mathbf{r}, t)] \} \quad (\text{C.2})$$

where, m is the mass of a particle, $\tilde{p}(\mathbf{r}, t)$ is the pressure, $\tilde{\mathbf{v}}(\mathbf{r}, t) \equiv \mathbf{v}_d(\mathbf{r}, t)$ is local velocity field, and η_1 is the coefficient of shear viscosity [69]. Here, the expressions have been written for a fluid assumed to be in a two dimensional plane. Further, we have ignored any contributions coming from a bulk viscosity [69, 72].

We focus on studying small deviations from local equilibrium. Note, in the process of studying small deviations from equilibrium, we are implicitly studying small amplitude variations in a compressible fluid, which by definition is a *sound wave* if we consider longitudinal fluctuations.

Next, we choose a reference frame that moves with the fluid velocity, say $\tilde{\mathbf{v}}_0$ that we will take to be zero for a fluid at rest. We then linearize the above equations by considering small perturbations to first order, as follows

$$\tilde{\rho} = \tilde{\rho}_0 + \epsilon \tilde{\rho}_1 = \rho + \delta\rho, \quad (\text{C.3a})$$

$$\tilde{p} = \tilde{p}_0 + \epsilon \tilde{p}_1 = p + \delta p, \quad (\text{C.3b})$$

$$\tilde{\mathbf{v}} = \tilde{\mathbf{v}}_0 + \epsilon \tilde{\mathbf{v}}_1 = 0 + \mathbf{v}. \quad (\text{C.3c})$$

Defining the current density as $\mathbf{j}(\mathbf{r}, t) = \rho \mathbf{v}(\mathbf{r}, t)$ and linearizing Eq. (C.1) and Eq. (C.2) with respect to small perturbations, one obtains to first order

$$\frac{\partial}{\partial t} \delta \rho(\mathbf{r}, t) + \nabla \cdot \mathbf{j}(\mathbf{r}, t) = 0, \quad (\text{C.4a})$$

$$m \frac{\partial}{\partial t} \mathbf{j}(\mathbf{r}, t) + \nabla \delta p(\mathbf{r}, t) = \frac{\eta_1}{\rho} \{ \nabla^2 \mathbf{j}(\mathbf{r}, t) + \nabla [\nabla \cdot \mathbf{j}(\mathbf{r}, t)] \} \quad (\text{C.4b})$$

Dividing the momentum conservation equation by m , and defining $\frac{\eta_1}{m\rho} = \nu_1$,

$$\frac{\partial}{\partial t} \mathbf{j}(\mathbf{r}, t) + \frac{\nabla \delta p(\mathbf{r}, t)}{m} = \nu_1 \{ \nabla^2 \mathbf{j}(\mathbf{r}, t) + \nabla [\nabla \cdot \mathbf{j}(\mathbf{r}, t)] \} \quad (\text{C.5})$$

We now take the Fourier transform of Eqs. (C.4a) and Eq. (C.5) in position space, i.e., transform $\mathbf{j}(\mathbf{r}, t) \rightarrow \mathbf{j}_{\mathbf{k}}(t)$, $\delta p(\mathbf{r}, t) \rightarrow \delta p_{\mathbf{k}}(t)$ and $\delta \rho(\mathbf{r}, t) \rightarrow \delta \rho_{\mathbf{k}}(t)$ with $\mathbf{k} = (k, 0)$ being the k -space vector, that we will take to be in the x -direction. Further, let us define components of the current density vector as $\mathbf{j}_{\mathbf{k}}(t) = (j_{\mathbf{k}}^l(t), j_{\mathbf{k}}^t(t))$, where $j_{\mathbf{k}}^l(t)$ is the longitudinal part of the current density, pointing in the direction of k -vector (x direction in this case) and $j_{\mathbf{k}}^t(t)$ is the transverse component, pointing in a direction perpendicular to k -vector (y -direction in this case). We thus obtain the following equations in Fourier space

$$\frac{\partial}{\partial t} \delta \rho_{\mathbf{k}}(t) - ik j_{\mathbf{k}}^l(t) = 0, \quad (\text{C.6a})$$

$$\frac{\partial}{\partial t} j_{\mathbf{k}}^l(t) - \frac{ik \delta p_{\mathbf{k}}(t)}{m} = \nu_1 [-k^2 j_{\mathbf{k}}^l(t) - k^2 j_{\mathbf{k}}^l(t)] - \nu_2 k^2 j_{\mathbf{k}}^l(t), \quad (\text{C.6b})$$

$$\frac{\partial}{\partial t} j_{\mathbf{k}}^t(t) = -\nu_1 k^2 j_{\mathbf{k}}^t(t). \quad (\text{C.6c})$$

Note, by taking the Fourier transform, we have managed to decouple the longitudinal fluctuations in Eq. (C.6b) and transverse fluctuations, Eq. (C.6c). However, the longitudinal fluctuations are coupled to density fluctuations, Eq. (C.6a), that eventually gives rise to a finite sound speed in the longitudinal direction. Conversely, as seen in Eq. (C.6c), transverse waves are purely diffusive and de-coupled from any density fluctuations.

C.1.1 Longitudinal Current Density

We now focus on the longitudinal current density, Eqs. (C.6a) and (C.6b) and drop the superscripts and subscripts l . An analogous calculation can be done for the transverse current density.

First, Eq. (C.6a) may be written in its integral form as

$$\delta\rho_k(t) = \delta\rho_k(0) + ik \int_0^t dt' j_k(t'). \quad (\text{C.7})$$

Recall, in the Navier-Stokes equation, we ignored any temperature fluctuations. Thus, as a working assumption, we are considering an ensemble with constant temperature and a fixed number of particles N . Thus, we write the variations in pressure as

$$\delta p = \left[\frac{\delta p}{\delta \rho} \right]_{N,T} \delta \rho \quad (\text{C.8})$$

From thermodynamics [70], we identify this as

$$\left[\frac{\delta p}{\delta \rho} \right]_{N,T} = \frac{1}{\rho \chi_T}, \quad (\text{C.9})$$

where χ_T is the isothermal compressibility of the system. Defining, $2\nu_l = \nu_l$, where ν_l is the longitudinal viscosity, we write Eq. (C.6b) as

$$\frac{\partial}{\partial t} j_k(t) - \frac{ik\delta\rho_k(t)}{m\rho\chi_T} = -\nu_l k^2 j_k(t). \quad (\text{C.10})$$

Inserting Eq. (C.7) into the above equation, we obtain

$$\frac{\partial}{\partial t} j_k(t) = -\frac{k^2}{m\rho\chi_T} \int_0^t dt' j_k(t') - \nu_l k^2 j_k(t) + \frac{ik}{m\rho\chi_T} \delta\rho_k(0) \quad (\text{C.11})$$

The longitudinal current density auto-correlation function is defined as [69]

$$C(k, t) = \langle j_k^*(0) j_k(t) \rangle. \quad (\text{C.12})$$

Multiplying Eq. (C.11) by $j_k(0)^*$ and ensemble averaging,

$$\frac{\partial}{\partial t} C(k, t) = -\frac{k^2}{m\rho\chi_T} \int_0^t dt' C(k, t') - \nu_l k^2 C(k, t), \quad (\text{C.13})$$

where $\frac{ik}{m\rho\chi_T} \langle \rho_k(0) j_k^*(0) \rangle$ vanishes by symmetry [69], as can be seen by multiplying Eq. (C.6a) with $\rho_k(0)^*$ and ensemble averaging the resultant expression, evaluated at $t = 0$. Further, it

can be shown that $\langle \frac{\partial \rho_{\mathbf{k}}(t)}{\partial t} \rho_{\mathbf{k}}^*(0) \rangle_{t=0}$ vanishes [69], producing the desired result.

The power spectrum of the longitudinal current density auto-correlation function can now be obtained as the Fourier transform of the longitudinal current density auto-correlation function or equivalently, as the real part of the one sided Laplace transform [70] of the current density auto-correlation function, evaluated at $s = i\omega$, which we call $P(\mathbf{k}, \omega) = \Re\{\mathcal{L}[C(\mathbf{k}, t)]\}_{s=i\omega}$. Thus, taking the Laplace transform of Eq. (C.13), we obtain

$$sP(\mathbf{k}, s) - P(\mathbf{k}, 0) = -\frac{k^2}{m\rho\chi_T} \frac{P(\mathbf{k}, s)}{s} - \nu_l k^2 P(\mathbf{k}, s), \quad (\text{C.14})$$

and therefore,

$$P(\mathbf{k}, s) = P(\mathbf{k}, 0) \frac{s}{s^2 + \omega_0^2 + s\nu_l k^2}, \quad (\text{C.15})$$

where, we have defined $\omega_0^2 = \frac{k^2}{m\rho\chi_T}$. Taking twice the real part, evaluated for $s = i\omega$, we finally obtain

$$P(\mathbf{k}, s) = 2P(\mathbf{k}, 0) \frac{\omega^2 \nu_l k^2}{[\omega^2 - \omega_0^2]^2 + (\omega \nu_l k^2)^2}, \quad (\text{C.16})$$

that is Eq. (4.7) in the main text. Note, for fluids, the constant $P(\mathbf{k}, 0) = v_{\text{th}}^2$ is basically square of the average thermal speed of particles [69].

FLUCTUATION DISSIPATION THEOREM

In this section, we will review the derivation for the appropriate form of the noise term that along with a second order hydrodynamical damping term satisfies the fluctuation dissipation theorem [64]. Consider the discrete set of equations

$$\begin{aligned}\frac{dp_n}{dt} &= t_n + f_n^{\text{Noise}} + f_n^{\text{Damping}}, \\ \frac{dx_n}{dt} &= \frac{p_n}{M},\end{aligned}\quad (\text{D.1})$$

where,

$$t_n = -\frac{\partial H}{\partial x_n} = -\frac{\partial U}{\partial x_n}, \quad (\text{D.2})$$

$$f_n^{\text{Damping}} = m\nu \left(\frac{dx_{n+1}}{dt} - 2\frac{dx_n}{dt} + \frac{dx_{n-1}}{dt} \right), \quad (\text{D.3})$$

and we need to determine the form of f_n^{Noise} that satisfies the fluctuation dissipation theorem. Here, p_n denotes the momentum, x_n the longitudinal displacement from its equilibrium position of the n -th particle with mass m and velocity dx_n/dt . The Hamiltonian is $H = K + U$, where $K = \sum_n \frac{p_n^2}{2m}$ is the kinetic energy and $U = \sum_n V[x_{n+1} - x_n]$ is the potential energy for a general inter-particle potential V that depends upon the relative displacement between neighbouring masses.

Taking the discrete (spatial) Fourier transform of Eqs. (D.1), i.e., $x_n = \frac{1}{\sqrt{N}} \sum_k \exp(-ikn)X_k$ and $p_n = \frac{1}{\sqrt{N}} \sum_k \exp(-ikn)P_k$ we obtain

$$\begin{aligned}\frac{dP_k}{dt} &= T_k + F_k^{\text{Noise}} + \nu [\exp(-ik) + \exp(ik) - 2] \frac{dX_k}{dt}, \\ \frac{dP_k}{dt} &= T_k + F_k^{\text{Noise}} - \nu\gamma_k P_k, \\ \frac{dX_k}{dt} &= \frac{P_k}{M}.\end{aligned}\quad (\text{D.4})$$

where, from the damping term we have defined

$$\gamma_k = 2 [1 - \cos(k)]. \quad (\text{D.5})$$

We define

$$F_k^{\text{Noise}}(t) = \sqrt{D(k)} \xi_k(t), \quad (\text{D.6})$$

where, $\xi_k(t)$ is a delta correlated white noise,

$$\langle \xi_k(t) \xi_{k'}(t') \rangle = \delta(t - t') \delta_{k, -k'} \quad (\text{D.7})$$

and $D(k)$ is to be determined.

The associated multi-dimensional Fokker-Planck equation [67] of Eqs. (D.4) takes the form

$$\partial_t \rho = \sum_k \left[-\partial_{P_k} (T_k \rho_k) - \frac{P_{-k}}{M} \partial_{X_{-k}} \rho_k + \nu \gamma_k \partial_{P_k} \left(P_k \rho_k + \frac{D(k)}{2\nu \gamma_k} \partial_{P_{-k}} \rho_k \right) \right] \quad (\text{D.8})$$

where, $\rho = \langle \prod_k \delta [P_k - P_k(t)] \delta [X_k - X_k(t)] \rangle$.

In order to determine $D(k)$, we assume the stationary solution of Eq. (D.8) to be the Boltzmann distribution, i.e.,

$$\rho = N \exp \left(-\frac{H}{k_B T} \right), \quad (\text{D.9})$$

where H is the Hamiltonian and N is a normalization constant. Substituting Eq. (D.9) into Eq. (D.8), we find that for a stationary distribution the left hand side must be zero. Consider, the first term on the right hand side

$$-\partial_{P_k} (T_k \rho_k) = -\rho_k \partial_{P_k} T_k - T_k \partial_{P_k} \rho_k \quad (\text{D.10})$$

$$= 0 - T_k \frac{\partial \rho_k}{\partial H} \frac{\partial H}{\partial P_k} \quad (\text{D.11})$$

$$= \frac{T_k P_{-k} \rho}{M k_B T}, \quad (\text{D.12})$$

where we have used $\frac{\partial H}{\partial P_k} = \frac{P_{-k}}{2M}$ since in Fourier space, the kinetic part of the Hamiltonian assumes the form $K = \sum_k \frac{P_k P_{-k}}{2M}$. Similarly, the second term on the right evaluates to

$$-\frac{P_{-k}}{M} \partial_{X_{-k}} \rho_k = -\frac{P_{-k}}{M} \frac{\partial \rho_k}{\partial H} \frac{\partial H}{\partial X_{-k}} \quad (\text{D.13})$$

$$= -\frac{T_k P_{-k} \rho}{M k_B T}, \quad (\text{D.14})$$

where we have used the relation $T_k = -\frac{\partial H}{\partial X_{-k}}$ (as can be checked for instance if the inter-particle potential is harmonic). Thus, the first two terms on the the right cancel out. Equating the third on the right of Eq. (D.8) to zero, we obtain

$$P_k \rho_k + \frac{D(k)}{2\nu \gamma_k} \frac{\partial \rho_k}{\partial H} \frac{\partial H}{\partial P_{-k}} = 0, \quad (\text{D.15})$$

$$P_k \rho_k - \frac{D(k)}{2\nu \gamma_k} \frac{\rho_k}{k_B T} \frac{P_k}{M} = 0, \quad (\text{D.16})$$

and therefore,

$$D(k) = 2\nu\gamma_k M k_B T. \quad (\text{D.17})$$

Now, from Eqs. D.6 and D.17, the noise term in position space is

$$f_n^{\text{noise}}(t) = 2\sqrt{2\nu M k_B T} \frac{1}{\sqrt{N}} \sum_k \exp(-ikn) \sin\left(\frac{k}{2}\right) \xi_k(t) \quad (\text{D.18})$$

Therefore,

$$\frac{N \langle f_n^{\text{noise}}(t) f_{n'}^{\text{noise}}(t') \rangle}{8\nu M k_B T} = \sum_k \sum_{k'} \exp(-i[kn + k'n']) \sin\left(\frac{k}{2}\right) \sin\left(\frac{k'}{2}\right) \langle \xi_k(t) \xi_{k'}(t') \rangle.$$

Substituting the relation from Eq. (D.7) in the above equation, we obtain

$$\frac{N \langle f_n^{\text{noise}}(t) f_{n'}^{\text{noise}}(t') \rangle}{4\nu M k_B T} = -\delta(t - t') \sum_k \exp[-ik(n - n')] (1 - \cos(k)).$$

Taking the Fourier transform of the above equation, noting that

$$\begin{aligned} \frac{1}{N} \sum_k \exp[-ik(n - n')] &= \delta_{n,n'} \\ \frac{1}{N} \sum_k \exp[-ik(n - n')] \cos(k) &= \frac{1}{2} (\delta_{n,n'+1} + \delta_{n,n'-1}), \end{aligned}$$

we find,

$$\langle f_n^{\text{noise}}(t) f_{n'}^{\text{noise}}(t') \rangle = -2\nu M k_B T \delta(t - t') (\delta_{n+1,n'} - 2\delta_{n,n'} + \delta_{n-1,n'}).$$

This relation can be satisfied by defining

$$f_n^{\text{noise}}(t) = \sqrt{2\nu M k_B T} [\xi_{n+1}(t) - \xi_n(t)] \quad (\text{D.19})$$

with

$$\langle \xi_n(t) \xi_{n'}(t') \rangle = \delta(t - t') \delta_{n,n'}. \quad (\text{D.20})$$

This is the fluctuation dissipation theorem we use in Eq. (5.3) in the main text.

LINEAR NON-QUASISTATIC REGIME

In the following supplementary section, we will solve for the analytic form of the transverse velocity field when the response of the random spring network falls in the linear frequency dependent regime. The derivation therefore rests on knowing the frequency dependent elastic moduli. In addition, we will see how the same solution can be arrived at by starting with a fractional diffusion equation in real space and time. Here, the fractional exponent can be read off from the super-diffusive exponent that characterizes the broadening of the shear front width at early times.

E.1 FROM OSCILLATORY RHEOLOGY

Consider the general frequency dependent constitutive relation for a linear visco-elastic material:

$$\sigma(s) = G(s)\gamma(s) , \quad (\text{E.1})$$

where, $G(s)_{s=i\omega} = G'(\omega) + iG''(\omega)$ is the (Laplace transformed) complex modulus, whose real and imaginary parts correspond to the storage and loss modulus respectively. The field $\sigma(s) \equiv \sigma_{xy}(s)$ denotes the shear stress and $\gamma(s) \equiv \gamma_{xy}(s)$ the shear strain. The general frequency dependent constitutive stress-strain relation Eq. (E.1) corresponds to the following convolution integral in the time domain,

$$\sigma(x, t) = \int_0^t G(\tau)\gamma(x, t - \tau)d\tau. \quad (\text{E.2})$$

Substituting into the equation of motion

$$\frac{\partial \sigma(x, t)}{\partial x} = \rho \frac{\partial^2 u(x, t)}{\partial t^2} \quad (\text{E.3})$$

and defining $v(x, t) = \frac{\partial u(x, t)}{\partial t}$, we obtain (interchanging the order of integration and differentiation),

$$\int_0^t G(\tau) \frac{\partial \gamma(x, t - \tau)}{\partial x} d\tau = \rho \frac{\partial v(x, t)}{\partial t}. \quad (\text{E.4})$$

Differentiating once with respect to time t , we find

$$\left[G(\tau) \frac{\partial \gamma(x, t - \tau)}{\partial x} \right]_{\tau=t} + \int_0^t G(\tau) \frac{\partial^2 \gamma(x, t - \tau)}{\partial x \partial t} d\tau = \rho \frac{\partial^2 v(x, t)}{\partial t^2}. \tag{E.5}$$

Since $\gamma(x, t) = \frac{\partial u(x, t)}{\partial x}$, the first term in the square brackets can be expressed as $G(t) \frac{\partial^2 u(x, 0)}{\partial x^2}$, which evaluates to 0, since there is no displacement field at $t = 0$. Therefore,

$$\frac{\partial^2}{\partial x^2} \int_0^t G(\tau) v(x, t - \tau) d\tau = \rho \frac{\partial^2 v(x, t)}{\partial t^2}. \tag{E.6}$$

Transforming back to Laplace time (noting that the first term is just the convolution integral), we obtain

$$G(s) \frac{\partial^2 v(x, s)}{\partial x^2} = \rho s^2 v(x, s) - \rho s [v(x, t)]_{t=0} - \rho \left[\frac{\partial v(x, t)}{\partial t} \right]_{t=0} \tag{E.7}$$

Since we are solving in the domain $x > 0$, our initial condition is $v(x > 0, 0) = 0$ and boundary condition is $v(x = 0, t) = v_0$. Thus, the two terms on the right are 0 leaving us with

$$\frac{\partial^2 v(x, s)}{\partial x^2} = \frac{\rho s^2}{G(s)} v(x, s). \tag{E.8}$$

This is an ordinary differential equation in x , solving which we obtain:

$$v(x, s) = \frac{v_0}{s} \exp \left(x \frac{s}{\sqrt{G(s)}} \right). \tag{E.9}$$

In oscillatory rheology, it is found that in the frequency dependent regime, the elastic moduli scale as $G(s) \sim s^{\frac{1}{2}}$. In the following, we thus express the term in the exponent more generally as: $\frac{s}{\sqrt{G(s)}} = s^{\frac{\alpha}{2}}$.

Let us define the sine-Fourier transform of a function $f(x)$ in the x - domain valid for $0 < x < \infty$ as

$$F(k) = \int_0^\infty f(x) \sin(kx) dx. \tag{E.10}$$

Taking the sine-Fourier transform of Eq. (E.9), we obtain

$$v(k, s) = \frac{v_0}{s} \frac{2k}{s^\alpha + k^2}. \quad (\text{E.11})$$

This can be written as

$$v(k, s) = \frac{2kv_0}{k^2} \left(\frac{1}{s} - \frac{s^{\alpha-1}}{s^\alpha + k^2} \right). \quad (\text{E.12})$$

Now, the Laplace inverse of

$$\left(\frac{s^{\alpha-1}}{s^\alpha + k^2} \right) \rightarrow E_{\alpha,1}[-k^2 t^\alpha], \quad (\text{E.13})$$

where $E_{\alpha,\beta}$ is the generalized Mittag-Liffler function [78]

$$E_{\alpha,\beta}(z) = \sum_{n=0}^{\infty} \frac{z^n}{\Gamma(\alpha n + \beta)}. \quad (\text{E.14})$$

Therefore, the inverse Laplace transform of Eq. (E.12) reads:

$$v(k, t) = \frac{2v_0}{k} \left(1 - E_\alpha[-k^2 t^\alpha] \right). \quad (\text{E.15})$$

and inverting in k space, we obtain the transverse velocity field :

$$v(x, t) = 2v_0 \int_0^\infty \frac{\sin(kx)}{k} \left(1 - E_\alpha[-k^2 t^\alpha] \right) dk. \quad (\text{E.16})$$

This equation can be expressed more concisely by defining a new variable $\omega = kt^{\frac{\alpha}{2}}$. Then, the integral can be represented in terms of just one similarity variable:

$$v(x, t) = 2v_0 \int_0^\infty \frac{\sin(\omega\eta)}{\omega} \left(1 - E_\alpha[-\omega^2] \right) d\omega, \quad (\text{E.17})$$

where $\eta = \frac{x}{t^{\frac{\alpha}{2}}}$ is the similarity variable.

As a check for the convergence of the integral solution, consider the special case where $\alpha = 1$. This corresponds to the ordinary diffusion equation. Then, the integrals can be solved by noting that

$$E_{1,1}(-k^2 t) = \exp(-k^2 t). \quad (\text{E.18})$$

Further,

$$\int_0^\infty \frac{\sin(kx)}{k} = \frac{\pi}{2}, \quad (\text{E.19})$$

and

$$\int_0^\infty \frac{\sin(kx)}{k} \exp(-k^2 t) = \frac{\pi}{2} \operatorname{erf} \left(\frac{x}{2t^{\frac{1}{2}}} \right). \quad (\text{E.20})$$

E.2 FRACTIONAL EQUATION

Although, we do not make extensive use of it, as an interesting mathematical aside, one way to model regimes of anomalous diffusion is to write down an analogue of Eq. (6.11), but with fractional derivatives (in time or space). A space fractional diffusion equation takes the form

$$\frac{\partial u}{\partial t} = D \frac{\partial^\alpha u}{\partial x^\alpha}, \quad (\text{E.21})$$

where $\alpha = \frac{2}{\xi}$. Here, we have used fractional derivatives with respect to the spatial coordinates only and the fractional derivatives are interpreted in the sense described by Caputo [77]. Note, if $\alpha = 1$, we recover the one dimensional wave equation (half-wave equation), while for $\alpha = 2$ ($\xi = 1$), we obtain the ordinary diffusion equation. Similar to ordinary derivatives, a Fourier- transform of Eq. (E.21) can also be defined and leads to the general kernel

$$u(k, t) \sim \exp(t(-ik)^\alpha), \quad (\text{E.22})$$

with a response time

$$t_r = \frac{1}{Dk^\alpha}. \quad (\text{E.23})$$

Note, for $\alpha = 2$, we recover Eq. (6.13). Moreover, Eq. (E.23) corresponds dimensionally to a similarity solution of the form $\left(\frac{x}{t^{\frac{1}{\alpha}}}\right)$. For $\alpha = 4/3$, this gives us $\left(\frac{x}{t^{\frac{3}{4}}}\right)$ that is consistent with the super-diffusive growth of the width at early times in Fig. (6.2).

Note, from our observations in Fig. (6.2), we could also have started with a time fractional version of the diffusion equation in real space-time variables [77, 78] :

$$\frac{\partial^\alpha u}{\partial t^\alpha} = D \frac{\partial^2 u}{\partial x^2}. \quad (\text{E.24})$$

Once again, we can take the Laplace transform in time domain and a sine-Fourier transform in x , to obtain Eq. (E.11) for the initial condition $v(0, s) = \frac{v_0}{s}$. Thus, the two approaches give the same solution. Note, the use of fractional derivatives naturally takes into account the non-locality implicit in the convolution in Eq. (E.2).

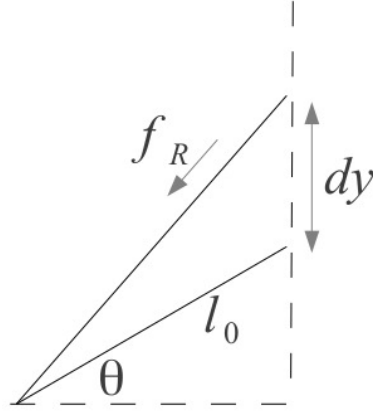


Figure E.1: A harmonic spring with equilibrium length l_0 , initially lying at an angle θ in the $x - y$ plane. One end of the spring is then moved up by an amount dy , to calculate the resultant force in the new position f_R .

E.3 NON-LINEARITY FROM HARMONIC SPRINGS

As a concluding remark, note that, although the spring networks we have considered are composed of harmonic springs, for high strains, the network response becomes non-linear. Although the actual mechanisms for the vanishing of the linear response in a disordered network of springs is fairly complex and involves a collective softness, the origins of nonlinearity can be traced to the simple picture depicted in Fig. (E.1). In particular, if we consider a spring with an equilibrium length l_0 lying at an angle θ in the $x - y$ plane, and move one of its ends by a small amount dy along the y -direction (for instance, the spring can be thought of the boundary spring that is sheared in the y -direction), then the force along the direction of the spring is

$$f = -(\sqrt{(l_0 \sin \theta + dy)^2 + (l_0 \cos \theta)^2} - l_0). \quad (\text{E.25})$$

By squaring and Taylor expanding the terms inside the square root, we find the force

$$f \approx -\left(dy \sin \theta + \frac{(dy)^2}{2l_0} \right). \quad (\text{E.26})$$

Consequently, the return force in the direction of shearing is

$$f_y \approx -\left(dy \sin \theta + \frac{(dy)^2}{2l_0} \right) \frac{(dy + l_0 \sin \theta)}{l_0}, \quad (\text{E.27})$$

that yields

$$f_y \approx -\frac{1}{l_0} \left(dy l_0 \sin^2 \theta + \frac{3}{2} (dy)^2 \sin \theta + \frac{dy^3}{2l_0} \right). \quad (\text{E.28})$$

Thus, the dominant non-linearity (second term on the right) is quadratic in displacement dy . For a more rigorous argument that also correctly accounts for the vanishing linear response, see [2].

IDEAS FOR FURTHER WORK ON THERMAL
AND QUANTUM FLUCTUATIONS

As discussed in Chapter 6, a two dimensional random network of springs becomes rigid when the mean connectivity $\langle z \rangle$ exceeds a critical isostatic value $z_c = 4$. Here, the onset of rigidity is a purely geometrical or mechanical phenomenon. In Chapter 5, we discussed that thermal fluctuations can introduce rigidity in a chain of (un-stressed) non-linear springs, that a-priori has no linear response. Similarly, a network of freely jointed chains that are often used as a simple model for polymers, can display a purely entropic elasticity with a shear modulus that grows linearly with temperature, i.e., $G \sim T$ [54].

Many systems however fall in an intermediate regime, where the rigidity arises from an interplay between network geometry and coupling to a source of fluctuation. In a recent study on such a model (a two dimensional random network of diluted springs), it is shown that the shear modulus scales sub-linearly with temperature, i.e., $G \sim T^\alpha$, with $0 < \alpha < 1$ [54]. Note, $\alpha = 1$ corresponds to the regime of purely entropic elasticity (such as freely jointed chains), while $\alpha = 0$ gives a shear modulus that is independent of temperature as for instance, can be expected for elastic spring networks well above the isostatic point, i.e., $z \gg z_c$.

However, so far much less is known about the role of quantum fluctuations (zero point motion) on the mechanical properties of fragile systems. For example, at the microscopic level, network glasses can be viewed as a random network of harmonic springs. An intriguing question then is: can the quantum zero point motion of network nodes induce the equivalent of an entropic (thermally induced) rigidity as the temperature is lowered ?

Thus, if amorphous materials can indeed be modelled as a random network of harmonic springs with a tune-able connectivity, then close the isostatic point, their elastic properties and specific heat can be expected to be profoundly effected by network connectivity and quantum and thermal fluctuations [80]. In this final chapter, we therefore discuss some initial ideas exploring this direction, by studying the effects of thermal and

quantum fluctuations on the rigidity of a random network of harmonic springs that are derived from jammed packings prepared at vanishingly small pressure. We discuss a simple method that allows us to approximately model both thermal and quantum fluctuations within a classical simulation, by coupling the system to a source of noise given by the Bose-Einstein spectrum. In the low temperature limit, this allows us to study the effects of quantum zero point motion within a purely classical approximation, while the high temperature limit, allows us to study the role of purely thermal fluctuations.

F.1 APPROXIMATE METHOD TO SIMULATE QUANTUM ZERO POINT ENERGY

Due to quantum fluctuations, the energy of the system at zero temperature, called the zero point energy, is larger than the potential energy minimum. This property is a direct consequence of the quantization of the energy of the vibrational modes. An intriguing, albeit approximate method, that allows us to incorporate zero point motion within a classical description of particle dynamics, is to consider a Langevin equation of the form Eq. (5.1), but with the source of Gaussian noise replaced with coloured noise with an appropriate power spectral density. This method thus consists of modelling the zero point motion as a quantum bath, that is analogous to a thermal bath, but with a different source of noise. In this way, the correct zero point energy for a harmonic oscillator can be obtained [68, 75, 73].

What is the nature of the noise term? In the next sub-section, we outline an intuitive method to see the appropriate power spectral density of the noise term that allows us to correctly obtain the energy of a simple harmonic oscillator. We then apply this method to study a one dimensional chain of harmonic oscillators and then, a two dimensional random network of harmonic springs.

F.1.1 Simple harmonic oscillator

Consider the equations of motion for a simple harmonic oscillator, akin to the Langevin equation that we considered in Chapter 5 Eq. (5.1), leaving the noise source $\Theta(t)$ as yet unspecified:

$$\frac{dx}{dt} = v, \quad (\text{F.1})$$

$$\frac{dv}{dt} = -\omega_0^2 x - \gamma v + \sqrt{2\gamma}\theta(t) \quad (\text{F.2})$$

where, x is the displacement from the equilibrium position, v is the speed, γ is the external drag and $\Theta(t)$ is a source of fluctuation. Here, we have set mass $m = 1$ and the oscillator frequency is ω_0 . Fourier transforming the equations Eq. (F.1) using $X(\omega) = \int x(t)e^{-i\omega t}$, $V(\omega) = \int v(t)e^{-i\omega t}$ we obtain

$$X(\omega) = \sqrt{2\gamma} \frac{\Theta(\omega)}{\omega_0^2 - \omega^2 + i\omega\gamma}, \quad (\text{F.3})$$

$$V(\omega) = \sqrt{2\gamma} \frac{i\omega\Theta(\omega)}{\omega_0^2 - \omega^2 + i\omega\gamma}. \quad (\text{F.4})$$

The power spectral density corresponding to the random variables $x(t), v(t)$ is $|X(\omega)|^2, |V(\omega)|^2$ respectively. Therefore, the ensemble averaged energy of the oscillator is

$$E(\omega) = \int \frac{d\omega}{2\pi} \left(\frac{1}{2} \omega_0^2 |X(\omega)|^2 + \frac{1}{2} |V(\omega)|^2 \right), \quad (\text{F.5})$$

$$= \int \frac{d\omega}{2\pi} \gamma \frac{\omega^2 + \omega_0^2}{(\omega^2 - \omega_0^2)^2 + \omega^2 \gamma^2} \Theta(\omega). \quad (\text{F.6})$$

Here, $\Theta(\omega)$ is the power spectral density of the noise.

For small damping γ , the poles of Eq. (F.6) are $\omega = \pm\omega_0 \pm i\gamma/2$, to leading order in γ . Solving by residues, we find that for a constant $\Theta(\omega)$, integration of Eq. (F.6) gives a constant that is independent of the drag γ . If we choose the constant $\Theta(\omega) = k_B T$ (independent of ω as in the Langevin equation), integration of Eq. (F.6), reproduces the classical equipartition theorem, where the energy is just equal to the thermal energy.

Similarly, for a frequency dependent $\Theta(\omega)$, integration of Eq. (F.6) gives $E \approx \Theta(\omega_0)$, to leading order in γ . Hence, by choosing

$$\Theta(\omega) = \hbar|\omega| \left(\frac{1}{2} + \frac{1}{\exp\left(\frac{\hbar\omega}{k_B T}\right) - 1} \right) \quad (\text{F.7})$$

and a value for γ small enough compared to the characteristic frequency ω_0 , we can ensure that the energy of the oscillator is given by the Bose-Einstein distribution Eq. (F.7) including the zero point energy.

Note, in these equation, no operators are involved. This is truly a classical approximation of the quantum zero point energy, where we are assuming that the quantum fluctuations are akin to thermal fluctuations, causing the particle position and velocity to fluctuate in time. For a detailed derivation of this classical approximation beginning with the coherent state description, see ref [68].

F.2 CHAIN OF HARMONIC OSCILLATORS

As a first step towards checking whether the above equations correctly reproduce the energy of a harmonic oscillator, we simulate a one dimensional chain of $N = 1024$ harmonic oscillators, where each particle is coupled to a source of noise $\Theta(t)$ and drag γ , and therefore satisfies an equation of the form Eq. (F.1). For more details on how to construct an approximate noise source in time domain that has the power spectral density given in Eq. (F.7), see section F.4.

In Fig. (F.1), we plot the numerically obtained energy (red circles) of the chain of harmonic oscillators against the Temperature, and compare it with the analytic expression given by the Bose-Einstein distribution Eq. (F.7), finding a reasonably good agreement. In these plots, we have used reduced units where energy is specified in units of ka^2 , where k is the bare spring constant and a is the lattice spacing. In Fig. (F.2), we also verify that in equilibrium, the energy is equally partitioned between the quadratic degrees of freedom (i.e., the kinetic and potential energies). Here, the equilibration time is set by the inverse of the drag coefficient γ .

F.3 RANDOM NETWORK OF HARMONIC SPRINGS

We now study a random network of harmonic springs derived from jammed packings (see Fig. 6.1) that have been prepared at a vanishingly small pressure so that the mean overlap between disks δ is nearly 0. For such networks of harmonic springs, the shear modulus scales linearly with the excess coordination number $G \sim dz = z - z_c$, where z is the average coordination number per node and $z_c = 4$ is the critical coordination num-

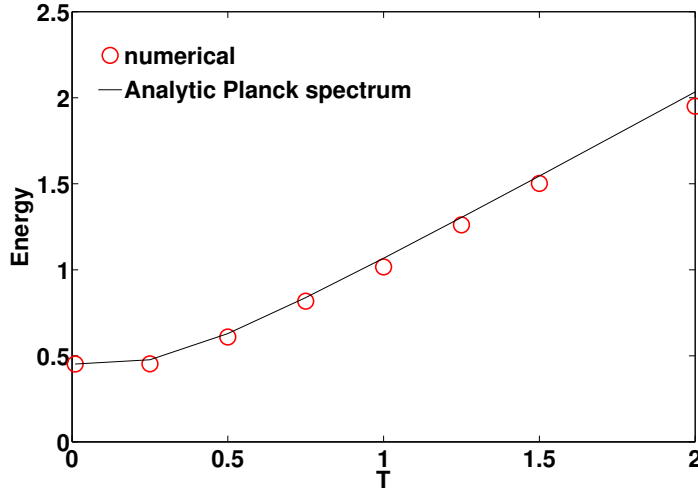


Figure F.1: Comparison of analytical Planck spectrum (solid black curve) against the energy of a chain of harmonic oscillators obtained numerically (red dots). Here, $\hbar\omega_0 = 1.0$. Note, unlike the case of a classical simulation where the energy at zero temperature would be zero, here the energy levels off to around 0.45, close to the expected zero point energy. Here, energy is measured in units of ka^2 , where k is the bare spring constant and a is the equilibrium lattice spacing.

ber in two dimensions. At the same time, the bulk modulus remains finite at the critical point and is nearly independent of dz as we move further away from the critical point.

We now couple the nodes of the two dimensional network of harmonic springs to a source of noise, modelled by the Bose-Einstein spectrum, Eq. (F.7) and study the equilibrium properties of the network. As a first step, in Fig. (F.3), we plot the numerically obtained energy (red circles) of this system against the Bose-Einstein distribution Eq. (F.7), where we find a reasonably good match for a range of ratios $\hbar\omega_0/k_B T$.

F.3.1 Fluctuation induced rigidity

Next, we study the long wavelength small frequency longitudinal and shear modes, using a procedure similar to the one

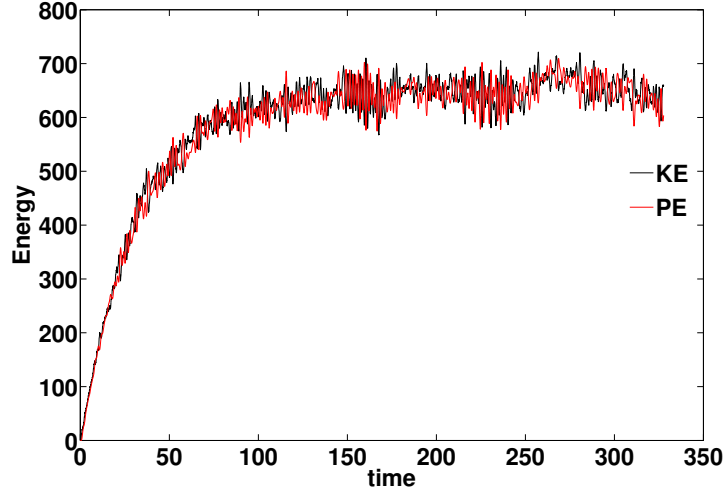


Figure F.2: Confirmation of the equipartition between kinetic (black) and potential (red) energies in a chain of harmonic oscillators at $\hbar = 1.0$ and $T = 1.25$.

outlined in Chapter 4. Note, the Bose-Einstein distribution has the following asymptotic forms:

$$\Theta(\omega) = \frac{1}{2}\hbar|\omega|; T \rightarrow 0 \quad (\text{F.8})$$

$$\Theta(\omega) = k_B T; T \rightarrow \infty, \quad (\text{F.9})$$

$$(\text{F.10})$$

that correspond to the quantum and classical limits respectively. In Fig. (F.4), we therefore probe these limits and plot the numerically obtained dispersion curves (obtained analogously to the procedure described in Chapter 5) for the shear modes, as a function of reduced temperature T (left panel) and reduced \hbar (right panel). As expected from the physics near the vicinity of the critical point, the slopes of the dispersion curves explicitly depend upon the energy of the fluctuation, i.e., the temperature or \hbar . Moreover, for random networks derived from jammed packings, the bulk modulus remains finite at the critical point and accordingly, the longitudinal dispersion curves remain nearly independent of temperature (see scaling in Figs. (F.6)-(F.7)).

In order to check the correctness of this procedure, i.e., the use of hydrodynamical modes to estimate the elastic modulus of spring networks, we plot in Fig. (F.5), the scaling of the shear (black circles) and bulk modulus (blue circles) as a function of the energy of pre-compression for spring networks derived

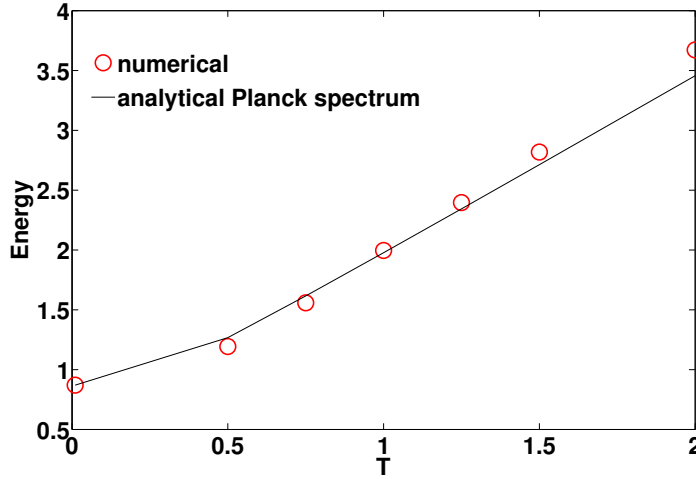


Figure F.3: Comparison of analytical Planck spectrum (solid black curve) against the energy for a random network of springs obtained numerically (red dots). Here, $\hbar\omega_0 = 1.0$. Note, unlike the case of a classical simulation where the energy at zero temperature would be zero, here the energy levels off to around 0.9, close to the expected zero point energy that is 1.0 in two dimensions. Here, energy is measured in units of ka^2 , where k is the bare spring constant and a is the average equilibrium lattice spacing.

from jammed packings with varying initial compression and with vanishingly small temperature, so as to probe the elasticity of the network that stems only from the geometry of the network. In particular, for an interaction potential of the form δ^α , where δ is the average initial overlap between disks, the shear modulus is expected to scale as $G \sim \delta^{\alpha-3/2}$ and the bulk modulus as $B \sim \delta^{\alpha-2}$. For harmonic interaction with $\alpha = 2$, this leads to $G \sim \delta^{1/2}$ and $B \sim \delta^0$. In this case, the energy of the packing due to pre-compression is $E \sim \delta^2$ (harmonic potential), and therefore, $G \sim E^{1/4}$ with an exponent 0.25. In Fig. (F.5), we find a scaling with an exponent approximately 0.23, close to the expected value, while the bulk modulus remains independent of the energy.

In Figs. (F.6-F.7), we show the analogous scaling we obtain when we couple the spring network that is close to the critical point, to a source of finite temperature and \hbar . In this case, we find that the scaling differs from that expected at a finite pre-compression. Rather, the shear modulus seems to scale as $G \sim (k_B T)^{0.4}$ and $G \sim (\hbar\omega_0)^{0.4}$, in units of the square of the inverse

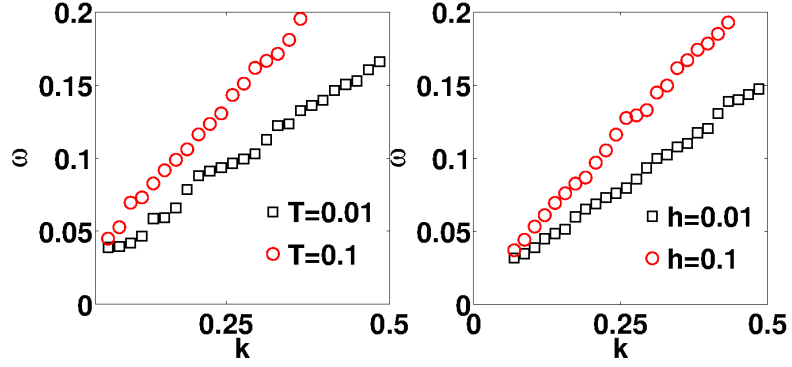


Figure F.4: The onset of shear rigidity due to thermal fluctuations (left panel) and classical approximation to quantum fluctuations (right panel). We define the shear rigidity as the square of the slopes of these curves.

lattice spacing. In these plots, the value of T and \hbar are chosen so that the energy induced by fluctuations is roughly comparable to the energies of the pre-compressed packings in Fig. (F.5) to allow for a more meaningful comparison.

F.4 SIMULATION

F.4.1 Planck Spectrum

The numerical implementation of the quantum bath reduces to generating a colored noise with a power spectral density $\Theta(\omega)$. Here, we adopt the numerical scheme suggested in reference [73, 74, 75].

For a continuous noise, we introduce the filter

$$H(\omega) = \sqrt{\Theta(\omega)}. \quad (\text{F.11})$$

and denote $H(t)$ as the inverse Fourier transform of $H(\omega)$. The noise $\Theta(t)$ can then be obtained by convolving $H(t)$ with a source of random noise $r(t)$, that has a power spectral density $R(\omega) = 1$. Therefore,

$$\Theta(t) = \int_{-\infty}^{\infty} H(s)r(t-s)ds. \quad (\text{F.12})$$

The power spectral density of the resulting noise is $|H(\omega)|^2R(\omega) = \Theta(\omega)$, which is the desired power spectral density.

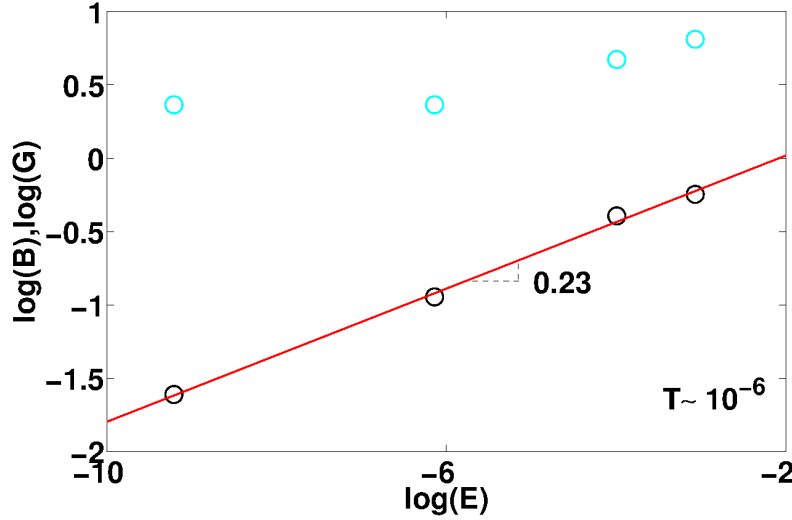


Figure F.5: The numerically computed shear (black circles) and bulk modulus (blue circles) plotted against the energy of the spring networks derived from jammed packings at various pre-compressions. These plots are obtained at a vanishingly small temperature, so the moduli scale with the pre-compression or network geometry. We find the bulk modulus is nearly independent of the pre-compression while the shear modulus scales approximately as $G \sim E^{1/4} \sim \delta^{1/2}$.

Numerically, this can be implemented as follows. The filter $H(\omega)$ is first discretized in $2N$ values with steps $d\omega$ over an interval $[-\Omega_{\max}, \Omega_{\max}]$:

$$H_k = H(kd\omega), k = -N \dots N - 1. \quad (\text{F.13})$$

On physical grounds, the cut-off frequency can be chosen to be around the maximum frequency for a harmonic oscillator $\sqrt{K/m}$, where K is the spring constant and m is the mass. Subsequently, we take the discrete Fourier transform of H_k :

$$H_n = \frac{1}{2N} \sum_{-N}^{N-1} H_k \cos\left(\frac{\pi}{N} kn\right). \quad (\text{F.14})$$

Finally, we perform the discrete convolution

$$\Theta_n = \sum_{-N}^{N-1} H_m r_{n-m}, \quad (\text{F.15})$$

where r is a normal random variable.

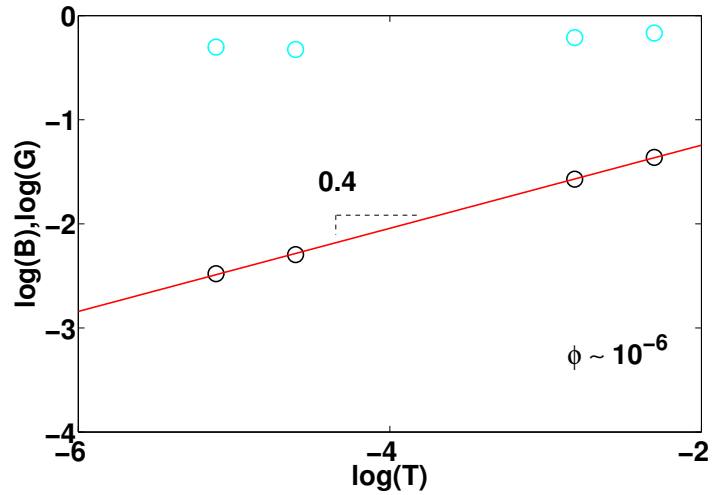


Figure F.6: The numerically computed shear (black circles) and bulk modulus (blue circles) plotted against the thermal energy for nearly isostatic spring networks derived from jammed packing at vanishingly small pre-compression ϕ .

F.4.2 Limiting forms

Note, the classical high temperature limit of the Planck spectrum is $k_B T$. Thus, the same procedure outlined above can be used to simulate a classical system coupled to a heat bath, as in Chapter 5. Further, for the numerical integration, we use a modified form of the velocity Verlet method that in the limit $\hbar \rightarrow 0, k_B T \rightarrow 0$ and drag $\gamma \rightarrow 0$, reduces to the velocity verlet method [71].

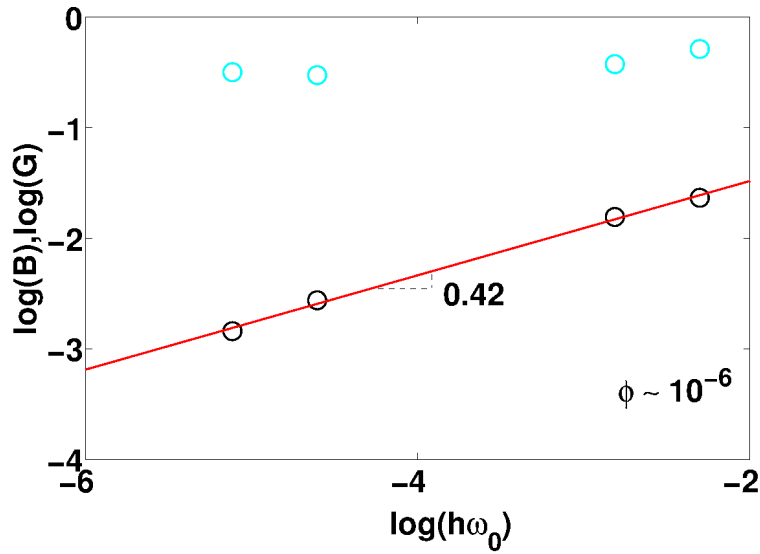


Figure F.7: The numerically computed shear (black circles) and bulk modulus (blue circles) plotted against the quantum energy for nearly isostatic spring networks derived from jammed packing at vanishingly small pre-compression ϕ .

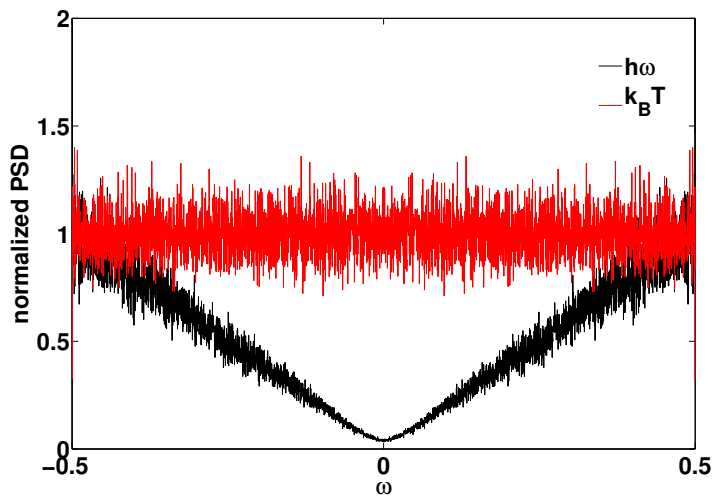


Figure F.8: Plots of the Planck spectrum obtained numerically for its asymptotic forms of high frequency (black) and high temperatures (red). The high frequency power increases linearly with frequency and corresponds to the quantum zero point motion, while the power spectrum density is a constant independent of frequency and proportional to $k_B T$ in the high temperature (classical) limit.

BIBLIOGRAPHY

- [1] V. Vitelli and M. van Hecke, *Euro Physics News* **43**, 6 (2012).
- [2] M. Wyart, H. Liang, A. Kabla and L. Mahadevan, *Phys. Rev. Lett.* **101**, 21 (2008).
- [3] W.G. Ellenbroek, Z. Zeravcic, W.V. Sarloos and M.V. Hecke, *Eur. Phys. Lett.* **109**, 34004 (2009).
- [4] B. Tighe, *Phys. Rev. Lett.* **107**, 15 (2011).
- [5] L. D. Landau and E.M. Lifshitz, *Theory of elasticity* (Pergamon press, 1970).
- [6] V. F. Nesterenko, *Dynamics of Heterogeneous Materials* (Springer-Verlag, New York, 2001), Chap. 1.
- [7] S.V.D Wildenberg, R.V. Loo and M.V. Hecke, arXiv:1304.6392 [cond-mat.soft] (2013).
- [8] S. R. Waitukaitis, L. K. Roth, V. Vitelli and H. M. Jaeger, *Eur. Phys. Lett.* **102** 2013.
- [9] S.Ulrich, N. Upadhyaya, B.V. Opheusden and V. Vitelli, arXiv:1307.7665 (2013).
- [10] A. J. Heeger, S. Kivelson, J. R. Schrieffer and W.-P. Su, *Rev. Mod. Phys.* **68**, 13 (1996).
- [11] S. Sen, J. Hong, J. Bang, E. Avalos, and R. Doney, *PhysicsReports* **462**, 21-66 (2008).
- [12] A. Spadoni and C. Daraio, *Proceedings of the National Academy of Sciences* **107**, 7230 (2010).
- [13] N. Boechler, G. Theocharis, and C. Daraio, *Nat. Mat.* **10**, 665 (2011).
- [14] V. F. Nesterenko, A. N. Lazaridi, and E. B. Sibiryakov, *Prikl. Mekh. Tekh. Fiz.* **36**, 19 (1995)[*J. Appl. Mech.Tech. Phys.*, **36**, 166 (1995)].
- [15] V. F. Nesterenko, *J. Phys. IV*, **4**, C8-729 (1994).

- [16] V. F. Nesterenko, C. Daraio, E. Herbold, S. Jin, *Phys. Rev. Lett.*, **95**, 158702 (2005).
- [17] S. Job, F. Melo, A. Sokolow, and S. Sen, *Granular Matter* **10**, 13 (2007).
- [18] A. N. Lazaridi and V. F. Nesterenko, *Prikl. Mekh. Tekh. Fiz.*, textbf26, 115 (1985)[*J. Appl. Mech. Tech. Phys.*, **26**, 405 1985)].
- [19] A. Sokolow, E.G. Bittle, S. Sen, *Europhys. Lett.*, **77**, 24002 (2007).
- [20] E. Somfai, J. N. Roux, J. H. Snoeijer, M. van Hecke, and W. van Saarloos, *Phys. Rev. E* **72**, 021301 (2005).
- [21] C. Daraio, V.F. Nesterenko, S. Jin Strongly nonlinear waves in 3d phononic crystals. In: Furnish, M.D., Gupta, Y.M., Forbes, J.W. (eds.) *Shock compression of condensed matter 2003*, Proceedings of the conference of the American physical society topical group on shock compression of condensed matter, vol 706, pp. 197200, AIP (2004).
- [22] E. J. Hinch and S. Saint-Jean, *Proc. R. Soc. A*, **455**, 3201 (1999).
- [23] C. Coste, E. Falcon, and S. Fauve, *Phys. Rev.E* **56**, 6104 (1997).
- [24] C. Daraio, V. F. Nesterenko, E. B. Herbold, and S. Jin, *Phys. Rev. E* **72**, 016603 (2005).
- [25] S. Sen, J. Hong, J. Bang, E. Avalos, and R. Doney, *Physics Reports* **462**, 21 (2008).
- [26] L. R. Gómez, A. M. Turner, M. van Hecke, and V. Vitelli, *Phys. Rev. Lett.* **108**, 058001 (2012).
- [27] L. R. Gómez, A. M. Turner and V. Vitelli, *Phys. Rev. E* **86**, 041302 (2012).
- [28] L. Vergara, *Phys. Rev. Lett.* **95**, 108002 (2005).
- [29] F. S. Manciu and S. Sen, *Phys. Rev. E* **66**, 016616 (2002).
- [30] M. P. Allen and D.J. Tildsey, *Computer simulation of liquids* (Oxford, New York, 1987).

- [31] C. Daraio, D. Ng, V. F. Nesterenko, F. Fraternali, *Phys. Rev. E* **82**, 036603 (2010).
- [32] V. F. Nesterenko, *J. Appl. Mech. Tech. Phys.* **5**, 733 (1984).
- [33] S. Sen, J. Hong, J. Bang, E. Avalos, and R. Doney, *Physics Reports* **462**, 21 (2008).
- [34] M. Manjunath, A.P. Awasthi, and P.H. Geubelle, *Phys. Rev. E* **85**, 031308 (2012).
- [35] S. van den Wildenberg, R. van Loo and M. van Hecke, *arXiv:1304.6392*, (2013).
- [36] K. Ahnert and A. Pikovsky, *Phys. Rev. E* **79**, 026209 (2009).
- [37] E. AVALOS, D. Sun, R.L. Doney and S. Sen, *Phys. Rev. E* **84**, 046610 (2011).
- [38] O.V. Zhirov, A.S. Pikovsky and D.L. Shepelyansky, *Phys. Rev. E* **83**, 016202 (2011).
- [39] A. Tichler *et al*, *Phys. Rev. Lett.*, **111**, 048001 (2013).
- [40] R. Zwanzig and M. Bixon, *Phys. Rev. A* **2**, 2005 (1970).
- [41] M.H. Ernst, E.H. Hauge and J.M.J. Leeuwen, *Phys. Rev. A* **4**, 2055 (1971).
- [42] M.H. Ernst, *Physica D* **47**, 198 (1991).
- [43] B.E. McDonald and D. Calvo , *Phys. Rev. E*, **85**, 066602 (2012).
- [44] M. Wadati, *J. Phys. Soc. Jap.* **59**, 12 (1990).
- [45] N. Upadhyaya, L. R. Gomez and V. Vitelli, *arXiv:1304.6692* , (2013).
- [46] V. Yakhot and Z. She, *Phys. Rev. Lett.*, **60**, 18 (1988).
- [47] O. Narayan and S. Ramaswamy, *Phys. Rev. Lett.*, **89**, 048001 (2002).
- [48] M. Kardar, *Statistical Physics of Fields*, (Cambridge University Press, 2007).
- [49] P. Rosenau, *Phys. Lett. A* **118**, 5 (1986).
- [50] A. Yethiraj, *Royal Socety of Chemistry*. **3**, 1099-1115 (2007).

- [51] D.E. Chang, J.I. Cirac and H.J. Kimble, *Phys. Rev. Lett.* **110**, 113606 (2013).
- [52] Z. Cheng, J. Shu, W.B. Russel and P.M. Chaikin, *Phys. Rev. Lett.* **85**, 7 (2000).
- [53] M. Sheinman, C.P. Broedersz and F.C. MacKintosh, *Phys. Rev. Lett.* **109**, 238101 (2012).
- [54] M. Dennison, M. Sheinman, C. Storm and F.C. MacKintosh, arXiv:1304.3500 (2013) .
- [55] A.S. Davydov, *J. Theor. Bio.*, **66**, 379 (1977).
- [56] T. Dauxois and M. Peyrard, *Physics of solitons* (Cambridge University Press, 2006).
- [57] C. S. O'Hern, L. E. Silbert, A. J. Liu, and S. R. Nagel, *Phys. Rev. E.* **68** 011306 (2003).
- [58] I. Atsushi, L. Berthier and G. Biroli, *J. Chem. Phys.* **138** 12A507 (2013)
- [59] N. Xu, T. K. Haxton, A. J. Liu, and S. R. Nagel, *Phys. Rev. Lett.* **103** 245701 (2009).
- [60] We are using "soliton" and "solitary wave" interchangeably to refer to a localized lump of energy; we do not assume anything about the equations being integrable.
- [61] For many waves or solitons, differentiating E with respect to P would give the group velocity or the speed of the wave's propagation, but this does not work for this case. (P is not the canonical momentum.)
- [62] N. Upadhyaya, A. M. Turner and V. Vitelli, arXiv:1304.6684 , (2013).
- [63] N.G. Van Kampen, *Stochastic processes in physics and chemistry* (Elsevier science publishers, 2007).
- [64] E. Arevalo, F.G. Mertens, Y. Gaididei and A.R. Bishop, *Phys. Rev. E.* **67**, 016610 (2003).
- [65] D.T. Gillespie, *Markov processes: an introduction for physical scientists* (Academic press, 1992).
- [66] D.S. Lemons, *An introduction to stochastic processes in physics* (The John Hopkins university press, 2002).

- [67] C.W. Gardiner, *Handbook of Stochastic Methods* (Springer, 1997).
- [68] C.W. Gardiner and P. Zoller, *Quantum noise* (Springer, 2000).
- [69] J.P. Boon and S. Yip, *Molecular Hydrodynamics* (McGraw Hill Inc, 1980).
- [70] J.P. Hansen and I.R. McDonald, *Theory of simple liquids* (Elsevier, 2006).
- [71] M.P. Allen and D.J. Tildsey, *Computer simulation of liquids* (Oxford, New York, 1987).
- [72] N. Upadhyaya, *Brownian dynamic simulation of dusty plasma*, Master thesis 2010, <http://hdl.handle.net/10012/5070>.
- [73] J.L. Barrat and D. Rodney, *J. Stat. Phys.*, **144**, 677-689 (2011).
- [74] I am grateful to Prof. Barrat for sharing a version of their simulation code to explain some details regarding their paper.
- [75] H. Dammak *et. al.* , *Phys. Rev. Lett.* **103**, 190601(2009).
- [76] M. Saadatfar and Muhammad Sahimi, *Phys. Rev. E.* **65**, 036116, (2002).
- [77] I. Podlubny, *Fractional differential equations* (Academic Press, 1999).
- [78] Y. Povstenko, *Fractional calculus and applied analysis*, **11**, 3, (2008).
- [79] H.V. Beijeren, arXiv:1106.3298 (2012).
- [80] M.F. Thorpe, *Journal of Non-Crystalline Solids*, **57** (1983) 355-370.

SUMMARY

In this thesis, we study energy transport and fluctuations in simple models of *fragile* matter : a unique state of matter that has a vanishingly small window of linear response since one or both of its elastic moduli (shear and bulk) are nearly zero. As a consequence, even the tiniest perturbations travel as non-linear waves. In addition, most models of fragile matter have an amorphous structure. It is the interaction of the non-linear waves with the underlying disorder and the resulting fluctuations, that constitutes the unifying theme explored in this thesis.

There are at least two seemingly distinct sources of fragility: a local source stemming from the strongly non-linear interaction potential between particles so that one can not expand around a potential minimum to define a spring constant, and a second, global source, whereby the collective response of the sample can be considered weakly linear.

As a model of the first kind, we consider a two dimensional packing of soft frictionless elastic disks that are just touching their nearest neighbours. The interaction potential between elastic disks is given by the nonlinear Hertz law that has no harmonic part. Consequently, for a packing in this state, the bulk modulus is vanishingly small and the smallest compressions imparted at the edges leads to nonlinear solitary like waves.

As a model of the second kind, we consider a two dimensional random network of harmonic springs where each node has on average around four nearest neighbours. Here, despite the contact interaction being harmonic, the network has a vanishingly small shear modulus. Consequently, even the tiniest shear strains elicit non-linear waves. There are many important similarities and differences between the nature of non-linear waves and the role played by disorder in the two models described above, which we are gradually beginning to understand.

In Chapters 2-4, we focus on models of the first kind, where we consider two dimensional packings of soft elastic frictionless disks such that, upon overlap, two disks interact with a non-linear potential given by the Hertz law. We begin our research work by first considering an ordered hexagonal packing of disks that are just in contact with their nearest neighbours, so

that the packing has a vanishing bulk modulus. Consequently, an impulse imparted at one of the edges leads to non-linear solitary waves that can be described by the one dimensional Nesterenko equation of motion whose solitary wave solutions are by now well established. We then introduce a simple model of disorder by creating an interface between two hexagonal packings with differing particle masses, and study the interaction of the solitary wave with the interface using a combination of simulations and simple analytical models, in particular, by invoking a quasi-particle approximation to the solitary wave.

We then study the propagation of the solitary like wave in a hexagonal packing with a random distribution of masses. We find that disorder effectively acts as a source of viscosity that causes the solitary-wave amplitude to decay as it propagates through the medium. For small variation in the mass distribution, we find two distinct regimes of attenuation: an initial exponential decay of the solitary-wave amplitude followed by a longer time, power law decay. We understand the exponential decay by invoking the quasi-particle approximation to the solitary wave. However, the decay in the power-law regime signals a new regime, where the solitary-wave ceases to exist. By contrast, we find the emergence of a new type of weakly non-linear shock-like front whose amplitude decays as a power law.

This observation provides our first link to the physics of energy attenuation in a strongly disordered medium such as in a hexagonal packing with a large variance in the distribution of masses and jammed amorphous packings of soft frictionless disks. In both cases, an initial impulse soon transitions into a triangular shock front whose amplitude decays as a power law with a rate that is independent of the amount of disorder.

The attenuation of the impulse has some interesting consequences. We find that disorder causes the energy, initially localized in an impulse, to be distributed throughout the amorphous packing (of finite size). In a system with no intrinsic mechanism to dissipate energy, the particles therefore continue to fluctuate forever. This we imagine as a granular analogue of temperature where the passage of the impulse effectively fluidizes the amorphous packing and where the energy of the initial impulse plays the role of temperature. As a consequence, the emergent mechanical state now has a finite bulk modulus (we started with an amorphous packing with a vanishingly small bulk modulus).

In Chapter 5, we study a simple one-dimensional model of fragile matter that is explicitly coupled to a source of thermal fluctuations. As the simplest toy model, we adopt a one-dimensional chain of strongly non-linear Hertzian springs coupled to a heat bath. We then study the propagation of an impulse along this chain and find that the dynamics of the solitary wave quasi-particle mimics that of a Brownian particle.

In Chapter 6-7, we shift our focus to models of fragile matter of the second kind, i.e, a two dimensional disordered network of harmonic springs. Here the loss of rigidity (vanishing shear modulus) is a collective phenomenon. By shearing one edge of the sample at a uniform rate we study the dynamics of the diffusing and propagating shear fronts. We find that the initial response of the network causes a super-diffusive spreading of the energy away from the boundary. However, after a critical time, the super-diffusive spreading transitions into a propagating shear front whose width continues to grow diffusively. Disorder in these networks thus directly manifests in the very large widths of the propagating shear fronts.

For large shearing rates, we find the onset of non-linearly propagating fronts. However, even though we maintain a constant influx of energy at the boundaries, we do not see steadily propagating nonlinear fronts. Instead, the front widths in the nonlinear regime continue to grow super-diffusively while the shearing rate dictates the speed of the propagating fronts. The super-diffusive spreading in both the linear and nonlinear regimes has very interesting connections with the nature of the fluidized states we found for the amorphous packing of disks interacting with the Hertz law potential, and is consistent with more generic transport properties of lower dimensional fluids.

Finally, we conclude with some initial observations on the emergence of rigidity in random spring networks as an interplay between the network geometry and the coupling to a source of quantum and thermal fluctuations.

SAMENVATTING

Dit* proefschrift is gewijd aan het onderzoek naar energietransport en fluctuaties in simpele modellen van *fragiele* materie: een unieke toestand van materie met een verwaarloosbaar lineair-respons regime, omdat een of beide elastische moduli (schuifmodulus, bulkmodulus) vrijwel nul zijn. Dat heeft tot gevolg dat zelfs de kleinste verstoringen zich als niet-lineaire golven voortplanten. Bovendien hebben de meeste modellen van fragiele materie een vormloze structuur. Het is de interactie van de niet-lineaire golven met de onderliggende wanorde en de resulterende fluctuaties dat het verbindende thema vormt van dit proefschrift.

Het blijkt dat er twee verschillende mechanismen zijn die leiden tot fragiliteit: een lokaal mechanisme, waarbij de interactiepotentiaal tussen deeltjes zodanig is dat men niet kan expanderen rond een minimum om zo een veerconstante te kunnen definiëren, en een tweede, globaal mechanisme, waarbij de respons van het systeem als geheel zwak lineair is.

Als model van het eerste type beschouwen we een tweedimensionale schikking van zachte, wrijvingloze elastische schijven die hun naaste burens net aanraken. Dientengevolge wordt hun interactiepotentiaal gegeven door de niet-lineaire wet van Hertz zonder harmonisch deel. Voor een schikking in deze staat is de bulkmodulus verwaarloosbaar klein en leiden de kleinste compressies uitgeoefend op de randen, al tot niet-lineaire solitaire golven.

Als model van het tweede type nemen we een (tweedimensionaal) willekeurig netwerk van harmonische veren, waarbij elke knoop gemiddeld ongeveer vier naaste burens heeft. Ondanks dat de interactie harmonisch is, heeft het netwerk een verwaarloosbaar kleine schuifmodulus. Daardoor brengt zelfs de kleinste schuif niet-lineaire golven voort. Er zijn veel belangrijke overeenkomsten en verschillen tussen de aard van de niet-lineaire golven en de rol van disorde in de twee beschreven modellen, die we geleidelijk beginnen te begrijpen.

In hoofdstukken 2-4 concentreren we ons op modellen van het eerste type, waarbij we tweedimensionale schikkingen van

* Many thanks to Thomas Beuman for generously summarizing the text in Dutch.

zachte elastische en wrijvingloze schijven beschouwen, zodanig dat bij een overlap de twee schijven interageren volgens een niet-lineaire potentiaal als gegeven door de wet van Hertz. We beginnen ons onderzoek door eerst een geordende hexagonale schikking van deze schijven te beschouwen. We vinden dat een stoot aan een van de randen leidt tot niet-lineaire solitaire golven, die beschreven kunnen worden door een eendimensionale Nesterenko bewegingsvergelijking, waarvan de solitaire-golfoplossingen bekend zijn. We introduceren dan een simpel model voor wanorde door een overgang te creëren tussen twee hexagonale schikkingen, met verschillende massa's van de deeltjes in elk, en bestuderen de interactie van de solitaire golf met de scheidslijn, met behulp van een combinatie van simulaties en simpele analytische modellen, in het bijzonder door gebruik te maken van een quasideeltjes benadering voor de solitaire golf.

Vervolgens bekijken we de voortplanting van de solitaire golf in een hexagonale schikking met een willekeurige massa verdeling. We zien dat de wanorde effectief een bron van viscositeit is, met als gevolg dat de amplitude van de solitaire golf afneemt terwijl deze zich door het medium voortbeweegt. Voor een kleine variantie in de massa distributie vinden we twee verschillende domeinen van verzwakking: in eerste instantie een exponentiële afname, gevolgd door een langere periode met een afname volgens een machtsverband. We kunnen de exponentiële afname begrijpen met behulp van de quasideeltjes benadering. De afname in het regime met het machtsverband, echter, wijst op een nieuw domein waarin een ruimtelijk lokale, voortschrijdende solitaire golf niet meer bestaat. In plaats daarvan zien we de opkomst van een nieuw type zwak niet-lineair, schokachtig, front, waarvan de amplitude afneemt volgens een machtsverband.

Dit geeft ons een eerste aanknopingspunt met de natuurkunde van energie-afname in een zeer wanordelijk medium, zoals een hexagonale schikking met een grote variantie in de massa distributie of geblokkeerde structuurloze schikkingen van zachte wrijvingloze schijven. In beide gevallen gaat een initiële stoot spoedig over in een driehoeksvormig schokfront, waarvan de amplitude afneemt volgens een machtsverband, in een mate die niet afhangt van de hoeveelheid wanorde.

De afname van de impuls heeft enkele verrassende implicaties. We vinden dat de wanorde ervoor zorgt dat de energie, oorspronkelijk gelokaliseerd in een stoot, verspreid raakt over de structuurloze schikking (van eindige grootte). Dientengevolge

zullen, in een systeem zonder intrinsiek mechanisme om energie te dissiperen, de deeltjes permanent fluctueren. Dit stellen wij ons voor als een granulaire analogie van temperatuur, waarbij de passage van de impuls effectief de structuurloze schikking vloeibaar maakt, en de energie van de oorspronkelijke stoot de rol speelt van temperatuur. Dit heeft tot gevolg dat de mechanische toestand die nu ontstaat een eindige bulkmodulus heeft (we begonnen met een structuurloze schikking met een verwaarloosbaar kleine bulkmodulus).

In hoofdstuk 5 bestuderen we een simpel ééndimensionale model voor fragiele materie dat expliciet is gekoppeld aan een bron van thermische fluctuaties. Als het simpelste model nemen we een ééndimensionale keten van niet-lineaire veren gekoppeld aan een thermisch bad. We bekijken de voortplanting van een impuls door deze ketting en vinden dat de dynamiek van het solitaire-golf quasideeltje beschreven kan worden als dat van een Brown's soort deeltje.

In hoofdstukken 6-7 verleggen we de aandacht naar een model van fragiele materie van het tweede type, namelijk, een tweedimensionaal wanordelijk netwerk van harmonische veren, waarbij het verlies van rigiditeit (verwaarloosbare schuifmodulus) een collectief fenomeen is. Door een rand van het systeem uniform te verschuiven bestuderen we de dynamiek van de diffunderende en voortschrijdende schuiffronten. We zien in de beginfase een superdiffusieve verspreiding van de energie, weg van de rand. Maar na een zekere, kritieke tijd gaat de superdiffusieve verspreiding over in een lopend schuiffront, waarvan de breedte blijft toenemen. De disorde in deze netwerken komt dus direct tot uitdrukking in de zeer grote breedtes van deze voortschrijdende schuiffronten.

Voor snelle verschuivingen zien we het begin van niet-lineaire voortplanting van fronten. Ondanks dat we een constante flux van energie aan de rand hebben, zien we geen regelmatig voortplantende niet-lineaire fronten. In plaats daarvan blijven de fronten zich superdiffusief verspreiden in het niet-lineaire domein, terwijl de verschuivingsnelheid de snelheid van de voortschrijdende front bepaalt. De superdiffusieve verspreiding, in zowel het lineaire als het niet-lineaire domein, vertoont zeer interessante gelijkenissen met de aard van de vloeibare toestanden die we vonden voor de structuurloze schikkingen van schijven die interageren volgens de Hertz potentiaal, en is consistent met meer algemene transport eigenschappen van vloeistoffen in lagere dimensies.

Ten slotte eindigen we met enkele initiële observaties omtrent het ontstaan van rigiditeit in willekeurige veernetwerken, als een wisselwerking tussen de netwerkgeometrie en de koppeling aan een bron van quantum- en thermische fluctuaties.

CURRICULUM VITAE

I was born in Hyderabad, India on the first of July, 1981. My parents moved to New Delhi in 1982, where I then obtained my school education. In 2004, I obtained a bachelors degree from the department of Electrical Engineering at the Indian Institute of Technology, New Delhi.

Between 2004-2007, I worked intermittently in semiconductor digital design, first for Biomorphic Microsystems and then Freescale Semiconductors , involved in designing and testing digital circuits for CMOS image sensors and universal serial bus (usb) interface. In 2008, I joined the University of Waterloo in Canada to pursue my masters studies with a thesis on the hydrodynamical description of the equilibrium properties of two-dimensional complex plasma. In 2010, I joined the Lorentz Institute, Leiden, Netherlands for a PhD in theoretical physics.

During my masters studies, I assisted in undergraduate courses on calculus and ordinary differential equations. During graduate studies at Leiden, I assisted in masters courses in fluid mechanics and quantum theory.

PUBLICATIONS

- Shear shocks in fragile networks , S.Ulrich, N. Upadhyaya, B.V. Opheusden and V. Vitelli, arXiv:1307.7665 (2013).
- Soliton attenuation and emergent hydrodynamics of fragile matter, N. Upadhyaya, L. R. Gomez and V. Vitelli, arXiv:1304.6692 (2013).
- Solitons and thermal fluctuations in strongly non-linear solids, N. Upadhyaya, A. M. Turner and V. Vitelli, arXiv:1304.6684 (2013).
- Transmission and reflection of strongly nonlinear solitary waves at granular interfaces, A. Tichler, L. R. Gomez, N. Upadhyaya, X. Campman, V. F. Nesterenko and V. Vitelli, Phys. Rev. Lett., **111**, 048001 (2013).
- Quantum buckling, N. Upadhyaya and V. Vitelli, Phys. Rev. E, **84**, 040601(R) (2011).
- A full account of compressional wave in 2D strongly coupled complex (dusty) plasmas: Theory, experiment and numerical simulation, N. Upadhyaya, V. Nosenko, Z. L. Miskovic, L.-J. Hou, A. V. Ivlev and G. E. Morfill, Eur. Phys. Lett., **94** 65001 (2011).
- Dispersion and damping of two-dimensional dust acoustic waves: theory and simulation, N. Upadhyaya, Z L Miskovic and L-J Hou New J. Phys., **12** 093034 (2010).
- Structure of 2D dusty plasmas in the presence of perpendicular ion flow, N. Upadhyaya, L.J. Hou and Z.L. Miskovic, Phys. Lett. A, **374** (2010).
- Modeling electrolytically top gated graphene, Z.L. Miskovic and N. Upadhyaya, Nano. Res. Lett., **5**,505-511 (2010).

MEANDERINGS

*And so, as I begin the long walk back,
there is much to reflect and remember.*

*Of a journey, that like all,
began being lost and then,
a hesitant knock.*

*Whence, the wise gatekeeper,
with a twinkle in his eyes,
winked me in,
to meander through his magical world...*

*Of crests and troughs,
and cracks and swirls.
Of incessant waves,
that were forever at play.*

*Of particles trapped in a box,
and their occasional escapades.
Of lights, sounds and action,
that orchestrated any new day.*

*But the absurd,
my ever so loyal companion,
hastens to remind me today...*

*That a beginning is,
inevitably entwined with an end,
and that back at the doorsteps,
all is but a little more unknown.
And I, just as lost.*

*Yet, not without solace.
For through my years of wandering restlessly,
as a mere remnant of those clouded memories,
I have often questioned the heavens.
And slowly, ever so slowly,
has an answer so manifest, unveiled.
Right here...*

*In those forever fleeting moments,
of innocence and beauty.
In the verses of a dear poet,
that miraculously reach me from across the seas.
In the kindnesses of the gatekeeper,
who welcomed me with open arms.
And in those gentle hands,
that continue to rock my cradle.*